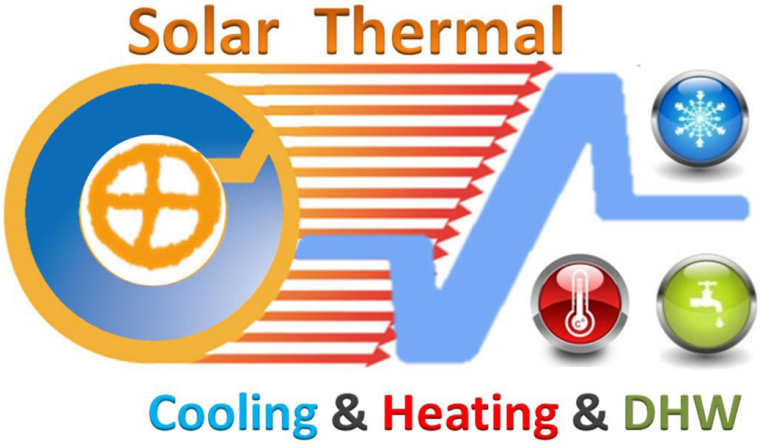

Solar heating and cooling in Northern and Central Europe

Pilot plants in Finland and Germany

VTT TECHNOLOGY 287

Solar heating and cooling in Northern and Central Europe

Pilot plants in Finland and Germany: Finnish-German joint research project within the European SET-plan strategy

Kari Sipilä, Francesco Reda, Riku Pasonen & Atte Löf

VTT Technical Research Centre of Finland Ltd

Maxime Viot & Kaj Pischow

Savo-Solar Oy

Martin Helm, Maximilian Möckl, Florian Menhart, Manuel Kausche, Peter Osgyan & Gloria Streib

ZAE Bayern

ISBN 978-951-38-8511-3 (Soft back ed.)
ISBN 978-951-38-8510-6 (URL: http://www.vttresearch.com/impact/publications)

VTT Technology 287

ISSN-L 2242-1211
ISSN 2242-1211 (Print)
ISSN 2242-122X (Online)
http://urn.fi/URN:ISBN:978-951-38-8510-6

JULKAISIJA – UTGIVARE – PUBLISHER

Teknologian tutkimuskeskus VTT Oy
PL 1000 (Tekniikantie 4 A, Espoo)
02044 VTT
Puh. 020 722 111, faksi 020 722 7001

Teknologiska forskningscentralen VTT Ab
PB 1000 (Teknikvägen 4 A, Esbo)
FI-02044 VTT
Tfn +358 20 722 111, telefax +358 20 722 7001

VTT Technical Research Centre of Finland Ltd
P.O. Box 1000 (Tekniikantie 4 A, Espoo)
FI-02044 VTT, Finland
Tel. +358 20 722 111, fax +358 20 722 7001

Juvenes Print, Tampere 2017

Preface

In the EU more than 70% of the EU-28's population live in urban areas, with the urbanization rate expected to continuously increase. In the EU area, cities use about 80% of the total energy and so environmental energy solutions are needed for a sustainable future in European cities.

Solar Thermal is a major renewable source for the provision of thermal energy, fulfilling demands for space heating, domestic hot water, process heat, and cooling. In terms of energy utilization and economics, an all-year operation of the system is beneficial, avoiding the need for storage of summer heat gain for heating purposes during the winter. Solar heat would rather be used directly during the heating period, and in the warm season a thermally driven chiller transforms the solar heat gain into useful cooling. Thus, the demand and supply of cooling would meet each other.

According to forecasts by the International Energy Agency (IEA), by 2050 solar technologies (1000 GW_{th}) could provide approximately 17% (1.5 EJ; 417 TWh) of the total energy used for cooling worldwide [IEA, 2012]. The SET-Plan driven potential is assumed by nearly 500 TWh in 2030 in contrast to the EU27 baseline scenario of about 100 TWh [EU 2007]. Solar collectors for hot water and space heating in buildings could reach an installed capacity of nearly 3500 GW_{th}, satisfying annually around 8.9 EJ (2472 TWh) of energy demand for hot water and space heating in the building sector by 2050. Solar hot water and space heating will account for 14% of space and water heating energy used in buildings by that time. Solar heating and cooling can reduce CO_2 emissions by some $800x10^6$ tonnes (Mt) per year by 2050.

Solar heating and cooling technologies are compatible with almost all sources of backup heat and are almost universally applicable due to their ability to deliver hot water, hot air and cold air. Solar energy is also an attractive option to decrease the demand for electricity and fight the increasing price of fuel-based energy as well as to decrease dependence on imported energy. Many installations have been realised and the technology has shown that significant energy savings and a reduction in CO_2 emissions are possible.

The project that is the subject of this report is an international co-operation between Savo-Solar Oy & VTT Oy in Finland and ZAE Bayern in Germany. The duration of the research project was 39 months, starting in September 2013 and ending in December 2016. It was structured into five subtasks, which were:

A) Concept and modelling phase
This section comprises the Identification, simulation and evaluation of promising fields of applications for solar thermal heating and cooling concepts for domestic and industrial energy supply under different climatic situations in central and northern Europe, with concern for their ecological and economic impact.

B) Component development: Highly efficient solar thermal flat-plate collector
A flat-plate solar collector for maximum solar gain applied under Northern Europe climatic conditions to be developed for heat absorption and industrial processes. Solar absorber with the highest optical performance and optimal flow design to be fitted with additional transparent front-side insulation as well as improved backside insulation to significantly increase the specific solar gain in solar cooling. The Savo-Solar MPE direct flow absorber is more effective in harvesting the energy per square meter than any of today's vacuum tube collectors. The challenge is to control the heat loses, the biggest of which is the convective loses through the front glass. Several solutions are in the research phase. Good results have been achieved using double glazing with a low-e coating in the second glass. As an alternative solution, a thin ETFE or FEP-Film with appropriate mounting and tensioning as well as high solar transmissions without an AR-coating could be applied. This latter measure seems to be more promising and easier to realize for the intended project goals.

C) District heating and biofuel-driven boiler backup
The Savo-Solar case study has district heating as a backup for a solar collector driven single-stage absorption chiller, when solar irradiation is not available.

The ZAE Bayern case study has a combination of an advanced single-stage absorption machine and a direct biomass-driven second-stage high temperature generator (HTG).

D) Component development: Compact absorption chiller comprising hydraulic rack
Absorption machines transform heat into cold by means of a sorption process between a refrigerant (e.g. Water) and a Sorbent (e.g. Lithium bromide) and can be used as a chiller or heat pump. In contrast to conventional vapour compression chillers/heat pumps, the required electricity consumption is almost negligible.

E) Solar heating and cooling system concept and demonstration
The system concept under investigation particularly fits the situation in Northern and Central Europe. During summertime, cooling is mainly done by converting solar heat from the flat-plate collectors into useful cold by an advanced single effect absorption process. At insufficient insolation, driving heat is provided by heat storage. In winter time the system operates as a thermally driven heat pump using district heating or local biofuel, e.g. wood or straw pellets, to upgrade ambient heat to a useful temperature level.

The commissioned solar heating and cooling system comprises an improved solar thermal collector and an advanced highly variable absorption chiller/heat pump for holistic heating and cooling of buildings with a high solar fraction at the Savo-Solar office building in Mikkeli, Finland.

The project will start by installing an array of an adequate number of Savo-Solar SF-100-03 standard collectors, which serve as a reference system for the same amount of optimized foil collectors in parallel. Heat from solar collectors are fed to the absorption chiller/heat pump, including the main hydraulic components in a pre-assemble rack for easy and quick onsite installation. Bought-in parts, such as a sensible heat buffer tank and dry air cooler complete the equipment for solar heating and cooling. Measurements through an adequate data collection system and analyses of the result will follow.

The project has a Steering Group, which has seven meetings during the project's lifetime. The StGr has seven Finnish participants, enlarged with four German participants:

Finnish participants:	
Karin Wikman	Tekes
Kaj Pischow	Savo-Solar Oy
Jari Nykänen/Auli Haapiainen-Liikanen	Etelä-Savon Energia
Petri Flyktman	Jyväskylän Energia Oy
Mika Oksanen	Helsingin seudun asuntosäätiö
Jukka Paloniemi	Caverion Oy
Kari Sipilä	VTT

German participants:	
Manuel Riepl	ZAE Bayern
Martin Helm	ZAE Bayern
Peter Osgyan	ZAE Bayern
Cristian Schweigler	ZAE Bayern

Thanks to the Steering Group for the good comments and discussions in our meetings.

SOLCH Project Group

Framework and Research Cooperation

FINLAND	GERMANY
VTT Vuorimiehentie 3 FI-02044 VTT www.vtt.fi Contact: Riku Pasonen, MSc (Tech) Tel: +358 40 574 8105 Fax: +358 20 722 7604 email: riku.pasonen@vtt.fi	**ZAE Bayern** Division 1: 'Technology for Energy Systems and Renewable Energy' Walther-Meissner-Straße 6 D-85748 Garching www.zae-bayern.de Contact: Manuel Riepl, MSc Tel: +49 89 329442-43 Fax: +49 89 329442-12 email: riepl@muc.zae-bayern.de
Savo-Solar Oy Insinöörinkatu 7 FI-50150 Mikkeli www.Savo-Solar.fi Contact: Kaj A. Pischow Tel: +358 40 555 3873 email: kaj.pischow@Savo-Solar.fi	**Scherdel Energietechnik GmbH** (Subcontract) Scherdelstrasse 2 D-95615 Marktredwitz www.econ-web.com Contact: Marco Bauer Dipl.-Phys. Tel: +49 9231 603-556 Fax: +49 9231 62938 email: marco.bauer@econ-web.de

VTT Technical Research Centre of Finland Ltd, Espoo Finland

VTT Technical Research Centre of Finland is the biggest multi-technological applied research organization in Northern Europe. VTT provides high-end technology solutions and innovation services. From its wide knowledge base, VTT can combine different technologies, create new innovations and a substantial range of world-class technologies and applied research services, thus improving its clients' competitiveness and competence. Through its international scientific and technology network, VTT can produce information, upgrade technology knowledge, create business intelligence and added value to its stakeholders. VTT is a part of the Finnish innovation field under the domain of the Ministry of Employment and the Economy. VTT is a not-for-profit organization.

Savo Solar Oy, Mikkeli Finland

Savo-Solar is a Finnish company manufacturing solar thermal collectors and absorbers. The uniqueness of the company's products is based on a vacuum coating process where the complete absorber can be coated, which means that the direct-flow design can be utilized. The Savo-Solar team has extensive experience and know-how in vacuum-coating techniques as well as in managing an international business. The company uses the latest manufacturing technologies in its processes and the quality system meets the ISO 9000 requirements. The company is expanding rapidly and via its products, it is supporting customers in their growth and other business targets. Savo-Solar invests in constant product development to fulfil also the future needs of the growing market.

Bavarian Center for Applied Energy Research (ZAE Bayern), Garching Germany

The Bavarian Center for Applied Energy Research (ZAE Bayern) is a registered, non-profit association. The association was founded in December 1991 and has its registered office in Würzburg. It was established to promote energy research as well as education, further training, consultation, information and documentation in all fields significant to energy research. The association supports a scientific research institute with three divisions in Würzburg, Erlangen and Garching, employing about 180 scientists, technicians, administrative personnel and students. The division in Garching, 'Technology for Energy Systems and Renewable Energy', is managed by the scientific director, Professor Dr Hartmut Spliethoff (TUM) and head of division Dr Andreas Hauer, who is the successor of the long/term head of division DiplPhys Wolfgang Schölkopf. The division develops and researches heat storage and conversion as well as electrochemical conversion and storage. Additional R&D is focused on biomass as well as geothermal and solar thermal systems.

Scherdel Energietechnik GmbH, Marktredwitz Germany

Scherdel Energy GmbH is a spin-off of the Scherdel Group set up to develop the new branch of business absorption heating and cooling technologies. The core competence of the Scherdel Group comprises technical springs, stamped and bent parts with elastic properties and weldment assemblies for the automotive market, as well as dedicated fundamental materials research, such as structure and durability tests, material and failure analysis. On behalf of the Technical University of Berlin and ZAE, a prototype for an absorption refrigeration system has been already manufactured for use in district heating systems, and successfully put into operation.

Contents

Summary

Solar heating and cooling technologies are compatible with almost all sources of backup heat and almost universally applicable due to their ability to deliver hot water, hot air and cold air. Solar energy is also an attractive option to decrease the demand for electricity and to fight against increasing prices of fuel-based energy as well as to decrease dependence on imported energy. Many installations have been realised and the technology has shown that significant energy savings and a reduction in CO_2 emissions are possible. In the solar cooling process, the demand and supply of cooling will meet each other.

The general objective of this Finnish–German cooperative research project has been to develop an innovative energy system for solar heating, cooling and domestic hot water preparation so as to broaden the application of improved solar thermal systems and absorption heat pumps/chillers for domestic and industrial buildings in Northern and Central European countries.

In this project a small scale (10 kW) solar cooling and heating (25 kW) system with a compact absorption chiller/heat pump and improved foil collectors has been developed and successfully demonstrated at the Savo-Solar office building in Mikkeli, Finland. By use of thermally-driven absorption instead of electrically-driven compressor heat pump technology, no additional grid stress or reserve capacity, either in summer or in winter, is caused. The demonstration consists of a solar-heat-driven (36 m^2 collectors) absorption chiller, heat storage and district heating or biomass boiler backup (15 kW) for the chiller. The absorption machine can be operated as a chiller or heat pump. Based on simulations, the most suitable V/S (heat storage volume/collector surface) is 55.6 l/m^2, so it means 2 m^3 in the Savo-Solar case.

A practical feasibility study of a biomass (wood chip) -driven double-stage absorption machine was conducted also at the ZAE Bayern laboratory in Munich, Germany. In combination with ground heat exchangers and solar collectors, it appears to be a very promising alternative for low-carbon heat and cold supply for buildings and industrial processes in the temperature range from 4 to 110 °C.

By adding a foil between the glass and aperture area, front-side heat losses have been reduced significantly by up to 11%, especially at higher temperatures, which are required to drive the absorption chiller during summertime. As the future of the solar thermal collector industry is seen to be in large scale applications, it is suggested that the developed techniques are transferred to larger scales as well.

Right now, the system itself shows adequate key performance results, but there is still a high optimization potential through adapting the control strategy to the special requirements and peculiarities of the building. The system size of a 10 kW

cooling capacity was chosen in order to cover the office needs. But from an economic point of view, the targeted size of the system would be at least 50 kW chilled water capacity. As renewable heat from the collectors is very rare in wintertime, an additional ground heat exchanger or the use of low temperature waste heat (e.g. from the coating machine) would increase the annual share of renewables for cooling and heating to more than 50% in total.

An energy efficiency ratio (EER) of more than 9 and a coefficient of performance (COP) of more than 0.7 for a chiller were reached in the pilot project.

The total investment cost of the solar driven chiller pilot project was EUR 69 550 (EUR 6955/kW_c), which consists of a solar field (35.0%), a chiller and hydraulics (21.5%), heat storage (10.6%), dry air cooling (17.7%) and district heating backup (15.1%). The driving cost of the pilot project was EURcent 4.7 per kWh of cooling energy. If we include the investment cost for the pilot project, the price of cooling energy is EUR 2.34/kWh_c. A commercial project price is evaluated to be about EUR 1.50/kWh_c.

Zusammenfassung

Solarthermische Heiz- und Kühltechnologie kann mit nahezu allen Backup-Wärmequellen kombiniert werden um versorgungssicher kaltes und warmes Wasser sowie konditionierte Luft bereit zu stellen. Ein hoher Anteil an Solarenergie hilft dabei den Elektrizitätsbedarf und die Abhängigkeit von steigenden fossilen Energiepreisen sowie Energieimporten zu reduzieren. Viele realisierte Projekte zeigen, dass diese Technologie signifikant Energie einsparen und den CO_2-Ausstoß reduzieren kann. Zudem passen solares Energieangebot und der Kältebedarf im Tagesverlauf gut zusammen. Das Hauptziel dieses bilateralen finnisch-deutschen Forschungsprojektes ist die Entwicklung und Erprobung eines innovativen Energiesystems zum solar thermischen Heizen, Kühlen und zur Warmwasserbereitung. Dieses Projekt erschließt neue Anwendungsgebiete für verbesserte solarthermische Systeme und Absorptionswärmepumpen und -kälteanlagen im Wohnungsbau und der Industrie für Nord- und Zentraleuropa.

In diesem Projekt wurde im kleinen Maßstab ein solarthermisches Heiz- und Kühlsystem mit kompakter Absorptionskälteanlage mit 10 kW Nennkälteleistung sowie Wärmepumpenfunktion mit 24 kW Nennwärmeleistung entwickelt und erfolgreich am Firmenstandort von Savo-Solar in Mikkeli, Finnland demonstriert. Durch den Einsatz der thermisch angetriebenen Absorptionstechnik, anstatt der elektrisch angetriebenen Kompressionstechnik, wird das Stromnetz, weder im Sommer noch im Winter, nicht zusätzlich belastet und kein weiterer Aufbau von Reservekapazität notwendig. Das installierte System besteht aus einem 36 m² großem Solarkollektorfeld das über einen Pufferspeicher die trocken rückgekühlte Absorptionskälteanlage antreibt. Simulationen zeigen ein optimales Verhältnis zwischen Speichervolumen und Kollektor Apertur Fläche bei 55,6 Liter pro Quadratmeter, sodass in diesem Fall bei Savo Solar insgesamt 2000 Liter Speichervolumen notwendig sind. Als Backupwärmequelle steht Fernwärme zur Verfügung. Zudem wurde im Labormaßstab auch eine direkte Biomassefeuerung (15 kW Feuerungsleistung) des Sorptionsprozesses erprobt. Dabei kann die Absorptionsanlage sowohl als Kälteanlage sowie auch als Wärmepumpe betrieben werden. Die Machbarkeit einer mit Biomasse betriebenen zweistufigen Absorptionsanlage wurde im Labor des ZAE Bayern in München bewiesen. In Verbindung mit Erdwärmesonden und Solarkollektoren erscheint dies als vielversprechende Alternative für eine kohlenstoffarme Wärme- und Kälteversorgung für Gebäude und industrielle Prozesse im Temperaturbereich zwischen 4 und 110 °C.

Durch die Integration einer dünnen Folie zwischen Apertur Fläche und Glasabdeckung des Solarkollektors konnten die vorderseitigen Wärmeverluste um bis zu 11 % reduziert werden. Dies ist vor allem bei den zum Antrieb der Absorptionskälteanlage notwendig hohen Temperaturen signifikant. Da die

Solarkollektorbranche in Zukunft verstärkt zu größeren Anlagen tendiert, sollten diese guten Ergebnisse auch auf den größeren Maßstab übertragen werden.

Bereits jetzt zeigt das Energiesystem angemessene Leistungszahlen. Es besteht jedoch noch erhebliches Einsparpotential, indem die Steuerungsalgorithmen auf die speziell vor Ort herrschenden Eigenheiten des Gebäudes angepasst werden. Die Systemleistung von nur 10 kW Kälte ist auf das Gebäude angepasst. Aus wirtschaftlichen Gründen sind jedoch Leistungsklassen über 50 kW anzustreben. Da solare Wärme von den Solarkollektoren im Winter nur spärlich zur Verfügung steht, könnte der regenerative Anteil an Wärme und Kälte auf über 50 % steigen, wenn zusätzlich Erdwärme oder Niedertemperaturabwärme aus der Beschichtungsanlage von Savo Solar genutzt würden.

In diesem Pilotprojekt beträgt die Systemkennzahl Energy Efficiency Ratio (EER) aktuell mehr als 9 und der Coefficient of Performance (COP) liegt über 0,7. Die Investitionskosten für das Demonstrationsprojekt der solar thermisch angetriebenen Kälteanlage summieren sich insgesamt zu 69 550 EUR (6955 EUR/kWC) und verteilen sich auf die Solarkollektoranlage (35,0 %), Kälteanlage und Hydraulik (21,5 %), Wärmespeicher (10,6 %), trockener Rückkühler (17,7 %) und Fernwärmebackup (15,1 %). Die Energiebetriebskosten für das Demonstrationsprojekt betragen 4,70 EURcent pro Kilowattstunde. Unter Berücksichtigung der Investitionskosten steigen die Kältegestehungskosten auf 2,34 Euro pro Kilowattstunde Kälte. Für eine kommerzielle Anlage sinken die Kosten auf circa 1,50 Euro pro Kilowattstunden Kälte.

Tiivistelmä

Aurinkoenergia on hyvin yhteensopiva lähes kaikkien muiden energian tuotantomuotojen kanssa tuottamaan lämmitystä ja jäähdytystä veden ja ilman välityksellä. Aurinkoenergia on myös keino vähentää sähkön käyttöä lämmityksessä ja jäähdytyksessä sekä polttoaineita, joiden hinnat vaihtelevat ja ovat usein myös tuontiriippuvia ja jotka aiheuttavat päästöjä ilmakehään. Aurinkojäähdytyksessä kulutus ja tuotanto kohtaavat sopivalla tavalla ja vältetään energian suurta varastointitarvetta.

Tämän Suomen ja Saksan yhteistyöprojektin tavoitteena oli kehittää pieni kompakti aurinkoenergialla, biopolttoaineella tai teollisuusprosessilämmöllä toimiva absorptiojäähdytin kiinteistön tai teollisuusprosessin jäähdytykseen Pohjois- ja Keski-Euroopan olosuhteisiin. Jäähdyttimen tulee toimia myös tarvittaessa lämpöpumppuna. Rinnakkain jäähdytys-lämmitysprojektin kanssa kehitettiin myös Savo-Solarin aurinkokeräintä SF100-03 varustamalla keräin muovikalvolla lasin ja absorptiopinnan väliin. Tavoitteena oli saada merkittävä parannus keräimen hyötysuhteeseen erityisesti suurilla keräimen keskilämpötilan ja ulkolämpötilan eroilla.

10 kW:n absorptiojäähdyttimen sovellutuskohteena oli Savo-Solar Oy:n toimistokiinteistö Mikkelissä. 15 kW:n aurinkolämpöteho tuotetaan Savo-Solarin aurinkokeräimillä (18 x 2 m^2). Jos lämmönlähteen tuottama lämpötila tai teho ei riitä jäähdyttimen ajamiseen, lisälämpö otetaan kaukolämmöstä. Absorptiokone toimii myös tarvittaessa 25 KW:n lämpöpumppuna. Järjestelmä on varustettu 2 m^3 kuumavesivaraajalla aurinkosäteilytehon vaihtelujen kompensoimiseksi ja ulos sijoitetulla ilmajäähdyttimellä, jonne ajetaan absorptiokoneen välijäähdytyslämpö ja tarvittaessa aurinkokeräinpiirin lämpö ylikuumenemisen välttämiseksi. Lämpöpumppumoodissa lämpö ajetaan teollisuushallin lattialämmitykseen. ZAE Bayernin pilot-kohteessa Münchenissä varalämmön lähteenä on puuhakkeella toimiva biokattila. Suunnitteluvaiheessa koko prosessi simuloitiin TRNSYS-mallilla, jossa todettiin mm. lämpövaraston sopivaksi mitoitusarvoksi 55,6 l/m^2 aurinkokeräinpintaa eli Mikkelin tapauksessa 2 m^3:n eristetty teräsäiliö varustettuna putkimallisella painovoimaisella lataus-purkausjakajalla. Jäähdytys-lämmityskäytössä lämpövarastoa voidaan hyödyntää 4–110 °C rajoissa.

Järjestelmä toimii tavoitteiden mukaisesti, ja 10 kW:n jäähdytysjärjestelmällä on päästy tavoitteisiin eli vähintään 0,7 COP:hen (jäähdytysteho/tarvittava lämpöteho) ja EER 9 -arvoon (jäähdytysteho/käytetty sähköteho). Kehittämällä ohjausstrategiaa ja optimointia paremmin sopivaksi rakennuksen erityistarpeisiin päästään vielä parempiin COP- ja EER-lukuihin.

Kalvolla varustettu aurinkokeräin paransi hyötysuhdetta 6 % verrattuna perinteiseen SF100-03-malliin jäähdytyskaudella 2016, ja maksimi 11 % parannus saavutettiin syyskuussa.

Jäähdytyskaudella 2016 (kesä-lokakuu) aurinkoenergiaa saatiin keräinten pinnalle 15253 kWh, josta hyödynnettiin 4711 kWh, eli järjestelmän hyötysuhteeksi saadaan keskimäärin 31% ±4%. Jäähdytysenergiasta n. 70 % tuotettiin auringolla ja 30 % kaukolämmöllä.

Pilottiprojektin investoinnit olivat 69 550 EUR (6955 EUR/kW_c), joka jakautui seuraavasti: 35 % aurinkojärjestelmälle, 21,5 % absorptiokoneelle + hydrauliikalle, 10,6 % lämpövarastolle, 17,7 % ilmajäähdyttimelle ja 15,1 % kaukolämpöliitännälle. Käyttökustannukset kesän 2016 kokemusten perusteella ovat 4,7 EURcent/kWh_c. Investoinnit huomioiden jäähdytysenergian keskihinnaksi saatiin 2,34 EUR/kWh_c. Kaupallisen 10 kW version omakustannusarvoksi arvioitiin n. 1,50 EUR/kWh_c. Kaupallisen aurinkojäähdyttimen koon pitäisi olla vähintään 50 KW_c. Lämpöpumppukäyttö pidentää absorptiokoneen vuotuista käyttöaikaa ja siten kannattavuus paranee.

List of symbols

CHP	Cogeneration heating plant
COP_c	Coefficient of performance in cooling
COP_h	Coefficient of performance in heating
Cp	Heat capacity of the indoor distribution system carrier fluid [kJ/(kg K)]
DH	District heating
DHW	Domestic hot water
$E_{i,in}$	Final energy consumption (electricity based systems) [kWh]
E_{P1}	Final energy consumption of the solar circulation pump (primary side) [kWh]
E_{P2}	Final energy consumption of the solar circulation pump (secondary side) [kWh]
E_{P3}	Final energy consumption of the circulation pump which supplies the desorber [kWh]
E_{P4}	Final energy consumption of the dry cooler circulation pump (chiller side) [kWh]
E_{P5}	Final energy consumption of the dry cooler circulation pump (dry cooler side) [kWh]
EER_c	Electricity efficiency ratio of cooling
EER_h	Electricity efficiency ratio of heating
FC	Free cooling
I_{sol}	Solar radiation
PER	Primary energy ratio [-]
Q_{CD}	Useful cooling distribution system supplied energy (building cooling needs) [kWh]
Q_{ch}	Cold energy produced by the chiller [kWh]
Q_d	Hot energy consumed by the desorber [kWh]
Q_{DH}	District heating supplied energy [kWh]
$Q_{DH,d}$	District heating supplied energy to the desorber [kWh]
$Q_{DH,b}$	District heating supplied energy to the building [kWh]
Q_{HD}	Useful heating distribution system supplied energy (building heating needs) [kWh]
$Q_{i,out}$	Useful supplied energy [kWh]
$Q_{i,in}$	Final energy consumption (non-electricity based systems) [kWh]
Q_{sol}	Heat produced by means of the solar thermal collectors [kWh]
$Q_{sol,\ DHW}$	Heat produced by means of the solar thermal collectors for supplying and DHW [kWh]
$Q_{sol,\ heating}$	Heat produced by means of the solar thermal collectors for supplying building heating energy[kWh]
$Q_{sol,\ chiller}$	Heat produced by means of the solar thermal collectors for supplying the chiller (desorber) [kWh]
Q_{WD}	Useful water distribution system supplied energy (DHW) [kWh]
$SF_{,c}$	Cooling solar fraction [-]

$SF_{,h}$	Building heating solar fraction [-]
$SF_{,h+DHW}$	*x*Building heating + DHW solar fraction [-]
$SF_{,DHW}$	DHW solar fraction [-]
$SF_{,tot}$	Total solar fraction [-]
SHC	Solar heating and cooling system
ε_{DH}	District heating primary energy factor [-]
ε_{el}	Electrical primary energy factor [-]

1. Introduction

Solar heating and cooling technology will play a vital role among the available options in sustainable energy systems. This has been identified by the European Commission in its Energy Roadmap 2050, as it can provide '*locally* produced' energy. Today, about 50% of the final energy demand is used for heating and cooling purposes. In the future, heat demand will be significantly reduced by behavioural changes and efficiency measures e.g. through nearly zero-energy buildings. However, since heat is not only used for space heating, but also for domestic hot water and process heating, roughly 50% of today's heat demand will remain by 2050.

1.1 Solar heating and cooling in Europe

The Solar Heating and Cooling Programme (SHC) of the International Energy Agency (IEA) was founded in 1977 as one of the first multilateral technology initiatives ('Implementing Agreements') of the IEA. Its mission is 'to enhance collective knowledge and application of solar heating and cooling through international collaboration to reach the goal set in the vision of solar thermal energy meeting of 50% of low temperature heating and cooling demand by 2050 (https://www.iea-shc.org/).

Solar worldwide resource capacity is shown in Figure 1.1.

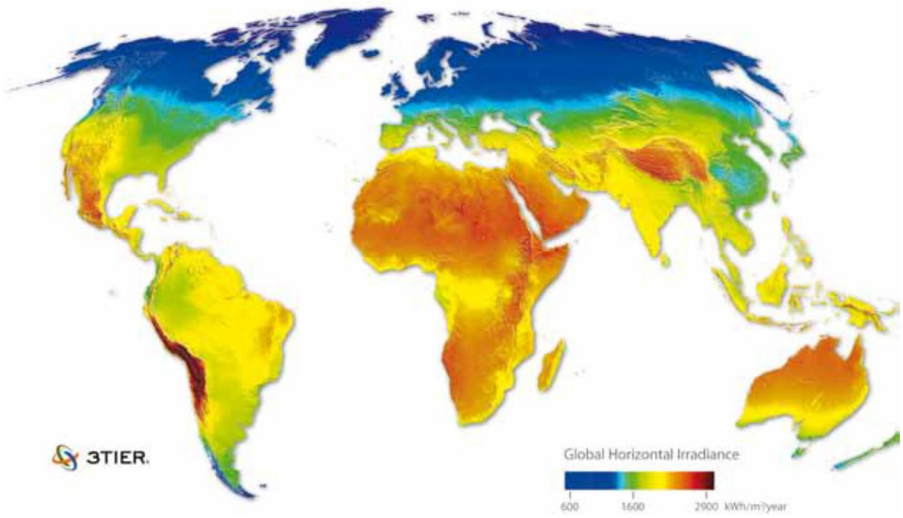

Figure 1.1. Worldwide Solar resource map (https://www.iea-shc.org/data/sites/1/publications/2012_SolarHeatingCooling_Roadmap.pdf) (kWh(m^2/y)).

'Solar technologies can supply the energy for all of a building's needs—heating, cooling, hot water, light and electricity—without the harmful effects of greenhouse gas emissions created by fossil fuels' states the IEA/SHC program. The so-called 'single effect' absorption chillers typically need heat with temperatures in the range of 70 to 100 °C, and achieve a coefficient of performance (COP) of about 0.7. Adsorption chillers are able to work at lower temperature ranges (down to 55 °C or lower, if it is a reasonable target), however this leads to an inferior COP (nearly 0.6 or lower) [Helm et al., 2016].

The main objective of the International Energy Agency (IEA) Task 38 (http://task38.iea-shc.org/) is the implementation of measures for an accelerated market introduction of solar air conditioning and refrigeration with focus on improved components and system concepts. The market introduction will be supported through activities in development and testing of cooling equipment for the residential and small commercial sector (http://task38.iea-shc.org/). Subsequent, the homepage of IEA SHC program/Task 48 provides many calculation tools and best practices in solar utilizing (http://task48.iea-shc.org /).

The total and newly installed solar thermal capacity 2005–2014 in Europe is shown in the Figure 1.2.

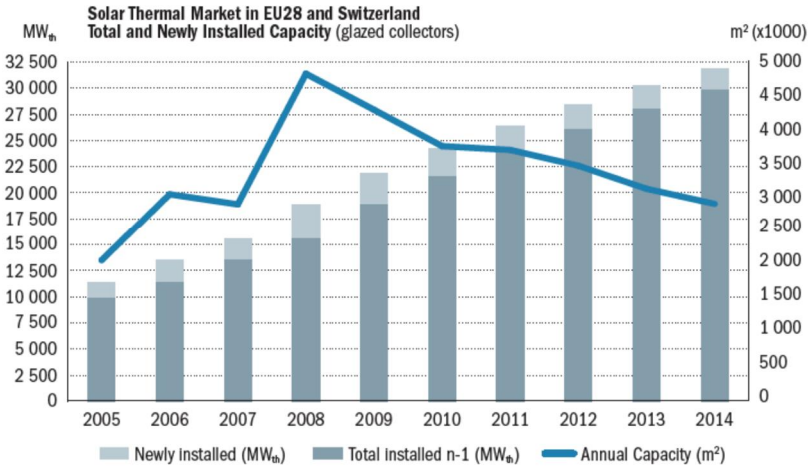

Figure 1.2. Solar Thermal Market in the EU27 and Switzerland. Total and Newly Installed Capacity.
http://www.estif.org/fileadmin/estif/content/market_data/downloads/2014_solar_thermal_markets_LR.pdf

Heating and cooling degree days are shown in Figure 1.3. Finland (8000 deg.-days/a) is colder than Germany (3000 deg.-days/a) based on heating degree days, but cooling degree days are close to each other, from 200 to 400. The cooling season is longer in Germany, but solar intensity is higher and the season is shorter in Finland. Building standards define indoor temperature in winter as being 20–21 °C and it cannot be allowed to rise over 26 °C in summer. We therefore require heating and cooling to keep indoor temperature within those values. In addition heating is needed for domestic hot water (DHW), which should be 55–58 °C.

European heating index (EHI) and European Cooling Index (ECI) are shown in Figure 1.4. The index is normalized, where 100 is equal to an average European condition. Using a reference degree-day number of 2600 corresponding to an annual average outdoor temperature just above 10 °C fulfils this normalization. Frankfurt in Germany is the typical space heating city in Europe, with a heating index of 100.

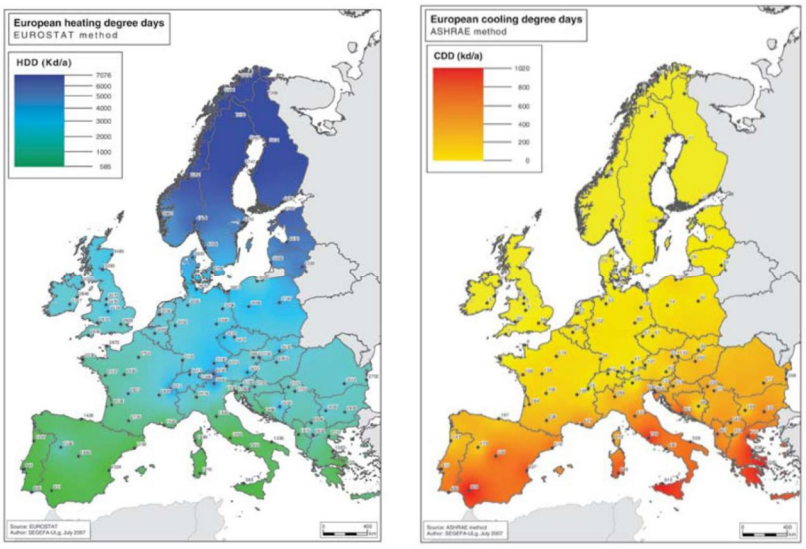

Figure 1.3. European heating (Eurostat) and cooling (ASHRAE) degree days. http://www.pvsites.eu/downloads/download/d2-2-european-climate-zones-and-bioclimatic-design

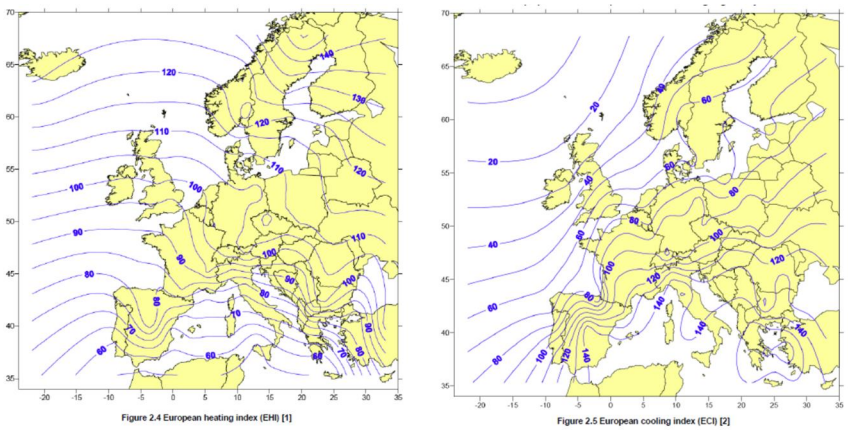

Figure 1.4. European heating index (EHI) and European Cooling Index (ECI). http://www.pvsites.eu/downloads/download/d2-2-european-climate-zones-and-bioclimatic-design

The recommended values in EN15251:2007 are 20 °C and 26 °C for winter and summer, respectively for the living space in a residential building. Figure 1.5 shows the minimum and maximum indoor temperatures in 16 EU countries. Inside the blue and green circles are shown the requirements in Finland and Germany.

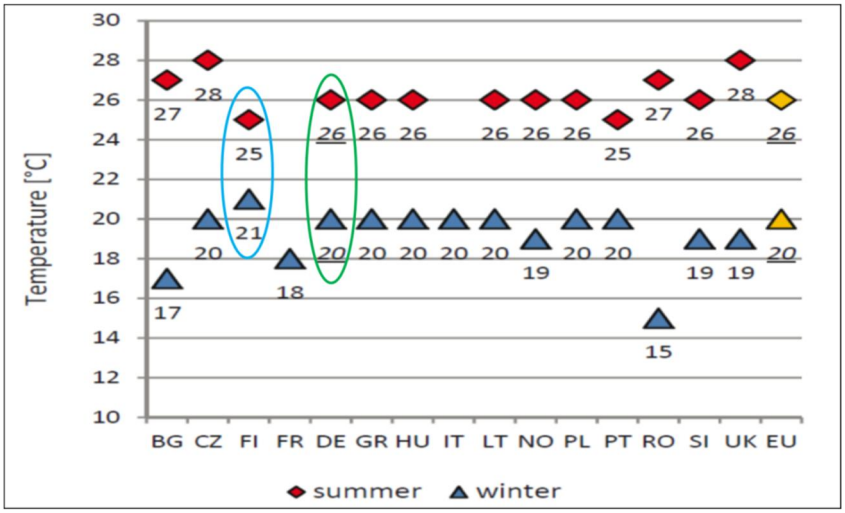

Figure 1.5. Recommended indoor temperatures for summer and winter in 16 EU countries.
http://www.pvsites.eu/downloads/download/d2-2-european-climate-zones-and-bioclimatic-design

2. Scientific and technical objectives of the project

The general objective of this Finnish-German cooperative research project has been to develop an innovative energy system for solar heating (15 kW), cooling (10 kW) and domestic hot water preparation in order to broaden the application of improved solar thermal systems and absorption heat pumps/chillers for domestic and industrial buildings in Northern and Central European countries.

Figure 2.1 describes proposed trivalent heating and cooling system with an integrated domestic hot water preparation comprises a highly efficient full aluminium solar thermal MPE- absorber, sensible heat storage with advanced stratification and an enhanced absorption chiller/heat pump for efficient heat transformation In solar cooling mode, the sorption chiller is driven by solar heat from a new improved flat-plate collector system with optimized efficiency at high temperatures, supplemented by heat from a district heating network or a biomass boiler as a backup heat source in times of insufficient insolation. With regard to moderate ambient temperatures during the summer season, a dry air-cooler is applied for rejecting the waste heat of the chiller. Waste heat rejection could also be used for pre-heating the hot tap water or for floor heating.

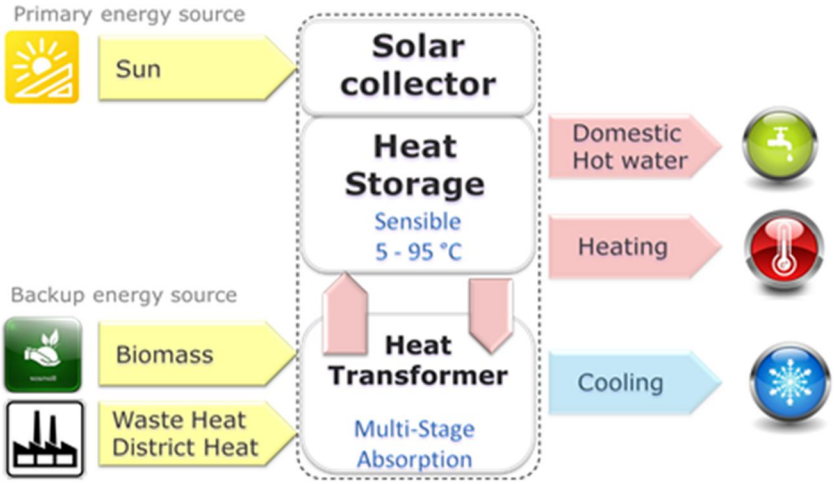

Figure 2.1. Sankey diagram with the main components and energy flows in the SHC-System.

During the heating season, solar heat can be used either directly for domestic heating or it can be buffered in heat storage at a temperature level up to 95 °C for later use. With the aid of the highly flexible sorption chiller/heat pump prototype, the useful minimum temperature of the storage is extended to 5 °C, thus enhancing the storage density by a factor of ≈ 2. Induced by the low storage temperature, the collector efficiency is increased in wintertime, allowing a high solar fraction even in icy weather conditions. The heat pump ensures a constant temperature level from the heating system at any time.

Compared to a conventional compression heat pump an increased temperature lift from the heat source to useful heat output only slightly affects the Coefficient of Performance COP, e.g. the ratio of useful heat and driving energy, in the sorption heat pump process. Further improvement is achieved when a direct biomass-driven second-stage generator is integrated into the heat pump cycle. By substituting a conventional biomass boiler system with about 40% of wood pellets and emissions are additionally saved. Thus, the potential of the available biomass for domestic heating and cooling is nearly doubled.

The project is an international co-operation between Savo-Solar Oy & VTT Oy in Finland and ZAE Bayern in Germany. The duration of the research project was 39 months, starting in September 2013 and ending in December 2016 and is structured into five subtasks, which are:

2.1 Concept and modelling phase

This section details the Identification, simulation and evaluation of promising fields of applications for solar thermal heating and cooling concepts for domestic and industrial energy supply under different climatic situations in central and northern Europe, with concern for their ecological and economic impact. Different concepts of solar thermal heating and cooling system are simulated and evaluated by reference to key ecological and economic figures. The most promising system will be realized as a pilot installation in phase E (Chapter 2.2).

2.1.1 Component development: Highly efficient solar thermal flat-plate collector

A flat-plate solar collector for maximum solar gain applied under Northern Europe climatic conditions was developed for heat absorption and industrial processes. For that purpose a full aluminium Multi-Port Extrusion (MPE) solar absorber with the highest optical performance (maximum α and F' and minimum ε) and optimal flow design was fitted with an additional transparent front-side insulation, as well as improved backside insulation so as to significantly increase the specific solar gain in solar cooling.

The Savo-Solar MPE direct flow absorber is more effective in harvesting the energy per square meter than any of today's vacuum tube collectors. The challenge is to control the heat loses, from which the biggest ones are the convective loses through the front glass. Several solutions were in the research phase and some are already in production, such as the vacuum flat-plate collector or the use of Teflon foil instead of double glazing. Good results have also been achieved using double glazing with a low-e coating in the second glass. Such a solution, however, may in practice be complicated and expensive and increases the collector weight. As an alternative solution, a thin (25-50 µm) ETFE or FEP-film with appropriate mounting and tensioning as well as high solar transmissions between 0.93 and 0.96, and also without AR-coating, could be applied. This measure was more promising and easier to realize for the intended project goals. Problems that had to be solved with regard to economic aspects were achieving film mounting without wrinkles or sagging at higher temperatures, combined with the thermal expansion of the film and the joining technique of the second glass cover under thermal stress.

At present, the Savo-Solar, with its SF_100-03 collector, produces a covered flat plate solar collector, with $\eta_0 = 0.92$, showing the highest optical efficiency ever scored. This is due to its nearly perfect heat transfer from the hot absorber plate to the working solar fluid by a full aluminium-absorber with many small-sized and well-bonded parallel flow channels. The thermal losses are average compared to today's flat-plate collectors and the constant and linear loss coefficients amount to $a_1 = 1.8\ W \cdot m^{-2} \cdot K^{-1}$ and $a_2 = 0.036\ W \cdot m \cdot^{-2} \cdot K^{-2}$, respectively. These values are valid

for a measuring range of 0–70 K over ambient as applied in the common solar key mark test for hot water and heating applications. So far, no reliable measurements have been done for the higher temperature range between 70 and 150 K over ambient, which is needed to drive a single-stage and two-stage absorption chiller, respectively, in North Europe. These measurements were carried out at the outdoor collector test facility at ZAE Bayern in Germany. Savo-Solar's goal was to carry out simulations optimizing the energy harvest by minimizing the heat loses, while keeping the transparency; their goal was also to build test collectors for testing in ZAE's test-rig in order to optimize the decrease of the thermal loses and to build the most effective high temperature flat-plate collector.

2.1.2 Pre-commercial design study: Biofuel-driven second-stage backup

The combination of an advanced single-stage absorption machine and a direct biomass-driven second-stage high temperature generator (HTG) promises a resource-conserving use of renewable biomass for heating and cooling purposes and ensures reliable energy supply at times of insufficient solar gain.

By implementing a biofuel-fired high temperature generator (HTG) alongside a single-stage absorption chiller, the absorption chiller system efficiency can be significantly increased from about 0.7 to 1.3. State-of-the-art gas-fired generators are based on conventional horizontal shell boiler designs. Yet, the large liquid solution inventory and the high volume of the generator vessel offer the opportunity for further improvement of the plant design.

A promising alternative is a high-temperature generator design based on a vertical boiling-tube arrangement, as used in large capacity power plants operating at high pressures. An earlier investigation by Kren [Kren, 2009] compared conventional shell-boilers to boiling-tube heat exchangers, pointing out that the boiling-tube design offers substantial advantages in terms of an increased heat transfer rate at given pressure drop in the flue gas flow passing the HTG. This kind of generator as shown in Figure 2.1 has been thermodynamically calculated, designed and evaluated by ZAE Bayern and successfully tested in several pilot installations. By applying biofuel, the current design of the heat exchanger and combustion chamber has to be revised in regard to particulate matter, the risk of condensation, extreme exhaust gas temperatures (hot spots) and pressure drop. Apart from the current vertical boiler-tube design, other concepts e.g. a pool-boiler concept with vertical flue gas tubes was been taken into consideration.

Therefore, a detailed analytical model (e.g. FEM-model) for the overall and local heat transfer coefficient, wall temperatures, and combustion efficiency was developed to ensure a proper design of the biomass-driven high-temperature generator. As a proof of concept, a functional model with 15 kW firing capacity was to be constructed and built. Subsequently, its operating characteristics was

demonstrated and scientifically analysed under test-rig conditions at ZAE Bayern with respect to fuel utilization, heat losses, and auxiliary power consumption. In addition to that, the following uncertainties and problems had to be investigated and solved:

- Metal Corrosion caused by the working fluid aqueous lithium bromide solution inside the HTG due to high local heat-exchanger-wall temperatures and by the ash content of the flue gas acting on the external heat exchanger surface.
- A particulate matter separator based on cyclone and electro-static technology for emissions reduction.
- Contamination of the heat exchanger surface and flow passages by combustion residues, sintering, and agglutination.
- Part load efficiency and variability: Quick and high load changes in the entire SHC-System demands enhanced variability of the biomass combustion down to 10% and at least 120% boost capacity in times of insufficient ambient heat sources.
- Reliable fuel feed (main error source in common pellet boilers) and long-term stability
- Auxiliary energy consumption for actuators, fans and ignition

2.1.3 Auxiliary energy consumption for actuators, fans and ignition

In a second step this HTG was connected to the single-effect absorption chiller/heat pump. The resulting multivariable double/single effect absorption machine driven by biofuel and/or solar heat ensures a reliable heating, cooling and hot water preparation throughout the year in a future decentralized low-carbon economy. Yet, the use of the natural refrigerant water R718 and the sub-atmospheric working pressure already avoid the emission of any climate damaging substances.

2.1.4 Component development: Compact absorption chiller, comprising a hydraulic rack

The absorption machines transform heat into cold by means of a sorption process between a refrigerant (e.g. Water) and a Sorbens (e.g. Lithium bromide) and can be used as chiller or heat pump. In contrast to conventional vapor compression chillers/heat pumps, the required electricity consumption is almost negligible. The design of this single-stage absorption chiller will be based on the ‘Phönix’ chiller developed earlier by ZAE Bayern. Following recent trends in solar cooling (e.g. IEA Solar Heating and Cooling Program, Tasks 25, Task 38, Task 48) the chiller design will be refined with regard to minimum auxiliary energy demand, compactness, optimized thermal sorption process parameters, elevated temperature levels for dry heat rejection and advanced part load control. Furthermore, the development focuses on optimized heat exchanger design and instrumentation for cost effectiveness and minimal maintenance effort, leading to

an affordable and reliable device. In addition, a simple connectivity for a reliable backup heat source (e.g. biomass boiler, district heating) and an efficient heat pump-mode was implemented.

As determined by the system concept, a high variability in the driving heat temperature level and a fast load change ability within minutes was required. Therefore, a component-oriented model based on a system of equations was set up to simulate the internal absorption process, characterized by equilibrium temperatures, salt concentrations, and specific flow rates in the main subsystems Evaporator, Absorber, Condenser, Generator and internal solution heat exchanger. Based on this theoretical model, the optimization of the following key values ensures an effective thermodynamic design of the chiller/heat pump.

- Minimisation of the specific solution flow from Absorber to the Generator, which is decisive for the required specific heat exchanger area, lithium bromide solution quantity, and its concentration change within the cycle, as well as the overall thermal coefficient of performance of the device.
- Minimisation of the entire heat exchanger surface area and optimized allocation to the main components concerning evaporator temperature and driving temperature differences.

Furthermore, advanced heat exchanger surface design and coatings had to be evaluated in regard to corrosion and fouling, which are primarily responsible for any long-term degeneration in capacity. An optimized flow channel and bundle design for refrigerant steam and aqueous lithium bromide solution were required to minimize internal pressure losses and maximize heat- and mass transfer of the absorption process. Moreover, a variable speed control of the solution pump was implemented for a significant improvement in the thermal COP in low part-load conditions. Thereby, the reliable wetting of the horizontal tube bundle and the solution distribution was revised according to ZAE patent EP 1 723 377 B1 in order to achieve complete utilization of the heat exchanger area in part-load conditions.

International research within the framework of the International Energy Agency's (IEA) Solar Heating and Cooling Programme, e.g. Task 38 and 48, has identified a high failure-proneness in the hydraulic connection of the main components of the solar collector field, storage, chiller, heat rejection and building distributor. So, a pre-fabricated hydraulic and adapted control system for all heat carrier loops were implemented in order to reduce the onsite engineering and installation effort to a minimum. This avoids critical onsite dimensioning and communication failures between different crafts and promises a significant cost reduction potential. Furthermore, a high hydraulic efficiency is granted.

Efficient heat rejection is crucial for the overall primary energy balance of sorption systems, as it dominates the auxiliary energy consumption. Most of the market available chillers are designed for cooling water supply/return temperatures less

than 31/36 °C. Thus a wet or hybrid cooling tower, with its well-known disadvantages concerning the risk of legionella, fogging and water consumption, was required. An appropriate heat exchanger bundle design and improved algorithms for automatized real-time crystallization protection, allow for an operation with increased reject heat temperatures from 37–45 °C for dry reject heat dissipation. Unfortunately, most market-available DDC control units are not powerful enough for complex control procedures. Thus a simplified algorithm has to be developed.

2.1.5 Solar heating and cooling system concept and demonstration

The system concept under investigation particularly fits the situation in Northern and Central Europe. During summertime, cooling is mainly done by converting solar heat from the optimized flat-plate collectors into useful cold by an advanced single-effect absorption process. At insufficient insolation, driving heat is provided by heat storage, highly efficient biofuel combustion or a district heating network. In wintertime the system operates as a thermally driven heat pump, using local biofuel, e.g. wood or straw pellets, to upgrade ambient heat to a useful temperature level. By replacing electricity and fossil fuels as the energy source for the chiller/heat pump, the sorption cooling and heating system operates with marginal primary energy consumption and CO_2 emission, even when only limited solar input is available. Furthermore, excessive stress to the electricity network to provide cooling or heating energy is avoided. In addition, the efficient heat conversion nearly doubles the biomass capability to cool and heat residential and industrial buildings or processes and extends the field of solar heating/cooling applications to regions without district heating or natural gas networks.

Commissioning of the solar heating and cooling system (SHC-system) comprises an improved solar thermal collector and an advanced highly variable absorption chiller/heat pump for holistic heating and cooling of buildings with a high solar fraction at the Savo-Solar office building in Mikkeli, Finland. The Savo-Solar office extension has an area of 195 m^2 and a volume of 1075 m^3. The high-grade pre-design and pre-assembly of the system promises low efforts and costs in planning and installation and ensures a reliable efficiency in seasonal operation.

The project will start by installing an array of an adequate number of Savo-Solar SF-100-03 standard collectors, which serve as a reference system for the same amount of optimized foil collectors. When the collector development delivers new improved foil collectors on the basis of SF-100-03, they were installed in parallel. This allowed the direct comparison of the solar field efficiency between standard and improved collector technology. Later on, ZAE Bayern and its industrial partner ECON provided the tested absorption chiller/heat pump, including the main hydraulic components in a pre-assemble rack for easy and quick onsite installation. Bought-in parts such as a sensible heat buffer and a dry air cooler completed the equipment for solar heating and cooling.

A detailed energetic analysis of the all-year operation of the system was carried out and a comparison with conventional systems was drawn by means of distinctive performance figures. The economics of the system was analysed regarding both the initial and current costs.

2.2 Research questions/objectives of the project

The following research questions have been identified and form the main objects of investigation.

a) Weather Forecast:
Are weather data freely available for a local prediction?
What is the precision of the irradiance and temperature weather forecasting?

b) Collector:
Would the foil implementation improve efficiency? (irradiance, temperature, angle, flow)?
Is the substitution of mineral wool economically achievable?
What is the endurance of the foil during seasonal operation conditions? (wrinkles, stagnation, etc.)

c) Biomass driven double-effect absorption chiller /heat pump:
Is the general system concept of a biomass driven absorption machine feasible?
What is the corrosion resistance of economically acceptable heat exchanger materials?
Are the part load efficiencies and variability sufficient for the heating and cooling system?
Are the fuel conversion ratios competitive?

d) Absorption Chiller / heat pump:
Can load changes be handled within a few minutes?
Is the installation compact and plug and play?
Is the system adaptive to part-load conditions?
Is there a high temperature lift and optimal use of driving exergy?

e) System:
What are the seasonal ratios of solar energy for cooling and heating?
Does district heating suffice to drive the system all year round?
Are High Electricity Efficiency Ratios feasible? EERC > 15?
Is the total thermal COPC in cooling greater than 0.7?

3. Focus of research, development and investigation

One of the tasks of the Finnish–German Joint Research Project 'Solar Heating and Cooling in Northern and Central Europe' was the development of a solar flat-plate collector with enhanced efficiency at 80 °C to 150 °C operating temperature in order to provide high temperature, driving heat to the absorption chiller. As this collector also serves as a low temperature ambient heat source for the absorption heat pump during wintertime, operating temperatures down to 4 °C might occur as well. There is therefore the risk of wetting of the back side insulation of the collector due to falling below the dew point of the ambient air. So, new concepts for improved back side insulation were investigated.

3.1 Foil collector investigation

The following section describes the work carried out at ZAE Bayern, Germany and at Savo-Solar Oy in Finland. This included full-scale prototyping, scientific test-rig measurements and onsite production-process handling checks.

3.1.1 Introduction to highly efficient flat-plate collectors

Regenerative heat can be provided by solar collectors in a clean way without greenhouse gas emissions. In most cases the collected heat from the solar irradiation is disposed to domestic hot water boilers or space heating systems. For these basic utilizations at typical working temperatures below 60 °C the efficiencies of standard flat-plate collectors are comparatively high (> 60% at 1000 W/m^2 solar irradiance). In addition, more advanced applications like solar cooling, which is one of the primary technologies in the present research project 'Solar Heating and Cooling in Northern and Central Europe', are also possible. Solar cooling is a technology where absorption chillers (= heat pumps) are driven by middle temperature heat from solar collectors. This process can therefore also be paraphrased as 'solar heat driven heat pumping'. For good system performance,

the absorption chillers need a driving heat at temperatures around 80 °C to 150 °C absolute or 60 K to 130 K ΔT over ambient temperature (summer case with a 20 °C ambient temperature). The collector efficiency at these elevated operating temperatures is usually rather low for standard collectors ($\eta \approx 60\%$ at 60 K ΔT, $\eta \approx 10\%$ at 130 K ΔT, both values at 1000 W/m^2 solar irradiance). To reduce the cost for the collector field and to reach economic operation of the solar cooling system as early as possible, the efficiencies of the relatively inexpensive standard flat-plate collectors were improved significantly in the target temperature range. In doing so it is crucial to maintain their good economy / low prices!

For a better understanding of the outlined relationships, Figure 3.1 shows the efficiency curves of three different types of solar thermal collectors over a temperature range from ambient temperature up to 200 K ΔT at 1000 W/m^2 solar irradiation (0.2 Km^2/W reduced temperature respectively). The target temperature range is marked by grey shading. The black line represents the efficiency curve of a Vaillant VFK 155, a state of the art flat-plate collector, whereas the green line displays the efficiency curve of a typical evacuated tube collector, the Viessmann Vitosol 300 T. The blue line finally depicts the predicted efficiency curve of an optimized flat-plate collector as it was developed in this project. The values for the efficiency curves of the commercial models VFK 155 and Vitosol 300 T are taken from the Solar Keymark database [Solar VFK 155, 2012], [Solar Vitasol 300 T, 2008]. Vacuum tube collectors like the Vitosol 300 T in general have very low heat losses due to their effective vacuum insulation. This results in the lowest slope of the efficiency curve of all three of the shown collector types. At the same time vacuum tube collectors intrinsically have a significantly lower conversion factor than flat-plate collectors (up to 10%-points lower). The conversion factor marks the zero-temperature-difference efficiency. The temperature difference is measured from the mean collector fluid to ambience. Usually the efficiency of solar collectors is calculated with the collector's aperture area as the reference area for solar irradiation input. Therefore, the lowered conversion efficiency of vacuum tube collectors is mostly due to their rather poor aperture- to absorber-area ratio.

In contrast, flat-plate collectors usually feature high conversion efficiencies of over 80%, but at the same time they have steeper slopes for their efficiency curves, as their insulation is not as perfect as that of vacuum tube collectors. An optimized flat-plate collector should, in respect of the efficiency curve, ideally be a hybrid between a standard flat-plate collector and a vacuum-tube collector. The result would be a collector with an efficiency curve similar to the blue one shown in Figure 3.1.

Here the conversion efficiency reaches almost the same high level as it does for standard flat-plate collectors but with a significantly improved thermal insulation, which leads to a more gently dipping slope in the efficiency curve. Thus, in the target temperature range, the efficiencies of such highly efficient flat-plate collectors should be up to 2 times higher than that of standard flat-plate collectors

and at the highest temperatures, they should still reach nearly two-thirds of the benchmarking vacuum tube collector efficiency values. The insulation improvement is mostly done by incorporating a second transparent front cover between the glass and the absorber.

The main objective of this work package within the project 'Solar Heating and Cooling in Northern and Central Europe' is the optimization of the existing commercial Savo-Solar SF100-03 flat-plate collector in order to develop a relatively low-priced but highly efficient collector suitable for applications with middle temperature demand, such as solar cooling with absorption chillers. In addition, the impractical mineral wool backside and side insulation would be changed for a less moisture sensitive and less dusty material if possible. All improvements to the collector were made without mayor alterations to the existing design and at low additional cost.

In the following chapters, first a thorough analysis of the existing commercial SF100-03 collector is done. Based on the results, the optimization potential is determined and the applied collector improvement techniques are described. Furthermore, all built prototype collectors, the correspondent collector test results and additional experiments are described and documented. Finally, the work is summarized and all necessary further steps are compiled with a view to developing a small-series model of a high performance flat-plate collector by Savo-Solar.

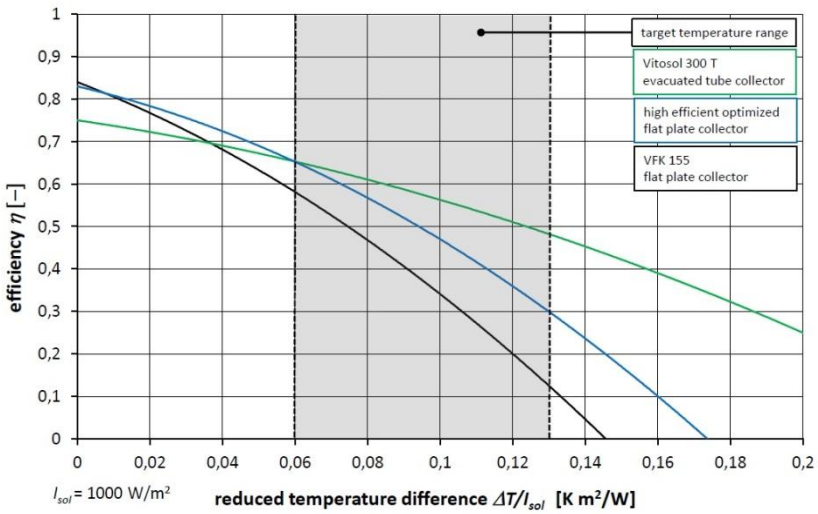

Figure 3.1. Efficiency curves of a typical flat-plate collector, the Vaillant VFK 155 (black line) [Solar VFK 155, 2012], a generic optimized highly efficient flat-plate collector (blue line) and a Viessmann Vitosol 300 T evacuated tube collector (green line) [Solar Vitasol 300T, 2008]. All curves are plotted for a solar irradiation of 1000 W·m^{-2}.

3.1.2 The Savo-Solar SF100-03 collector

The SF100-03 solar thermal collector is built by the Finnish company Savo-Solar in Mikkeli. Compared to typical flat-plate collectors like the Vaillant VFK 155 or the Viessmann Vitosol 300 F, the SF100-03 is distinguishable by its particular high conversion factor Figure 3.2 illustrates this feature by comparing the efficiency curves of the VFK 155 (black line), Vitosol 300 F (blue line) and the SF 100-03 (green line).

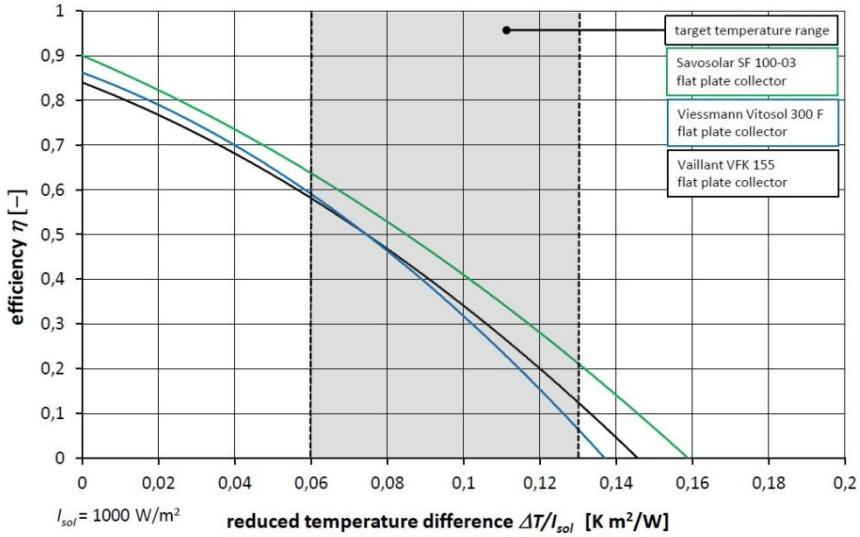

Figure 3.2. Efficiency curves of three commercial flat-plate solar collectors, the Savo-Solar SF 100-03 (green line), the Viessmann Vitosol 300 F (blue line) and the Vaillant VFK 155 (black line). All curves are plotted for a solar irradiation of 1000 W/m2. All values are extracted from up-to-date official test certificates from the Solar Keymark database [Solar SF100-03, 2012], [Solar VFK 155, 2012] and [Solar Vitasol 300F, 2014].

Just as in Figure 3.2 the target temperature range is highlighted by grey shading. It is clearly visible that the SF100-03 outperforms the VFK 155 and the Vitosol 300 F at all reduced temperature differences due to its high conversion factor of 90% paired with a good thermal insulation comparable to or slightly better than the ones used in the VFK 155 and Vitosol 300 F. In order to quantify the performance of the SF100-03, all relevant parameters of the three collectors from Figure 3.2 are gathered in Table 3.1.

Comparing the values from Table 3.2 it becomes clear that the Savo-Solar SF100-03 has a conversion factor of around 4 to 6%-points higher than the standard collectors VFK 155 and Vitosol 300 F. The total loss coefficients a_{100} at 100 Kelvin temperature difference do vary at a maximum of about 10% from the value of

4.9 $W \cdot m^{-2} \cdot K^{-1}$ of the SF 100-03. The corresponding efficiency η_{100} at a 100 Kelvin temperature difference for the SF 100-03 scores 41%, which is about 7%-points better than for the VFK 155 and even 9%-points better than the value of the Vitosol 300 F. The clearly higher-than-average efficiency of the Savo-Solar SF100-03 makes it an ideal starting point for the collector improvements.

At this point it has to be stated that the data from the Solar Keymark certificates used for Figure 3.2 and Table 3.1 are valid only up to a 70 Kelvin temperature difference. Therefore, the collector efficiency of the SF100-03 will be measured by the ZAE Bayern at up to a 110 Kelvin temperature difference or 0.11 $K \cdot m^{-2} \cdot W^{-1}$ reduced temperature differences respectively. The results of the high temperature efficiency test will be presented in the following section.

Table 3.1. Collector efficiency parameters of the Savo-Solar SF100-03, Vaillant VFK 155, Viessmann Vitosol 300 F. All data from Solar Keymark certificates [Solar SF100-03, 2012], [Solar VFK 155, 2012] and [Solar Vitasol 300F, 2014].

Measure-ment **Type**	η_0 - Conversion factor	a_1 $W \cdot m^{-2} \cdot K^{-1}$ Loss coefficient Linear	a_2 $W \cdot m^{-2} \cdot K^{-2}$ Loss coefficient Quadratic	a_{100} $W \cdot m^{-2} \cdot K^{-1}$ Total loss coefficient at 100 K ΔT	η_{100} - Efficiency at 100 K ΔT
SF100-03	0.90	3.60	0,013	4,9	0.41
VFK 155	0.84	3.29	0.017	5.0	0.34
Vitosol 300 F	0.86	3.14	0.023	5.4	0.32

a) Efficiency Measurements at Elevated Temperatures

As remarked previously, all the official Solar Keymark certification measurements, e.g. [Solar SF100-03, 2012], are limited to the rather low maximum temperature difference of a 70 Kelvin temperature difference according to the DIN-Standard [Deutsches Institut für Normung (DIN), 2006]. Strictly speaking, the extrapolation of efficiency curves to higher temperatures than the maximum temperature the collector was measured at is out of bounds. Nevertheless, to a certain extent (some 10 K to 20 K) such an extrapolation is possible, but one should be aware of the quickly rising degree of uncertainty the higher is the distance to the last measured point. In order to reveal the behaviour of the efficiency curve at elevated temperatures, a normal series production SF100-03 was measured at the ZAE Bayern test-rig during June 2014. This test was done on the basis of the European norm DIN EN 12975. Figure 3.3 depicts the result in comparison to the Solar Keymark certificate values.

The blue line depicts the Solar Keymark efficiency curve, the black line the ZAE Bayern measured curve. Inspecting the plot one can observe that there is only a slight offset between the two curves; the slopes and therefore also the loss coefficients are comparable to each other. The conversion efficiency difference can be read directly from Figure 3.3 and amounts to only 1.7%-points.

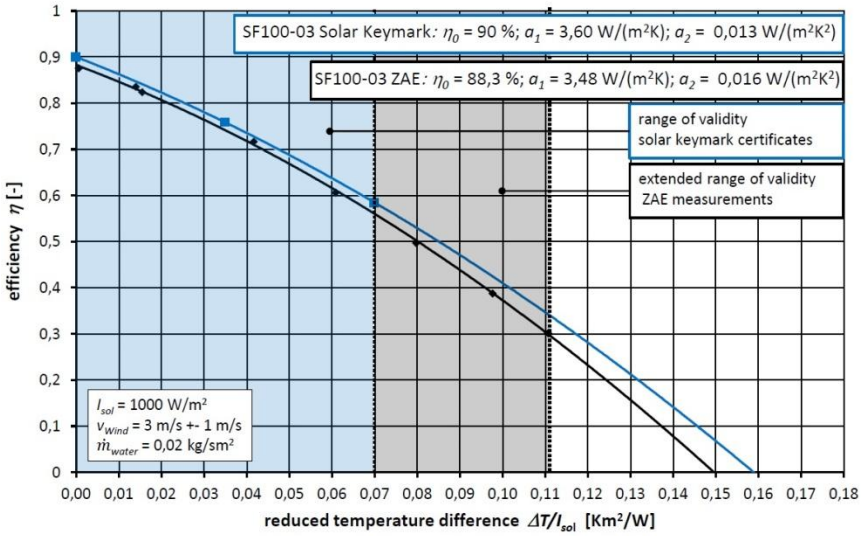

Figure 3.3. Comparison of efficiency curves obtained from ZAE measurements and Solar Keymark certificate values of the series production Savo-Solar SF100-03 collector. Grey shading highlights the extended range of validity of ZAE measurements.

Table 3.2 gives an overview of the collector efficiency (defined, [Henning H-S., Motta M., 2013]) parameters η_0, a_1 and a_2 plus the derived values of a_{100} and η_{100} and their relative and absolute differences, which make it easier to value the precision of the ZAE Bayern measurement in contrast to the Solar Keymark data. The combined or total loss coefficient a_{100} at a 100 Kelvin temperature difference is 0.2 $W \cdot m^{-2} \cdot K^{-1}$ higher for the ZAE Bayern measurement. In relation to the absolute mean value of a_{100} = 5.0 $W \cdot m^{-2} \cdot K^{-1}$ of both sets of values, this results in a difference of just 4%. Also the η_{100} values show only little deviation of -3%-points absolute or -7.6% relative. Thus, the results confirm the fully satisfactory precision of the ZAE Bayern test-rig used for the prototype collector testing in this project.

According to a previous analysis, the overall accuracy of the test-rig is usually smaller than +-3%. Nevertheless, during all the performed tests the series SF100-03 was always measured in parallel to the prototypes in order to have a certain well-known standard to rely on. Even with reasonable diligence while performing the outdoor tests, ambient conditions are still somewhat uncontrollable. Small

offsets, as observed in this reference experiment, occur frequently. To minimize the impact of these fluctuations on the absolute efficiency values, the experimentally determined relative differences to the reference collector are used as the decisive quantities and directly show the effect of certain changes to the collector design.

Table 3.2. Collector efficiency parameters for the Savo-Solar SF100-03, the Solar Keymark versus ZAE Bayern test-rig measurements.

Measurement / **Type**	η_0 - Conversion factor	a_1 $W \cdot m^{-2} \cdot K^{-1}$ Loss coefficient Linear	a_2 $W \cdot m^{-2} \cdot K^{-2}$ Loss coefficient Quadratic	a_{100} $W \cdot m^{-2} \cdot K^{-1}$ Total loss coefficient at 100 K ΔT	η_{100} - Efficiency at 100 K ΔT
Solar Keymark	0.90	3.60	0.013	4.9	0.41
ZAE	0.88	3.48	0.016	5.1	0.38
Absolute Differences	-0.017	-0.12	+0.003	+0.2	-0.03
Relative Differences	-1.9%	-3.4%	+20.7%	+4.0%	-7.6%

In this context it should be mentioned that the comparability of collector test results is rather limited. Strictly speaking, all measurements performed by the ZAE Bayern should only be compared among themselves and not directly with Solar Keymark certificate data (offsets are very likely).

b) Highly efficient Direct Flow Absorber

The reason why the conversion factor of the SF100-03 collector reaches the high value of 90% according to its Solar Keymark certificate is mainly the incorporation of a novel full area direct flow absorber. In the following section the mechanism behind the conversion factor improvement is described briefly. The conversion factor η_0 of a solar thermal collector is influenced by three parameters according to the following equation (1):

$$\eta_0 = F' (\alpha \cdot \tau) \qquad (1)$$

Here α denotes the absorbers surface absorptivity coefficient and τ the transmission coefficient of the front glass. Both coefficients are evaluated for the solar radiation spectrum. The expression $(\alpha \cdot \tau)$ in brackets is the so-called effective transmission-absorption product which includes also the part of the solar radiation that is finally absorbed after multiple reflections between glass and absorber. This share $(\alpha \cdot \tau)$ of the incoming radiation is converted to heat at the absorber surface. Therefore, the product $(\alpha \cdot \tau)$ could also be called the collector's true optical

efficiency. However, the conversion factor η_0, also sometimes referred to as the 'optical efficiency', is per definition the collectors efficiency measured at a zero temperature difference between the mean fluid temperature of the collector and ambient temperature. Thus, to determine η_0 correctly, one needs to account for the small but existing temperature difference between the hot absorber surface and the slightly cooler fluid. This is done by introducing F´. Vice versa, if the mean absorber surface temperature was known, one could also use the true optical efficiency ($\alpha \cdot \tau$) as the conversion factor. In this case, the relevant temperature difference would be calculated between the absorber surface and ambience. This is not done though, since it is a lot easier to determine the collector's fluid mean temperature by inlet and outlet temperature measurement and subsequent averaging than evaluating the entire surface temperature of the absorber.

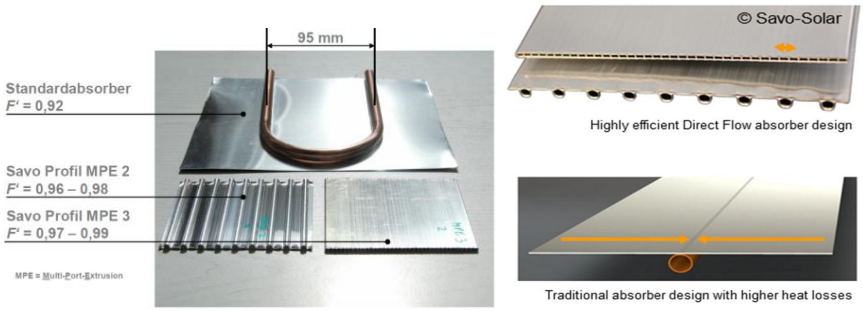

Figure 3.4. Photograph of standard absorber piping configuration in contrast to two highly efficient absorber profiles type MPE 2 and MPE 3 from the Savo-Solar.

For practical considerations one can rely on the rule of thumb that F´ gets close to 1 if the heat transfer from the absorber surface to the fluid is nearly perfect. In order to improve the conversion factor η_0 the decisive factors F´ and ($\alpha \cdot \tau$) have to be maximized. The transmission-absorption product ($\alpha \cdot \tau$) effectively cannot be enhanced further as the optical properties of modern absorber surfaces and solar glasses are already optimized with regard to an industrial applicability of the measures. The state-of-the-art value for α is 95% and 96% for ($\alpha \cdot \tau$) respectively. In contrast the F´ of standard absorbers used in typical flat-plate collectors like the VFK 155 reach only values of around 0.92. This gives a potential of almost 8%-points of improvement in the conversion factor. Providing that the thermal coupling of the absorber sheet to the piping is sufficient, the piping distance is the key factor that controls F´ according to [Duffie, J.A., 2006]. Figure 3.4 depicts three different absorber configurations, a standard absorber design and two advanced Savo-Solar absorber profiles. Here it is clearly visible that the absorber piping distances of the standard absorber (≈ 95 mm) are reasonably greater than they are at the Savo-Solar absorber profiles (< 10 mm).

The Savo-Solar full area direct flow absorber is assembled out of the depicted aluminium extrusion profiles type MPE 2 and MPE 3 (MPE = Multi Port Extrusion) which show only slightly different F´ values. Several ZAE Bayern collector

measurements suggest the assumption of 0.97 for the MPE 2 profile and 0.98 for the MPE 3 on average. It has to be noted that measuring F´ is only possible by back-calculating it from the determined η_0 value by assuming that the specified values for α and τ from the technical data sheet are true. The MPE 2 profile absorber is currently in use in the Solar-Keymark certified SF100-03 collector. To check if different fluid flow rates have an influence on F´ under typical operating conditions a special test was conducted with one of the prototype collectors using the MPE 2 absorber. Figure 3.5 shows the results of the conducted experiments. Additionally, for the full efficiency curve measurement of the prototype SF100-03 with double FEP front foil insulation (black line), which was carried out similarly to the Solar Keymark standard, two measurement points are taken with the same system at two different flow rates per square meter of collector aperture area, 105 $L \cdot h^{-1} \cdot m^{-2}$ (high flow) and 60 $L \cdot h^{-1} \cdot m^{-2}$ (low flow). The additional points are plotted above in the same diagram together with the full efficiency curve of the prototype taken at a flow rate of 70 $L \cdot h^{-1} \cdot m^{-2}$. One can see that both of the additional two points show higher efficiencies than the black prototype efficiency curve. Furthermore, there is no significant difference between the high flow and the low flow point. These findings are at first sight contradict the expectation that efficiency should be greater with higher flow rates. The general problem of this measurement method is that the expected differences in collector efficiency with a variable flow rate are of similar magnitude as the typical measurement error of ± 3%. Thus the flow rate effect on the efficiency should be negligible for practical values between 50 $L \cdot h^{-1} \cdot m^{-2}$ and 100 $L \cdot h^{-1} \cdot m^{-2}$. To evaluate the variation in efficiency for different flow rates, another approach could be tested: The entire efficiency curve (0 to 100 K over ambient temperature) for the collector can be measured for three different flow rates under as steady as possible ambient conditions. In this case, the difference should be more visible, since deviations in efficiency for single measurement points are smoothed out due to an averaging effect of the polynomial curve-fitting process. Nevertheless, the results are expected to be more for academic interest than being practically relevant. Concluding this section, it can be recorded that the novel full area direct flow absorber design of the Savo-Solar SF100-03 enables it to have a high conversion factor of 88% to 90%. Moreover, the extra 5% to 6%-points in the conversion factor compared to standard collectors like the Vaillant VFK 155 are practically independent of the flow rate under typical working conditions.

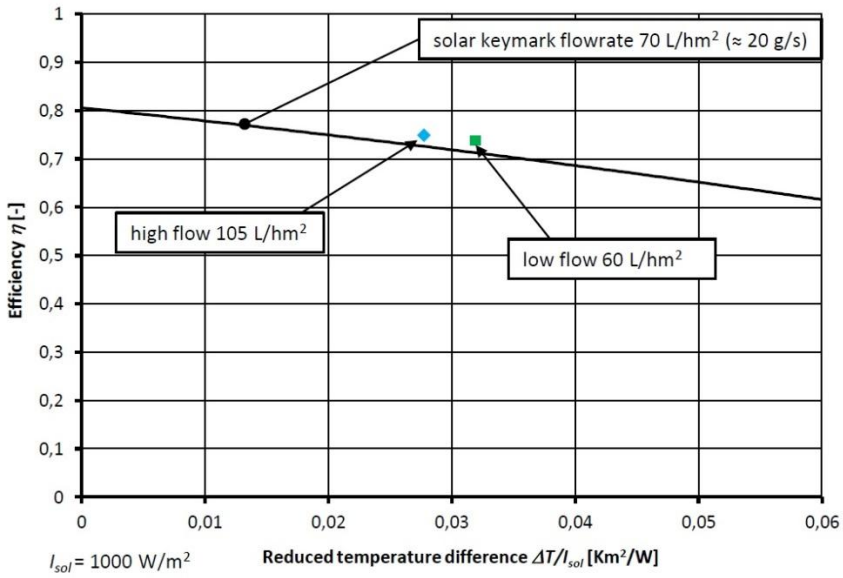

Figure 3.5. Experiment to determine the efficiency change of the SF100-03 with different flow rates.

3.1.3 Optimisation potential

Picking up the main objective of this project, the optimization of the Savo-Solar SF100-03 collector in order to obtain a highly efficient collector for elevated temperatures of 80 °C to 150 °C, in this section the practical optimization potential shall be determined. The best way to start this analysis is by looking at the actual loss structure of a typical single-front glass flat-plate collector, which is pictured in Figure 3.6. Here the blue rectangular area represents the 'optical losses'. In the SF100-03 these are already reduced compared to other standard solar collectors like the Vaillant VFK 155. Compendiously, this reduction is done by incorporating a highly efficient direct flow absorber. The thermal losses can be split into front-side losses, side and backside losses. In typical flat-plate collectors, the backside and side losses cannot easily be reduced further as they are already at a relatively low level due to the widely-used opaque insulation materials (mineral wool, PU-foams, etc.) at these faces. It is clearly visible in Figure 3.6 that around two-thirds of the total thermal losses occur at the front side. Hence for an effective collector, improvement the front-side losses have foremost to be reduced.

In order to diminish the collector's front-side losses, several measures can be applied. The most common ones are incorporating multiple front covers [Giovanetti, 2013], the use of transparent heat insulation materials [Giovanetti, 2011] or heavy gas filling (argon, krypton, SF_6 etc.) of the sealed gap between

absorber and front glass [Savo-Solar, 2014]. The two latter solutions, transparent heat insulation materials and heavy gas filling, usually show good initial performance results, but at the same time some severe problems are associated with the use of these measures. Collectors with transparent heat insulation materials are to this day not inherently stagnation proof [Giovanetti, 2011] and heavy gas filling is generally susceptible to performance degradation due to permeation of the enclosed gases through the sealant.

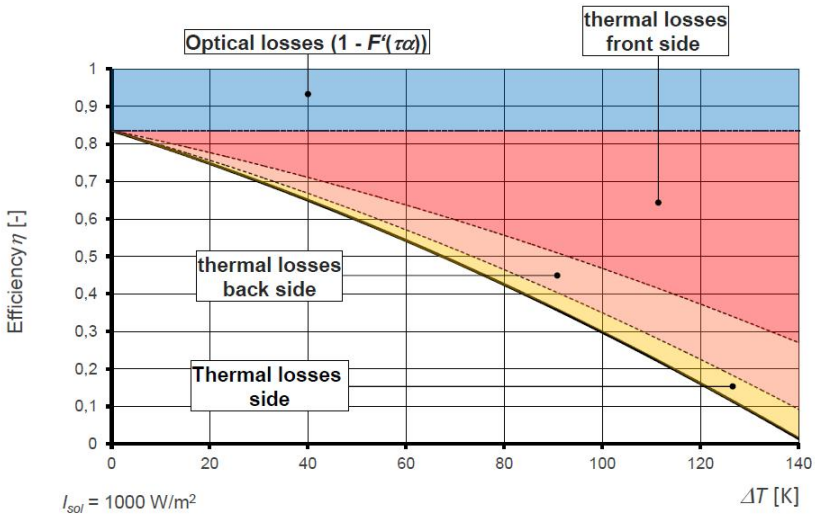

Figure 3.6. Loss structure of a typical flat plate solar collector visualized directly in the efficiency plot.

The most reasonable and preferred loss reduction method of the three previously mentioned is the use of multiple covers at the collector front. In a precursor-project at ZAE Bayern [Beikircher, 2010] it was shown that thin strained fluoropolymer films are well suited as a second cover under the front glass. The 25 µm to 50 µm foils made from ETFE or FEP are stagnation proof, show very good solar transmission values of 94% (ETFE) to 96% (FEP), are lightweight (<50 g·m^{-2}) and relatively cheap (3 to 7 €·m^{-2}). As the materials are fluorinated plastics, their durability is outstanding [Beikircher, 2010]. Even UV degradation is very low as they are protected behind the front glass and in addition are virtually transparent to UV radiation (very low absorbed dose) [DuPont, 1999].

The main challenge in using foils as collector covers is the mounting in the gap between absorber and front glass without sagging or build-up of wrinkles during operation. Nevertheless, the foil insulation concept will also be applied in this project to improve the collector's efficiency. Based on [Beikircher, 2010] the optimization potential when integrating a front-side foil insulation in the SF100-03 collector is illustrated in Figure 3.7.

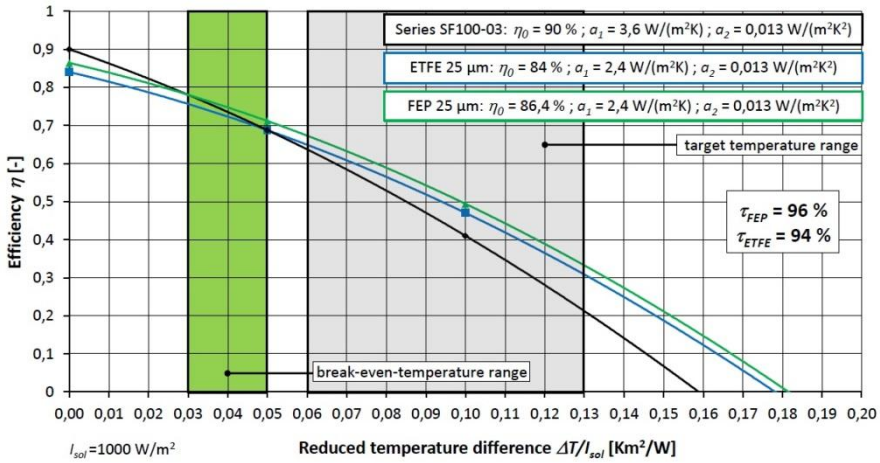

Figure 3.7. Optimization potential for a front-side foil insulation in the Savo-Solar SF100-03 collector.

Here the black line depicts the plain SF100-03 collector efficiency curve (Solar Keymark certificate values). The blue and green lines show the predicted efficiency curves for the same collector with a 25 µm ETFE (blue) or 25 µm FEP (green) foil insulation between the absorber and front glass. For the potential calculation, the results from [Beikircher, 2010] are used: It was experimentally determined that foil insulations typically reduce the linear loss coefficient a_1 by 1.2 $W \cdot m^{-2} \cdot K^{-1}$. At the same time the foil reduces the conversion factor by 3.5% to 6%-points due to the transmission reduction. At last the specific combination of transmission- and thermal loss reduction yields a typical break-even-temperature range of foil insulation between a 30 to 50 Kelvin temperature difference at 1000 $W \cdot m^{-2}$, depending on the fluoropolymer used. Again the target temperature range in Figure 3.7 is marked by grey shading. At the end of the target range (130 Kelvin temperature difference) the estimated absolute improvement reaches about 12%-points for FEP and 10%-points for ETFE respectively, which corresponds to a relative improvement of nearly 60%.

Table 3.3 gives an overview of all relevant parameters of the three depicted curves from Figure 3.7. Compared to the front side the backside and side insulation cannot easily be improved further, as stated in the introduction. The reason is the high quality mineral wool that is currently in use in the SF100-03, which exhibits comparatively low heat conductivity.

Table 3.3. Predicted collector efficiency parameters for front-side foil insulated series SF100-03 with different foil materials

Measurement Type	η_0 - Conversion factor	a_1 $W \cdot m^{-2} \cdot K^{-1}$ Loss coefficient Linear	a_2 $W \cdot m^{-2} \cdot K^{-2}$ Loss coefficient Quadratic	a_{100} $W \cdot m^{-2} \cdot K^{-1}$ Total loss coefficient at 100 K ΔT	η_{100} - Efficiency at 100 K ΔT
SF100-03	0.90	3.60	0.013	4.9	0.41
25 µm ETFE	0.84	2.40	0.013	3.7	0.47
25 µm FEP	0.86	2.40	0.013	3.7	0.49

In Figure 3.8 the insulation value or heat transition coefficient of several insulation materials including the mineral wool type Isover GW Solar 3.5 N are shown for a mean temperature of 60 °C. It becomes clear that for reducing the backside thermal losses of the SF100-03 (1-D calculated to be just 0.74 $W \cdot m^{-2} \cdot K^{-1}$) while keeping the insulation thickness of 50 mm the only way would be to change the mineral wool type GW Solar 3.5 N from Isover to a material with even lower heat conductivity, e.g. polyisocyanurate (PIR) foam.

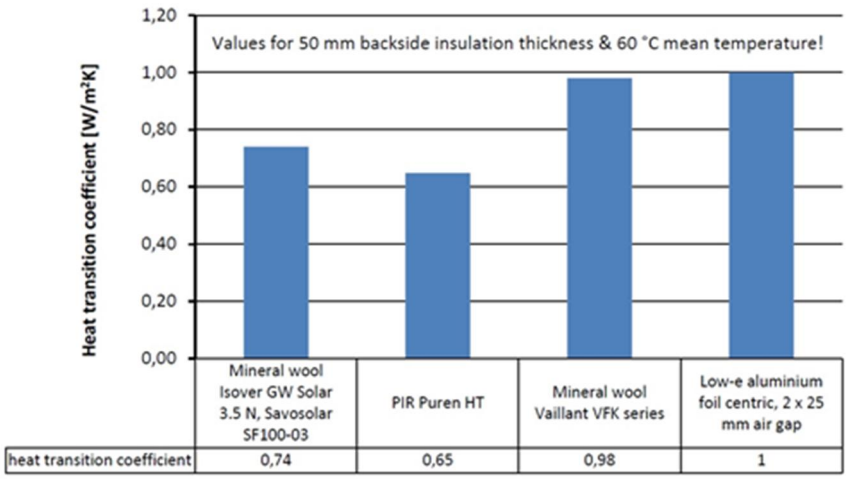

Figure 3.8. Comparison of heat transition coefficients for different insulation materials at constant thickness of 50 mm and 60 °C mean temperature.

This is not recommendable since the PIR foam loses its good insulation properties at persistent high temperature operation due to outgassing of the heavy gas filling from its pores. In addition, the temperature resistance of PIR is only specified up to 200 °C, which could feasibly be reached by a highly efficient flat-plate collector during summer stagnation. In contrast, mineral wool is typically specified up to

250 °C. The concept of a single backside low-e aluminium foil insulation [Beikircher, 2010] is water proof and lightweight, but it cannot reduce the backside thermal losses, as its heat transition coefficient is about 0.25 $W \cdot m^{-2} \cdot K^{-1}$ higher than the Isover mineral wool's coefficient.

Hence, the focus in the backside insulation upgrade is more on a substitution of the mineral wool, which is disadvantageous in terms of moisture sensitivity and moisture storing capacity, and because of its cumbersome handling properties. Thus, two novel moisture proof concepts are developed and tested for their performance:

a) Low-e foil cladded PU-foam plus air gap hybrid insulation and
b) Sheet metal heat shield with double air gap insulation supported by a wooden framework.

In the following, all the relevant technical details of the developed front-side foil insulation and the two new backside insulation concepts for the Savo-Solar SF100-03 collector are described and documented.

3.1.4 Implementation of front-side foil insulation

Front-side loss reduction is crucial for the development of highly efficient flat-plate collectors on the basis of standard collectors. As was previously described, the selected method in this project to realize the front-side loss reduction is the use of a thin-strained fluoropolymer foil in the space between the glass and absorber. This method was thoroughly researched and tested in a project at ZAE Bayern. For further information on the theoretical background of foil insulations, the final report [Beikircher, 2010] represents the key source.

The loss reduction of foil insulations works by effective convection suppression in the gap between the absorber and glass. Roughly described, the mechanism works as follows: The thermos fluid dynamic regime is changed in a beneficial way (= lowered heat transfer) by dividing the gap into two halves. In the optimum case the distances between absorber to foil and foil to glass are exactly sized to a dimension where free convection just does not start to propagate in the two resulting gaps at working temperatures. Each gap now features the same or an even lower heat transfer coefficient as the single one before without foil. Thus, the thermal resistance of each gap now has the same value as the resistance of the single gap before. That means that the overall heat transfer coefficient from absorber to front glass over the two gaps is now approximately halved compared to the case without foil (effect analogy to total resistance of a serial connection of two resistors that each have the same resistance as a single one before).

Figure 3.9 from [Beikircher, 2010] illustrates the changes in the front-side heat transfer coefficient between two parallel 45° inclined surfaces with variable gap

width at different driving temperature differences. The lower surface represents the hot absorber, the cooler upper surface the front glass. The mean temperature of the setup is 50 °C. Below the convection limit, marked by labelling 'start of convection' the heat transfer coefficient behaves inversely proportional to the plate distance.

Directly at the convection limit the lowest heat transfer coefficient is reached. With growing distance, the coefficient increases once again but finally levels out/falls slightly at gap widths greater than approximately 3 cm. For different temperature levels, driving temperature differences and inclinations, the plot will always vary (indicated by the dotted curve for 30° and 40 K difference), but the qualitative behaviour will be the same as at first approximation.

Using foil insulation finally results in a reduction of the linear loss coefficient a_1 of around 1.2 $W \cdot m^{-2} \cdot K^{-1}$. In order to reach this decrease, minimum distances of 10 mm between glass and foil / foil and absorber must be applied according to [Beikircher, 2010]. Nevertheless, a certain security margin should be added to account for slight sagging of the foil or the glass. Therefore 12 mm to 15 mm distances should be reasonable for practical applications. The special requirements in this project concerning the front-side foil insulation were primarily making as little modifications to the existing collector design as possible and secondarily adding only little extra height to the collector.

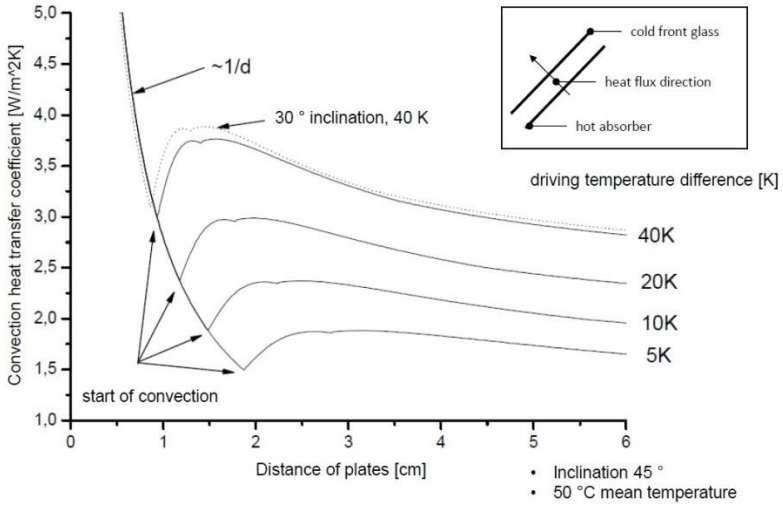

Figure 3.9. Convection heat transfer coefficient between two parallel plates at 45° inclination, 50 °C mean temperature, varying driving temperature differences and plate distances [Beikircher, 2010].

Hence, the design of the foil-mounting concept was the main task during the front-foil insulation development for the Savo-Solar SF100-03 collector. Finally, a novel design differing highly from the basic proposals shown in [Beikircher, 2010] was elaborated that could meet both demands at once. Usually the foil integration is done by straining the foil on the collector's base frame and fixing it with a clamping bar. The novel concept of this project features a two-step foil mounting procedure: The foil is strained in a so-called second frame first which is subsequently connected to the basis SF100-03 frame. With this procedure the handling of the strained foil is similar to inserting the collector's front glass. Furthermore, the production process for the collector is nearly the same till the step when the glass is usually glued in. Besides these, manufacturing aspects the second frame design gives the opportunity to lower the position of the foil inside the base frame of the SF100-03. This would not be possible with a foil mounting at the level of the front glass.

Figure 3.10 (1) depicts a section of the SF100-03 collector frame with the assembled foil-mounting demonstrator (2). The second frame of the demonstrator is represented here by a simple L-bar. It is used together with a PU-foam coated clamping bar to hold the foil in position. The PU-foam coating is essential to enhance the friction between metal/plastic and foil in order to prevent any creeping or relaxation of the foil tension during service. A more advanced design of the second frame is shown in Figure 3.10 (3). Here the clamping bar is made from a plastic extrusion part which fits exactly in the base frame. Moreover, the second frame is in this case purpose-shaped so that the front glass can be fixed in the same way as it is done for the normal SF100-03 collector. Even the original plastic corner pieces that are injection moulded can still be used with this design. The additional height adds up to just 9 mm. To take up the forces and stabilize the second frame during foil straining, a support and handling frame made from item aluminium profiles is placed in the middle. It is connected to the second frame via 10 small adjustable stands that are equally distributed at the circumference.

In the following step the foil is placed on top of the second frame and prepared for straining, which is done by simple weights. The weights are connected to the foil by tightly screwed aluminium L-bars. Again PU-foam is used to enhance the friction between the bars and the foil to obtain a good connection and in the end an even distribution of the tension. In order to prevent sagging and formation of wrinkles up to a certain temperature, the foil needs to be strained with an appropriate tension. Due to the special behaviour of each foil-material, the optimum tension values have to be determined experimentally. For the 25 µm ETFE foil from Nowofol, values for a wrinkle-free operation up to 120 °C mean collector fluid temperature were identified during a previous project. According to these values the foil was strained with slightly higher values of 16 MPa in the foil extrusion direction (short side) and 8 MPa normal to the foil extrusion direction (long side).

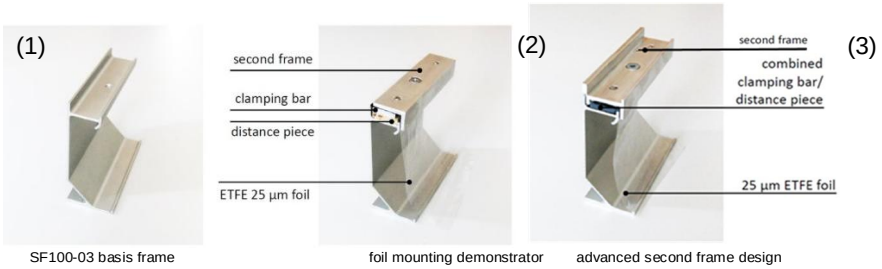

Figure 3.10. Collector frame (1) with foil mounting demonstrator (2) and advanced second frame design (3).

Figure 3.11 illustrates the straining process and the direction of the different applied tensions. The difference of the tensions depending on the extrusion direction comes from the phenomenon that the extruded foils exhibit a rather strong thermal shrinkage/anti-shrinkage. In the extrusion direction the foil elongates the first time it is heated up to a certain temperature. The higher the temperature, the higher is this anti-shrinkage effect. Normal to the extrusion direction, the effect is contrary: The foil shrinks when heating up for the first time. Thus the tensions have to be higher on the short side and lower on the long sides as the anti-shrinkage of the foil will take up a part of the initial tension, whereas on the long sides it will increase the initial tension value obtained by the straining process.

When the straining is completed the foil is clamped to the second frame by the PU-foam coated clamping bars which are connected to the frame by screws, see Figure 3.12. Here also the auxiliary corner connector plates are visible that hold together all four parts of the second frame till it is finally connected to the base frame. On the middle photograph the support and handling frame is still in position whereas on the right it is removed whilst the auxiliary corner connector plates are still attached. Now the full tension is held solely by the collector frame. On top of the second frame, the front glass is mounted by a combination of PU-foam sealing and tape fixation.

Figure 3.11. ETFE foil on second frame ready for straining (1) and after (2).

All prototypes with front foil insulation from this project use the same foil-mounting method based on the second frame concept. The performance of the developed foil-mounting during service will be described in the section regarding the test results of the prototypes.

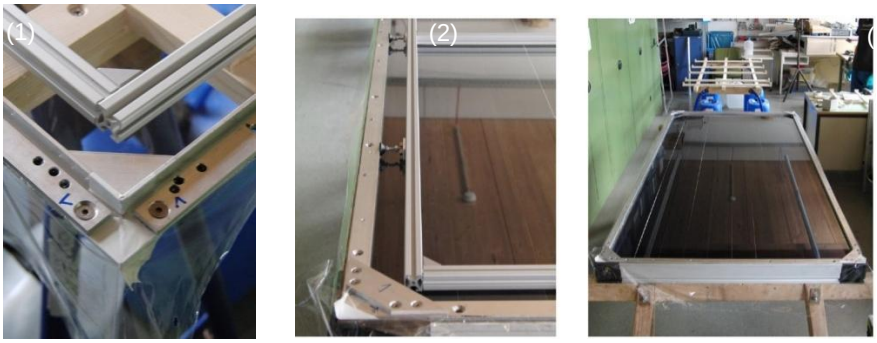

Figure 3.12. Strained foil clamped to the second frame by screwed clamping bars (1). SF100-03 collector base frame connected with second frame including the strained foil (2). Foil collector assembly (3).

3.1.5 Novel back side insulation concepts

As mentioned earlier, the backside insulation improvement in this project is focused on the development of moisture insensitive material that exhibits comparable performance as the current mineral wool insulation. Moisture is a serious problem as it can accumulate in solar collectors due to day-night cycles with temperatures falling below the dew point at some spots in the collector's body. Hence, anaesthetic condensation at the front glass can occur, with a more severe consequence being a significant increase in the mineral wools thermal conductivity compared to dry values. Thus, it is very important to use materials that are not susceptible to moisture penetration and if possible the amount of porous media in the collector should be reduced in general. The two concepts developed during this project are described and documented in the following.

a) Ow-e foil cladded PU-foam plus air gap hybrid insulation

As shown in Figure 3.13, high temperature resistant PU-foams (Polyisocyanurat = PIR) exhibit around 10% lower heat conductivities than typical mineral wool insulation. Moreover, they are less susceptible to moisture penetration and accumulation and show better handling, with less formation of dust. In contrast the main problem with these materials is still their limited resistance against the highest temperatures above 200 °C, which are very likely to be reached by highly efficient flat-plate collectors during summer stagnation. Even at more moderate temperatures between 100 °C and 200 °C, a degradation of the material is

probable due to outgassing of the heavy gas filling from the pores of the foam and the related increase in the heat conductivity. To avoid this complex of problems while still benefitting from the good insulation values, a hybridization with an air gap insulation seems to be favourable.

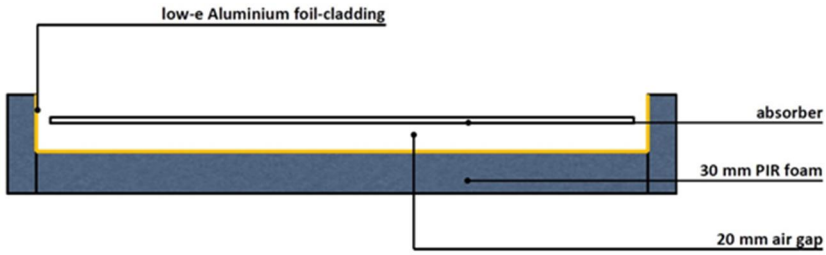

Figure 3.13. Graphical representation of hybrid PIR-foam & air gap insulation.

Figure 3.13 depicts a graphical representation of the hybrid backside insulation setup. It consists of 30 mm low-e foil cladded PIR foam at the backside, followed by a 20 mm air gap towards the absorber. The setup has two advantages:

1. Due to the insulating air gap between the absorber and back side insulation the maximum temperatures at the PIR-foam are effectively reduced.
2. The amount of porous material that is primarily responsible for moisture storage issues in collectors is almost halved.

Furthermore, the low-e aluminium foil cladding helps to further reduce the radiative heat transfer from the absorber to the foam. As a first approximation the overall heat transition coefficient for this setup should be around 0.8 $W \cdot m^{-2} \cdot K^{-1}$ at 60 °C mean insulation temperature, which is quite similar to the value of 0.74 $W \cdot m^{-2} \cdot K^{-1}$ for the currently used Isover GW Solar 3.5 N mineral wool. A major drawback of this hybrid insulation is the lacking mechanical support for the absorber. This problem can be solved by either using a stripe of insulation material that bridges the gap in the middle of the collector or by using a supporting bar. The latter option would also help stabilizing the frame in respect to the relatively high forces that have to be taken up due to the strained foil from the front-side insulation.

b) Sheet metal heat shield with double air gap insulation supported by framework

Further developing the principle idea of the PIR-foam & air gap hybrid insulation, one arrives at a double air gap insulation with two chambers separated by a thin low-e surface barrier, e.g. aluminium foil or thin sheet metal.

With this setup there is no need for any porous insulation medium at the collector's backside. Thus, the moisture storing capacity is minimized and the insulation inherently cannot be degraded by humidity accumulation. However, the heat

transition value of such a backside foil insulation system (1.0 $W \cdot m^{-2} \cdot K^{-1}$ at 50 mm with 60 °C) should be about 35% higher compared to state-of-the-art mineral wool insulation like the Isover GW Solar 3.5 N (0.74 $W \cdot m^{-2} \cdot K^{-1}$ at 50 mm with 60 °C). Another issue arising with this concept is not only the question of how to mechanically support the absorber but also how to support the foil or sheet metal without creating substantial heat bridges that would reduce the insulation effect. In this project a new concept is tested. A 0.4 mm thin aluminium sheet is placed on a pine-wood framework made from 5 mm thick strips. The framework is lattice-window formed and consists of a cross in the middle of the collector and a complete frame at the circumference. For better understanding, Figure 3.14 depicts a cross-section of the setup.

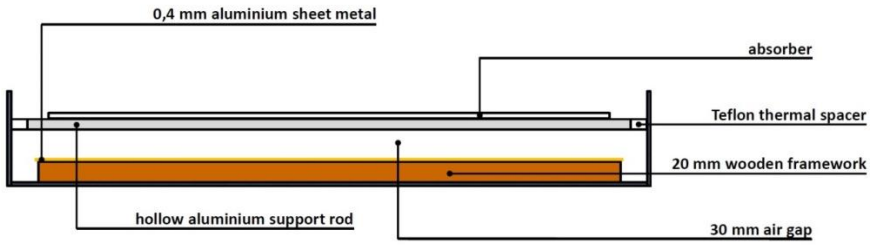

Figure 3.14. Graphical representation of 0.4 mm aluminium sheet metal on wooden framework insulation.

The necessary absorber support is done by mounting a squared hollow aluminium rod to the sides of the collector frame. In order to reduce the thermal bridge unavoidably created by the rod, thermal spacers made from Teflon are used at the sides. Due to the rigid design, the rod can be used to effectively strut the forces that are put on the collector frame by the strained front foil. The real installation inside a prototype collector is shown in Figure 3.15.

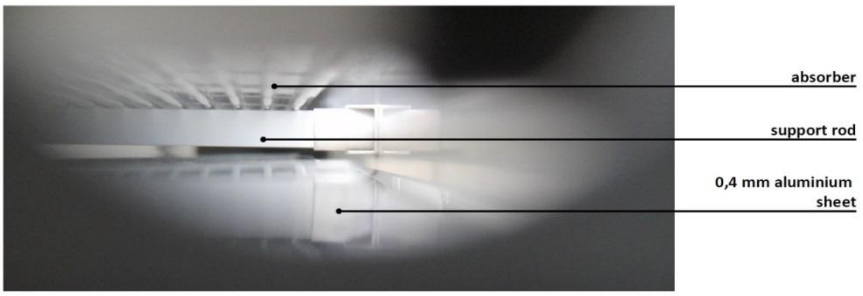

Figure 3.15. Photograph of the realized 0.4 mm aluminium sheet metal insulation.

Here in contrast to the series collector, no side insulation is used at all. Thus, the design is absolutely free of any porous and moisture sensitive insulation material.

The prototype results regarding this new backside insulation setup are documented in the following section.

3.1.6 Prototype collectors and test results

This chapter represents a collection of all test results achieved with the different collector prototypes. In total five collectors were built, four of them were real-sized and one was quarter-sized for foil tension tests. A short description for each collector is followed by the particular test results and further derived findings.

Prototype 0: One-Fourth Scale Model Collector Foil Tension Tests

To check the feasibility and to find reasonable values for the right straining tension, the newly developed foil-mounting concept was tested with a quarter-sized model collector. The smaller aperture area of 1 m x 0.5 m allowed for a fast and easy test of the different concepts. In order to achieve the highest possible portability of the results, the model collector was built from the same components as the SF100-03 series type, including the same backside and side insulation. Figure 3.16 shows a photograph of the assembled system with already strained 25 µm ETFE foil.

Figure 3.16. Prototype 0: Quarter-scale model for foil straining tests.

After checking the principle feasibility of the second frame concept, stagnation tests with different foil tensions were performed. This was done in order to determine the possible minimum tension values while still avoiding sagging and build-up of wrinkles up to high working temperatures of 150 Kelvin temperature difference. A drawback of the small model collector is its higher frame stiffness compared to the real-sized 2 m x 1 m collector. Thus the onset temperature for the build-up of wrinkles is possibly overestimated here. Nevertheless, the results give a first impression of the necessary minimum straining tension values. Table 3.4 contains the results in compacted form:

Table 3.4. Test results temperature dependent wrinkle build-up experiment with 25 µm ETFE foil.

Test number	**1**	**2**	**3**	**4**
Straining tensions in MPa (short side / long side)	16 / 8	14 / 7	10 / 5	5 / 5
$\Delta T < 100$ K	●	●	●	●
100 K $< \Delta T <$ 150 K	●	●	●	●
150 K $< \Delta T$	●	●	●	●

For all tests no significant (< 5 mm) sagging of the 25 µm ETFE foil occurred up to the stagnation temperature. Green shading marks zero wrinkles, yellow indicates small wrinkles at the sides (mainly due to imperfect tension distribution during the straining process) and red marks larger wrinkles in the middle of the aperture area. The best results were obtained with relatively high tensions of 16 MPa on the short and 8 MPa on the long side. Nevertheless, for the 16/8 test at temperature differences above 150 Kelvin temperature difference, wrinkles also occurred. This should be a particular case of foil creeping due to imperfect clamping of the foil and the following prolonged period between straining and the experiment of about 4 weeks. Considering all cases only values greater than 14 MPa short side and 7 MPa long side are recommendable. Thus all subsequent prototype tests were performed with foil tensions of 16/8 MPa.

Prototype 1: Single front-side foil insulation 25 µm ETFE, rear and side insulation mineral wool

The first real-size prototype built during this project was an all-series SF100-03 with additional front-foil insulation. A 25 µm ETFE foil was mounted according to the previously described second frame concept. No changes were made to the backside and side insulation in order to determine the isolated effect of just the front-foil insulation Figure 3.17. shows a schematic cross-section of the prototype. The distance from foil to glass is set at 15 mm, which results in a rather wide gap width of 25 mm between absorber and foil. Thus if necessary the overall collector height could theoretically be lowered about 10 mm without any negative effect on the performance by decreasing the gap widths to e.g. 17 mm absorber-to-foil and 13 mm foil-to-glass. Contrary to this finding is the fact that during service, the absorber position is usually not tightly fixed. In the case of the SF100-03 it can move up to 10 mm to the front due to thermal elongation. Hence in this case a slightly worse space utilization helps to maintain good performance under all typical working conditions.

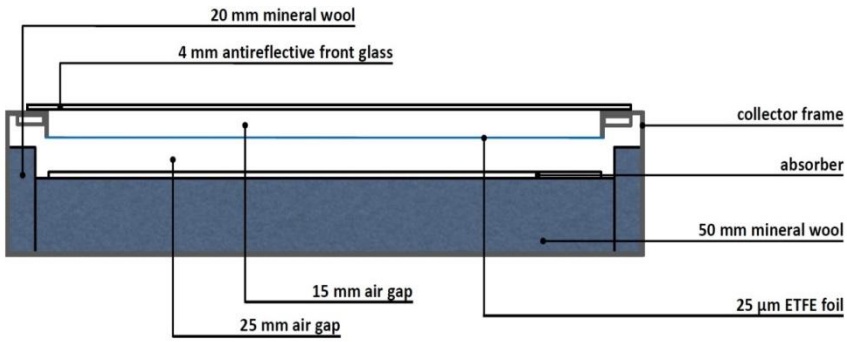

Figure 3.17. Internal schematic structure of prototype 1 with single 25 µm ETFE front-side foil insulation, backside and side insulation according to standard SF100-03.

Prototype 1 is shown in Figure 3.18 during the measurement on the ZAE outdoor test-rig (right side). The outer appearance is very close to the series SF100-03 model (left side), which is measured in parallel as a reference. As mentioned previously, all collector tests at ZAE are performed in a way strongly oriented to the norm DIN EN 12975.

Figure 3.18. Prototype 1 on ZAE Bayern outdoor test-rig (right) and reference collector SF100-03 series type (left). Prototype 1 shows small wrinkles in the middle of the aperture area at 110 °C fluid mean temperature.

Figure 3.19 depicts the measured efficiency curves for the series collector (black line) and the prototype (blue line). The prototype performs very good in the target temperature range (indicated by grey shading). At every reduced temperature difference upwards starting from 0.05 $K \cdot m^{-2} \cdot W^{-1}$ it shows higher efficiencies than the reference SF100-03.

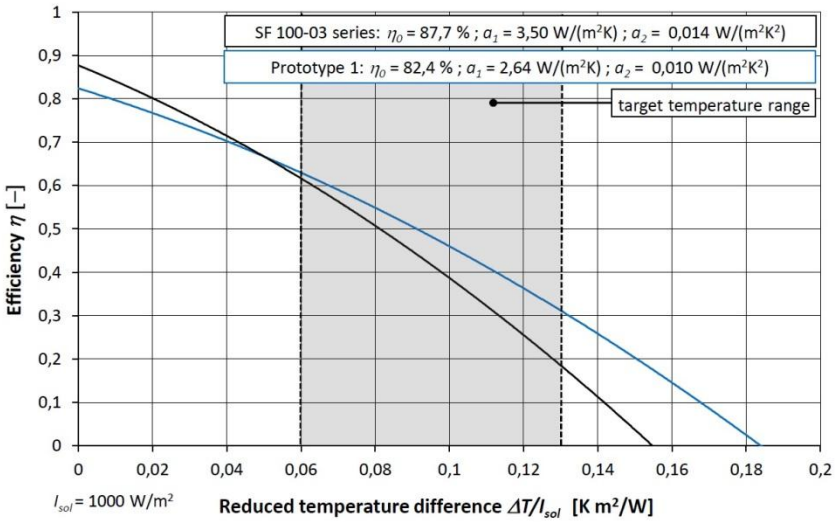

Figure 3.19. Collector efficiency test result prototype 1 with 25 µm ETFE front-side foil insulation, backside and side insulation as in series collector (blue line). Reference collector SF100-03 series model (black line).

For a more precise evaluation of the improvements, the determined collector efficiency parameters of both collectors are given in Table 3.5. Prototype 1 exhibits a total loss coefficient a_{100} at a 100 Kelvin temperature difference of 3.64 $W \cdot m^{-2} \cdot K^{-1}$. Together with the typical η_0 reduction by the ETFE foil of about -6%-points, this leads to an efficiency value η_{100} at a 100 Kelvin temperature difference of 0.46, so 7%-points more than the series SF100-03. Furthermore, comparing the measured values with the predicted ones for a foil-insulated SF100-03 results in excellent agreement. Thus, the prediction method proposed originally in [Beikircher, 2010] is proven once again: A front-foil insulation using fluoropolymer films (e.g. ETFE 25 µm) with properly dimensioned gap widths (> 10 mm) provides a reduction in a_{100} of 1.3 to 1.4 $W \cdot m^{-2} \cdot K^{-1}$ and an improvement in η_{100} of 6% to 7%-points. Moreover, the experiment clearly shows that the new foil mounting system based on the second frame concept works fine. During the measurements at elevated temperatures (130 to 150 °C), only minor wrinkles appeared in the middle of the aperture area, see Figure 3.18.

Table 3.5. Experimentally determined collector efficiency parameters SF100-03 series collector and prototype 1 (ETFE 25 µm front-side foil insulation, backside and side insulation as in series SF100-03). Measurement was performed in parallel under identical conditions.

Measure-ment **Type**	η_0 - Conversion factor	a_1 $W \cdot m^{-2} \cdot K^{-1}$ Loss coefficient Linear	a_2 $W \cdot m^{-2} \cdot K^{-2}$ Loss coefficient Quadratic	a_{100} $W \cdot m^{-2} \cdot K^{-1}$ Total loss coefficient at 100 K ΔT	η_{100} - Efficiency at 100 K ΔT
SF100-03 series	0.877	3.50	0.014	4.9	0.39
Prototype 1	0.824	2.64	0.010	3.64	0.46
Prototype 1 (prediction)	0.840	2.40	0.013	3.7	0.47

Prototype 2: Single front-side foil insulation 25 µm ETFE, rear and side insulation hybrid PIR & air gap.

The second prototype, again based on the SF100-03, features front-side 25 µm ETFE foil insulation and novel low-e aluminium foil cladded 30 mm PIR-foam plus 20 mm air gap hybrid backside insulation as well as 20 mm aluminium foil cladded PIR-foam side insulation. Figure 3.20 shows the corresponding schematic cross section. As previously explained, the absorber is resting on a single PIR foam insulation strip in the middle of the collector, see Figure 3.13.

Prototype 2 was measured in parallel to a SF100-03 series type reference collector, see Figure 3.21. Prototype 2 also performs significantly better than the series collector. No wrinkles showed up during the entire testing time or thereafter.

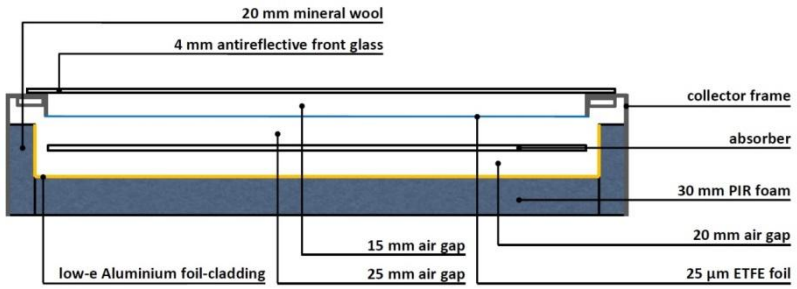

Figure 3.20. Prototype 2 schematic cross-section. Front-side foil insulation and backside hybrid insulation low-e aluminium foil cladded 30 mm PIR-foam & 20 mm air gap, low-e aluminium foil cladded 20 mm PIR-foam side insulation.

Figure 3.21. Prototype 2 (right) and series SF100-03 reference collector (left) on ZAE test-rig.

In turn, Figure 3.22 displays the measured efficiency curves for the series collector (black line) and the prototype (blue line). Starting at around 0.07 $K \cdot m^{-2} \cdot W^{-1}$ reduced temperature difference, prototype 2 exhibits an advance in efficiency compared to the SF100-03 reference. For a quantitative evaluation, Table 3.6 gives an overview of all experimentally determined collector efficiency parameters.

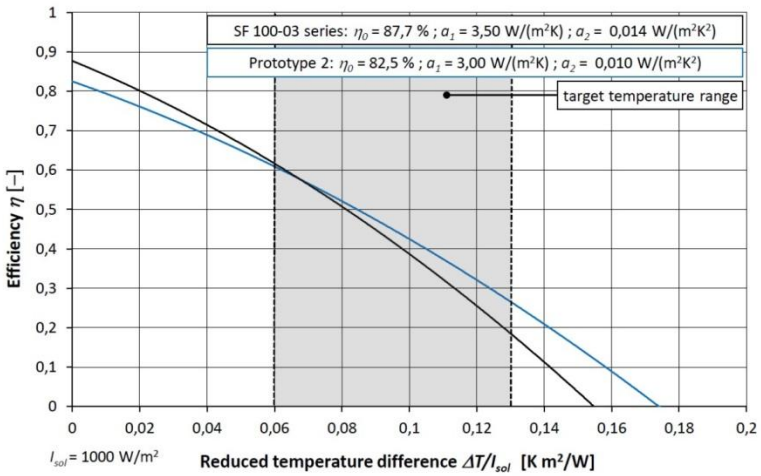

Figure 3.22. Collector efficiency test result prototype 2 featuring 25 µm ETFE front-side foil insulation, 30 mm PIR-foam & 20 mm air gap backside and 20 mm PIR-foam side insulation (blue line). Reference collector SF100-03 series model (black line) was measured in parallel.

As expected the conversion factors of prototype 2 and the reference collector are in good approximation equal to the values obtained from the prototype 1 test. The total loss coefficient a_{100} at 100 Kelvin temperature difference is lowered by 0.9 $W \cdot m^{-2} \cdot K^{-1}$ and analog the efficiency η_{100} at a 100 Kelvin temperature difference is 4%-points higher. Thus, prototype 2 represents an example for a highly efficient flat-plate collector with a less moisture sensitive backside and side insulation.

Table 3.6. Experimentally determined collector efficiency parameters SF100-03 series collector and prototype 2 (ETFE 25 µm front-side foil insulation, low-e aluminium foil cladded 30 mm PIR-foam & 20 mm air gap hybrid backside insulation, low-e aluminium foil cladded 20 mm PIR-foam side insulation). Measurement was performed in parallel under identical conditions.

Measurement	η_0 -	a_1 $W \cdot m^{-2} \cdot K^{-1}$	a_2 $W \cdot m^{-2} \cdot K^{-2}$	a_{100} $W \cdot m^{-2} \cdot K^{-1}$	η_{100} -
Type	Conversion factor	Loss coefficient Linear	Loss coefficient Quadratic	Total loss coefficient at 100 K ΔT	Efficiency at 100 K ΔT
SF100-03 series	0,877	3,50	0,014	4,9	0,39
Prototype 2	0,825	3,00	0,010	4,0	0,43

Nevertheless, it performs slightly worse than prototype 1 (0.3 $W \cdot m^{-2} \cdot K^{-1}$ with higher a_{100} and 3%-points less η_{100}) due to the different backside and side insulation. Hence the resulting backside heat transition values of the reference SF100-03 and prototype 2 are as follows:

Series collector mineral wool: 0.74 $W \cdot m^{-2} \cdot K^{-1}$
PIR-foam & air gap hybrid: ca. 1 $W \cdot m^{-2} \cdot K^{-1}$

Prototype 3: Single front-side foil insulation 25 µm ETFE, rear insulation 0.4 mm aluminium sheet on wooden framework.

Also the second novel backside insulation system consisting of a 0.4 mm aluminium sheet metal on a wooden framework with two air gaps is tested in a front-side foil insulated prototype. The concept in this case is quite outstanding because of the complete removal of all porous insulation material from the collector. The schematic cross-section is depicted in Figure 3.23.

As can be seen here, no side insulation is used in prototype 3. This was done mainly because foil insulation systems to the sides are difficult to integrate and at the same time probably not very effective. It was previously described that the absorber rests on a hollow aluminium support rod. This rod also serves as a strut

to reinforce the frame in order to minimize bending caused by the foil tension. Prototype 3 is tested according to the same procedures as the foregoing prototypes. The experimentally determined efficiency curve in direct comparison with the reference collector SF100-03 is presented in Figure 3.24.

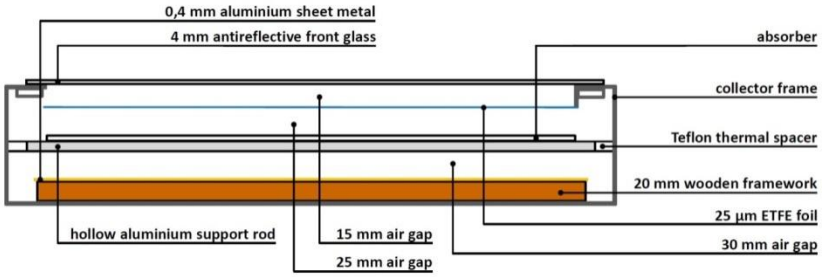

Figure 3.23. Prototype 3 schematic cross-section. Front-side foil insulation and 0.4 mm aluminium sheet metal on wooden framework backside insulation. No side insulation!

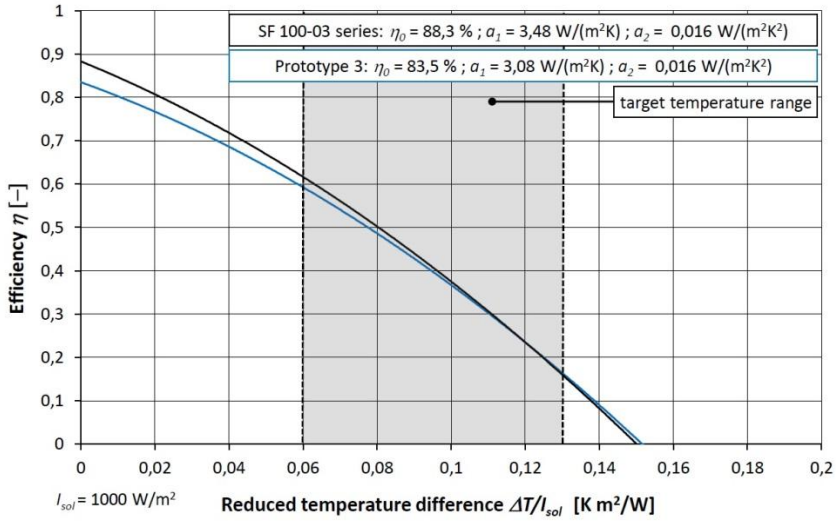

Figure 3.24. Collector efficiency test result prototype 3 featuring 25 µm ETFE front-side foil insulation and 0.4 mm aluminium sheet metal on wooden framework double air gap backside insulation, no side insulation (blue line). Reference collector SF100-03 series model (black line) measured in parallel.

Compared to the first two prototypes, model number three does not exhibit an acceptable break-even temperature below the target temperature range. Just

starting from 0.13 $K \cdot m^{-2} \cdot W^{-1}$ the prototype shows better efficiencies than the reference SF100-03. Thus, it would be counterproductive to use the prototype 3 design in a real application. Table 3.7 contains the identified collector efficiency parameters. For prototype 3 the total loss coefficient a_{100} is only about 0.4 $W \cdot m^{-2} \cdot K^{-1}$ lower than the corresponding value of the reference collector. The typical improvement of 1.3 $W \cdot m^{-2} \cdot K^{-1}$ by the front-side foil insulation is attenuated by the insufficient backside and missing side insulation. Hence also η_{100} is slightly worse (1%-point) checked against the reference collector's value.

Table 3.7. Experimentally determined collector efficiency parameters SF100-03 series collector and prototype 3 (ETFE 25 µm front-side foil insulation, 0.4 mm aluminium sheet metal on wooden framework double air gap backside insulation, no side insulation). Measurements in parallel under identical conditions.

Measurement	η_0	a_1	a_2	a_{100}	η_{100}
	-	$W \cdot m^{-2} \cdot K^{-1}$	$W \cdot m^{-2} \cdot K^{-2}$	$W \cdot m^{-2} \cdot K^{-1}$	-
Type	Conversion factor	Loss coefficient Linear	Loss coefficient Quadratic	Total loss coefficient at 100 K ΔT	Efficiency at100 K ΔT
SF100-03 series	0.883	3.48	0.016	5.1	0.38
Prototype 3	0.835	3.08	0.016	4.7	0.37

However, the incorporated backside insulation design is free of any porous material and insensitive to moisture accumulation and related degradation effects. Compared to the mineral wool Isover GW Solar 3.5 N used in the SF100-03 series collector, the sheet metal on framework insulation has a 0.9 $W \cdot m^{-2} \cdot K^{-1}$ higher heat transition value. In absolute values (50 mm layer with 60 °C mean temperature):

Series collector:	0.74 $W \cdot m^{-2} \cdot K^{-1}$ (mineral wool)
Sheet metal insulation:	ca. 1.4 to 1.6 $W \cdot m^{-2} \cdot K^{-1}$ (Uncertainty due to removed side insulation!)

Prototype 4: Double front-side foil insulation 2 x 25 µm FEP, rear and side insulation PIR-foam & air gap.

The fourth and last prototype was built to test a further improved front-side insulation concept featuring a double 25 µm FEP foil insulation. Based on the second frame concept, another u-profile spacer is used and a second foil is integrated. The overall collector height is 15 mm [EN 12975-2:2006, 2006]. Figure 3.25 depicts a schematic cross-section of this three-fold covered collector.

In the case of double front-side foil insulation, it is crucial to use only materials with the highest possible transmission coefficients for solar radiation. Using FEP (fluorinated ethylene propylene) with 96% solar transmittance is in this case mandatory in order to maintain a sufficiently high conversion factor. For the backside insulation the same concept as in prototype 2 is applied. Differing from prototype 2, the absorber support is done by the support rod, as in prototype 3. To get a better impression of the assembly.

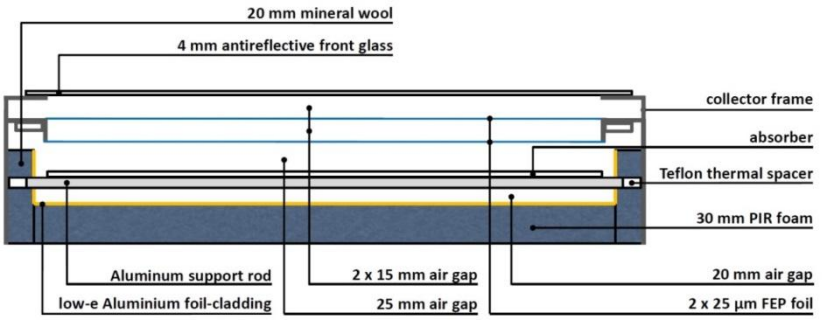

Figure 3.25. Prototype 4 double front-side foil insulation and backside hybrid insulation low-e aluminium foil cladded 30 mm PIR-foam & 20 mm air gap, low-e aluminium foil cladded 20 mm PIR-foam side insulation.

Figure 3.26 shows a photograph of the insulation system. All faces pointing towards the absorber are low-e cladded to reduce the radiative heat transport. In addition to the mechanical supporting function the support rod serves again as in prototype 3. For the prototypes 1, 2 and 3 with single front foil insulations the strut function is not absolutely necessary whereas for prototype 4 with its double front-foil insulation, it becomes more beneficial. However, it still represents a certain heat bridge.

Figure 3.26. Prototype 4 rear insulation assembly: 30 mm low-e foil cladded PIR-foam and 20 mm air gap.

Together with the front glass the double front foil insulation forms a triple layer cover system. The two foils are almost invisible from the top due to their high transmittance and the structured front glass. Figure 3.26 shows a close-up photograph of the front side with a laser beam used to create intensive reflexes at each of the four layers. These are front glass, two FEP foils and (rather dull) the

absorber. Prototype 4 is again measured according to the typical procedure, see Figure 3.27 . As in the foregoing efficiency plots, the reference collector efficiency curve is represented by a black line and the measured prototype curve is drawn in blue. Additional to these two curves, a green line depicts the calculated efficiency curve for prototype 4 with changed backside insulation.

Instead of the actually measured PIR-foam & air gap hybrid, the effect of series SF100-03 mineral wool insulation is extrapolated here. The conversion factor is slightly lower for prototype 4 compared to the first three prototypes with single front foil, but still at a relatively good level above 80%. Especially when using mineral wool backside insulation, the breakeven temperature stays at around 0.05 $K \cdot m^{-2} \cdot W^{-1}$ and the performance in the target temperature range is further improved compared to prototype 1. The hybrid PIR-foam & air gap insulation is not recommendable though for prototype 4, as the overall performance would be decreased too much and the effort of the double foil insulation does not pay off.

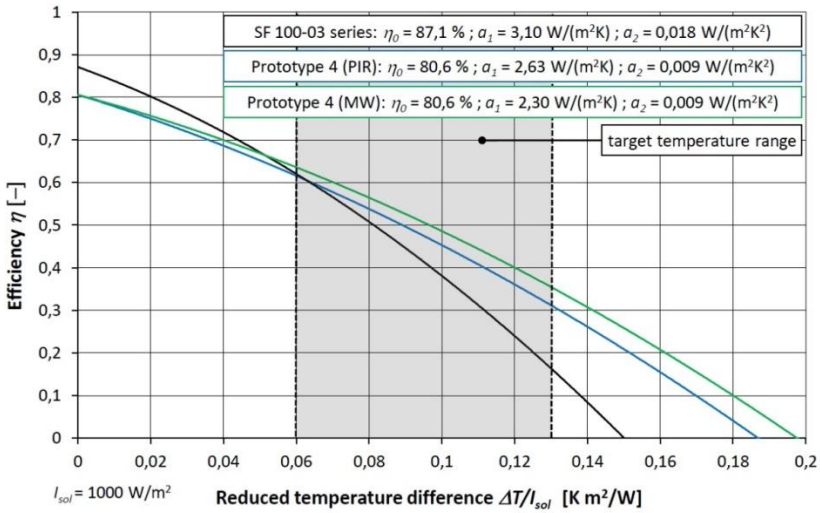

Figure 3.27. Collector efficiency test result prototype 4 featuring 2 x 25 µm FEP front-side double foil insulation, 30 mm PIR-foam & 20 mm air gap backside and 20 mm PIR-foam side insulation (blue line). Calculated curve for prototype 4 with alternative 50 mm mineral wool backside insulation (green line). Reference collector SF100-03 series model (black line) measured in parallel.

According to Table 3.8 with a double foil insulation the total loss coefficient a_{100} can be reduced by 1.7 $K \cdot m^{-2} \cdot W^{-1}$ whereas η_{100} increases by 11%-points to a high value of 0.49%. The double foil concept looks promising but still has to be further investigated and tested, especially for its durability and stagnation proofness (which should theoretically be no problem, as all the used materials, including FEP, can resist the high expected temperatures).

Table 3.8. Experimentally determined collector efficiency parameters SF100-03 series collector and prototype 4 (2 x FEP 25 µm double front-side foil insulation, 30 mm PIR-foam & 20 mm air gap backside and 20 mm PIR-foam side insulation. Additional calculated values for prototype 4 with alternative 50 mm mineral wool backside insulation). Measurement was performed in parallel under identical conditions.

Measurement **Type**	η_0 - Conversion factor	a_1 $W \cdot m^{-2} \cdot K^{-1}$ Loss coefficient Linear	a_2 $W \cdot m^{-2} \cdot K^{-2}$ Loss coefficient Quadratic	a_{100} $W \cdot m^{-2} \cdot K^{-1}$ Total loss coefficient at 100 K ΔT	η_{100} - Efficiency at100 K ΔT
SF100-03 series	0.871	3.10	0.018	4.9	0.38
Prototype 4 PIR & air gap	0.806	2.63	0.009	3.5	0.45
Prototype 4 Mineral wool	0.806	2.30	0.009	3.2	0.49

3.1.7 Overview prototype results

In order to recap and rank the results of all four experimental prototypes, Figure 3.28 again shows all measured efficiency curves in comparison. Analog Table 3.10 contains the measured efficiency parameters. In Figure 3.28 and Table 3.9 mean values of the four conducted SF100-03 measurements are used as a reference.

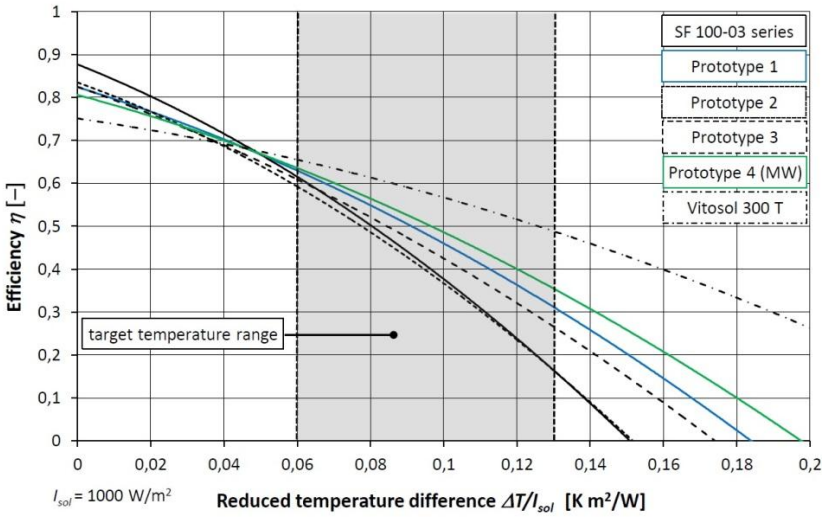

Figure 3.28. Overview of efficiency curves of all prototypes 1 to 4. In addition, curves of the reference collector Savo-Solar SF100-03 (full black line) and a state-of-the-art evacuated tube collector Viessmann Vitosol 300 T (dot-dash black line) are depicted for direct comparison.

Table 3.9. Overview experimentally determined relative differences in collector efficiency parameters. Calculated for each prototype with the particular values of the parallel measured reference collector.

Measurement	η_0	a_1	a_2	a_{100}	η_{100}
	-	$W \cdot m^{-2} \cdot K^{-1}$	$W \cdot m^{-2} \cdot K^{-2}$	$W \cdot m^{-2} \cdot K^{-1}$	-
Type	Conversion factor	Loss coefficient Linear	Loss coefficient Quadratic	Total loss coefficient at 100 K ΔT	Efficiency at 100 K ΔT
Prototype 1	-0.053	-0.86	-0.004	-1.26	+0.07
Prototype 2	-0.052	-0.50	-0.004	-0.09	+0.04
Prototype 3	-0.048	-0.40	+-0	-0.40	-0.01
Prototype 4 Mineral wool	-0.065	-0.80	-0.009	-1.70	+0.11

It is clearly visible that prototypes 1 and 4 show the best results with up to 11%-points more in η_{100}. Nevertheless, the evacuated tube collector still performs significantly better at high temperature differences but at much higher cost! As it was described previously the most important values of the collector experiments are the identified relative changes between the prototypes and the reference SF100-03, particular for each single measurement. Thus, Table 3.9 gives the

relative values of $\Delta\eta_0$, Δa_1, Δa_2, Δa_{100} and finally $\Delta\eta_{100}$. The determined relative differences can be used for estimating the performance of other collectors when incorporating front-side foil insulations (Prototypes 1 and 4) or combinations of front-side foil insulations with moisture insensitive backside insulations (Prototypes 2 and 3).

Table 3.10. Overview experimentally determined collector efficiency parameters. Solar Keymark certificate values for Vitosol 300 T evacuated tube collector are added for reference purposes.

Measurement **Type**	η_0 - Conversion factor	a_1 $W \cdot m^{-2} \cdot K^{-1}$ Loss coefficient Linear	a_2 $W \cdot m^{-2} \cdot K^{-2}$ Loss coefficient Quadratic	a_{100} $W \cdot m^{-2} \cdot K^{-1}$ Total loss coefficient at 100 K ΔT	η_{100} - Efficiency at 100 K ΔT
SF100-03 series	0.877	3.40	0.016	5.0	0.38
Prototype 1	0.824	2.64	0.010	3.64	0.46
Prototype 2	0.825	3.00	0.010	4.0	0.43
Prototype 3	0.835	3.08	0.016	4.7	0.37
Prototype 4 PIR & air gap	0.806	2.63	0.009	3.5	0.45
Prototype 4 Mineral wool	0.806	2.30	0.009	3.2	0.49
Vitosol 300 T	0.751	1.24	0.006	1.84	0.57

3.1.8 Summary and outlook for foil collector development

In this work package a solar flat-plate collector with enhanced efficiency at 80 °C to 150 °C operating temperature was developed. Several concepts for a highly efficient flat-plate collector were tested and evaluated on the basis of Savo-Solar SF100-03 series model. Typically, around two-thirds of the thermal losses of flat-plate collectors occur at the transparent cover. Thus the focus was to effectively improve the front-side insulation while keeping a high conversion factor. This was done by incorporating highest transmittance fluoropolymer (ETFE & FEP) foil insulations in the gap between the absorber and front glass. In this context a new foil-mounting system based on a second frame was developed and successfully tested. It allows a separated foil straining and subsequent integration in the parallel assembled collector. Furthermore, two novel moisture insensitive backside

insulation concepts were developed and tested that can be used as a replacement for mineral wool.

The new concepts and ideas where experimentally studied with five collector prototypes. The results show that single front foil insulation systems effectively reduce the total loss coefficient of the collector a_{100} at a 100 Kelvin temperature difference above ambient temperature by 1.3 $K \cdot m^{-2} \cdot W^{-1}$. In combination with the high transmittance of the used 25 µm ETFE foil, high η_{100} values (efficiency at 100 Kelvin temperature difference) around 46%, 7%-points more than the SF100-03 series collector, are possible. Moreover, the developed advanced double front-foil insulation with 2 x 25 µm FEP facilitates even higher η_{100} values of around 49%-points, due to the abundant loss reduction of 1.7 $K \cdot m^{-2} \cdot W^{-1}$, while maintaining a high conversion factor above 80%. The general applicability of the new moisture insensitive backside insulation designs (PIR-foam & air gap, 0.4 mm sheet metal on wooden framework) was demonstrated. However, the concepts showed 1.5 to 2 times higher heat transition coefficients compared to state-of-the-art mineral wool. Hence the use of these insulation designs in a highly efficient flat-plate collector is not recommended.

The next step towards the implementation of the front-side foil insulation in a series collector should be the development of an easy to handle foil-mounting system using the second frame concept. Furthermore, the development of a glass-foil element should be considered. In this case the front glass is glued into the second frame first and the foil is strained subsequently. Thus, the foil tension is held by the glass without any additional support frame. Such a glass-foil element can be handled easily and fixed to the base frame in the same way as it is usually done with the glass alone. Regarding the double front-foil insulation, tests on the stability at high temperatures and stagnation proofness have to be made. In addition, the performance of the double FEP insulation should be experimentally determined in combination with state-of-the-art mineral wool backside insulation.

3.2 Biomass-driven absorption chiller/heat pump – feasibility study

This section describes the simulation, development and feasibility study of a multivariable double stage absorption chiller with heat pump mode driven by wood pellets. The main objective was a reliable, resource-saving and low-carbon heat and cold supply to buildings as well as industrial processes between the temperature levels of 4 to 110 °C with regionally harvested renewable energy. By using thermally-driven absorption instead of electrically-driven compressor heat pump technology, no additional grid stress or reserve capacity, neither in summer nor in wintertime, is caused. Furthermore, biomass itself serves as an unrivalled cheap renewable energy storage compared to any other technology (PV, Wind, Solar thermal, Batteries, Power to Gas, hot water storages, etc.)

3.2.1 Introduction and objectives

Biomass already heavily contributes to the German 'Energiewende' and European Energy Technology Plan (SET Plan) objectives all year round. In 2011 about 11% of the primary energy consumption in Germany was fulfilled by renewable biomass. But, realistic evaluations pointed out a maximum potential of about 22% of the overall energy consumption. For additional growth, new efficient and resource-saving technologies have to be developed. Concurrently, huge efforts have to be taken in the near future to initiate and expedite the 'Wärmewende' in the housing and industrial sector, which consume roughly about one third of the primary energy in Germany.

Besides economically exploiting new resources, a more efficient use of biomass is mandatory. In this context, condensing technology in biomass boilers (standard fuel efficiencies approx. 90% max.) promises an efficiency increase to about 110%, but is struggling with extremely corrosive sewage, dirt and other nasty problems. In connection with a standard thermally driven sorption machine, the system fuel efficiency might reach 160%, if neglecting transmission heat losses. Higher efficiencies of up to 220% and increased variability in thermal energy provision could be achieved by the following proposed concept, where biomass combustion directly fires a double-effect absorption machine for heat and cold supply. Figure 3.29 depicts exemplary temperature levels T0 to T3 and specific targeted energy conversion ratios in three different operation modes. Depending on the needs, the system is supposed to lift 0.4 portions of heat from T0 to T2 level by means of one portion of biomass energy or provide 2.2 portions of medium tempered heat at T1 and 1.2 portions of cold at T0 level simultaneously. For sure, the system can operate in any mixed mode as well as allowing for multivariable and efficient energy conversion subjected to customer needs.

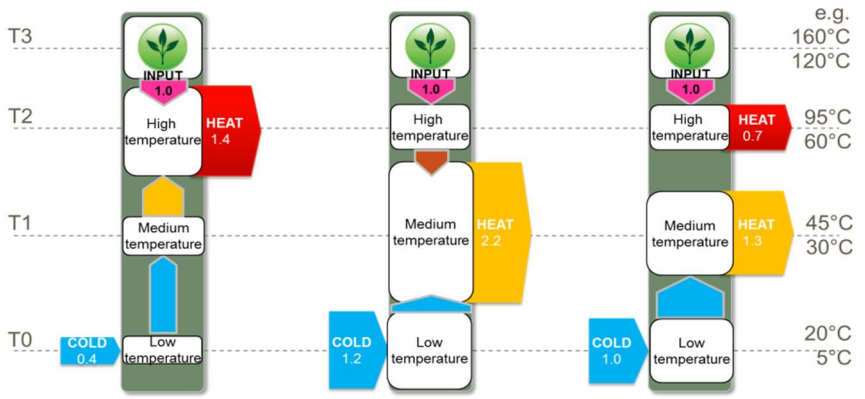

Figure 3.29. Sankey-scheme of energy flows and standard temperature levels for Cold and Heat supplied by the absorption chiller /heat pump device in three different operation modes with reference to one unit energy input.

3.2.2 Background and theory

So far as is known, such a system of a multivariable direct biomass-fired high temperature desorber (HTD) has not yet been built. Therefore, standards and norms of similar proceedings have to be considered. Some examples of an absorption chiller combined with a biomass boiler can be found in the literature [Moretti et al., 2013], [Obernberger, 2008], but in all these examples the heat from the biomass combustion is transferred by a heat transfer medium (thermal oil, steam, pressurized water e.g.) between the biomass boiler and the desorber of the absorption machine. Thus, complex planning, installation and control effort as well as safety and efficiency aspects due to high system temperatures inhibit this energy and resources saving technology platform.

In this investigation the heat from the biomass combustion is directly used to regenerate the aqueous lithium bromide solution of the absorption machine. Consequently, no additional circle for the heat transport between boiler and absorption machine is needed. This allows for a higher driving temperature of the desorber, so a double-effect-absorption chiller can be realized. Thus, efficiency increases up to 72% compared to single-stage absorption systems and additionally the simplified configuration reduces heat losses significantly.

At the outset, legal restrictions have to be checked to verify which construction methods are permitted and which points have to be considered. The relevant norm and standards under German federal law are:

- DIN 18842: Fireplaces fired by solid fuel - Gravimetric fired appliances for pellets and other solid fuels – Requirements and test methods
- DIN EN 13384-(1-5): Chimneys – Thermal and fluid dynamic calculation methods

- DIN EN 12309 (1-7): Gas-fired absorption and adsorption air-conditioning and/or heat pump appliances with a net heat input not exceeding 70 kW
- DIN EN 13445 (1-5): Unfired pressure vessels
- DIN EN 16147: Heat pumps with electrically driven compressors
- RICHTLINIE 97/23/EG DES EUROPÄISCHEN PARLAMENTS UND DES RATES vom 29. Mai 1997 zur Angleichung der Rechtsvorschriften der Mitgliedstaaten über Druckgeräte

Subsequently, a literature search was performed concerning mass- and heat transfer in both technologies: biomass boilers and absorption machines. Based on ZAE Bayerns long-standing experience in directly gas or flue gas driven desorbers, as presented in Figure 3.30, important parameters like critical heat transfer coefficients of 1300 $kW \cdot m^{-2}$, constructive and burnout parameters, or air/fuel ratio have been identified and evaluated [Zuber & Tribus, 1958], [Kren, 2009], [Bin Gadhi et al., 1987], [Shi et al., 2009].

Additional information is provided comprehensively in the following publications:

- 2007_Paper-Bauer-Messung-Temperatursensoren-in-BM-Feuerung
- 2008_Bauer_Modellierung des dynamischen Verhaltens der Wärmeübertragung in einem Rauchrohr-Wärmeübertrager
- 2009_Bauer_Bestimmung Rauchgas Massenstrom
- 2009_Bauer_Modelling of grate combustion in a medium scale biomass
- 2012_Schnetzinger_Abbilden des instationären Betriebs eines Pelletkessels

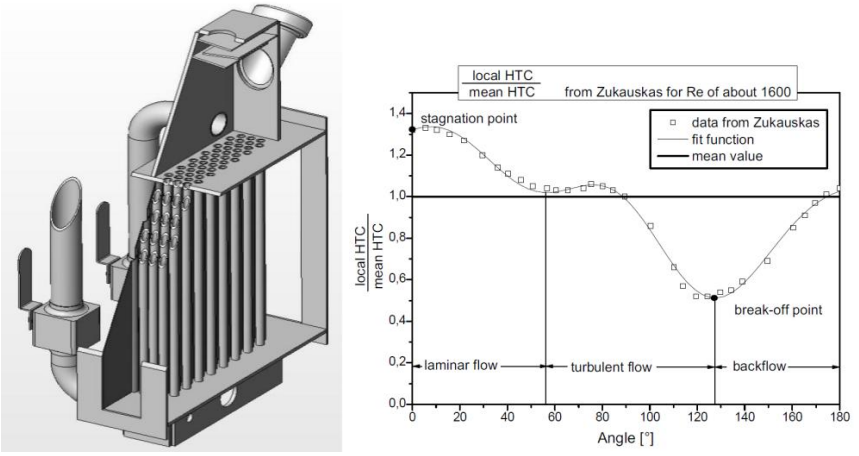

Figure 3.30. CAD section cut through a gas fired HTG prototype(left) and local outer heat transfer coefficient vs. radial contact angle of the flue gas (right).

This leads to a steady-state process parameter simulation, which has been set up in the programming environment of Engineering Equation Solver (EES), following

the suggestions of Keith 2016 for single- and double-effect absorption chillers. Standard UA-values of E1=1.5, A1=0.8, C1 and C2 =3.5, D1=0.8 kW·m^{-2}·K^{-1} have been implemented for the single-stage module and the condenser of the biomass desorber D2. The biomass-driven pool boiling desorber D2 (nominal capacity of 15 kW) simulation itself comprises a combustion calculation, convective and radiative heat transfer in the combustion (leanness λ 2.2) and flue gas section (according to Zukauskas), heat conductivity of the heat exchanger, as well as heat and mass transfer on the lithium bromide side. Heat transfer coefficients at the flue gas side are less than 100 m^{-2}·K^{-1}, while combustion temperature does not exceed 1800 °C. Neither in heavy nor part load, will heat transfer coefficients exceed the critical values, causing burnout or intense corrosion of the heat exchanger material. Maximum wall temperatures on the flue gas side compute to less than 320 °C, which is far from the maximal allowed temperature of 600 °C. The maximum pressure in the desorber does not exceed 1.5 bar, so no European Pressure Equipment Directive has to be complied with. In most cases, the vessel pressure will not exceed 1.0 bar during operation.

Predictive values in temperature, concentration and pressure of the combined process of biomass driven desorber D2 and single-stage absorption machine are presented in Figure 3.31. External temperature and flow conditions are 10 °C chilled (1.7 m^{3}h^{-1}) and 37 °C cooling water (2.5 m^{3}h^{-1}).

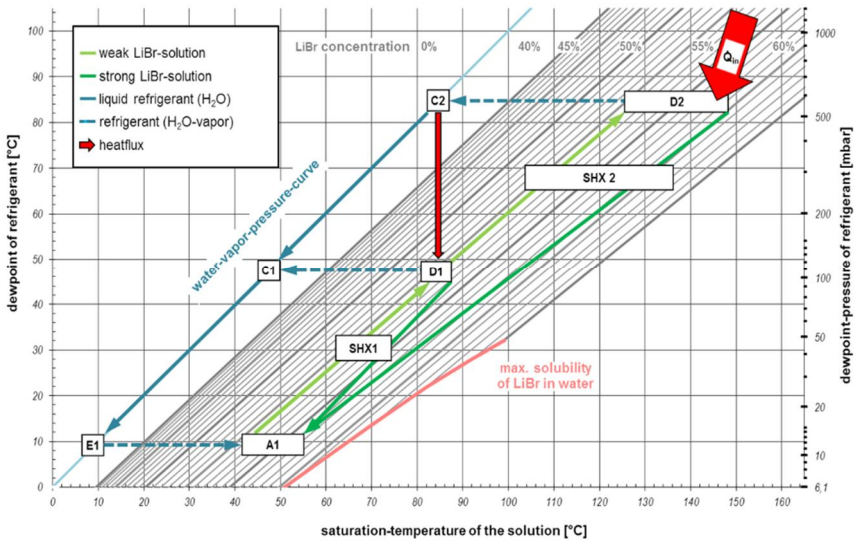

Figure 3.31. Saturation temperature, pressure and concentration parameters of the main components Evaporator E1, Absorber A1, Solution heat exchanger SHX1 and SHX2, Condenser C1, Desorber D1, secondary Condenser C2 and Desorber D2 in Duehring-Diagramm.

3.2.3 Biomass fired test-rig setup and testing procedure

Proof of concept has been carried out on a small scale (14 kW combustion capacity) laboratory test-rig functional model. The aim is to prove the feasibility and functionality of the idea directly with a wood-pellets-fired LiBr / H_2O high-temperature-generator. For this purpose, an existing pellet boiler was modified so that it can withstand the high temperatures and the corrosiveness of the aqueous salt solution at 170 °C. Starting from the existing geometry of the combustion chamber and the fuel analysis, calculations were carried out and new heat exchange surfaces have been designed. In this first step, the entire unit is made out of stainless steel to avoid any negative effects on the thermodynamic process from corrosion. To restore the decreased resistivity after welding, the tank surfaces were pickled and passivated. Finally, the high-alloy stainless steel container design was checked by FEM strength analysis and tested for leaks after assembly to ensure high vacuum conditions.

The current design comprises a direct fired reversing chamber where most of the combustion heat is transferred by radiation. Subsequent, the flue gas enters vertical flue gas pipes in a circular tube and shell lithium bromide boiler. Emerging vapour is separated at the top and flows towards the condenser. In front of it, an additional demister prevents any contamination with solution caused by entrained lithium bromide droplets. A spiral condenser was constructed and equipped with gauge glasses to guarantee an easy and good observation of the process. In order to evaluate the biomass fired desorber under various operating conditions, a conditioning and mixing circuit adjusts temperature and concentration of the lithium bromide solution to simulate an entire absorption machine. Highly accurate measuring equipment detects all main thermodynamic relevant states as shown in Figure 3.32, which allow for a detailed and precise process analysis by means of the predefined key values coefficient of performance, combustion efficiency and system performance.

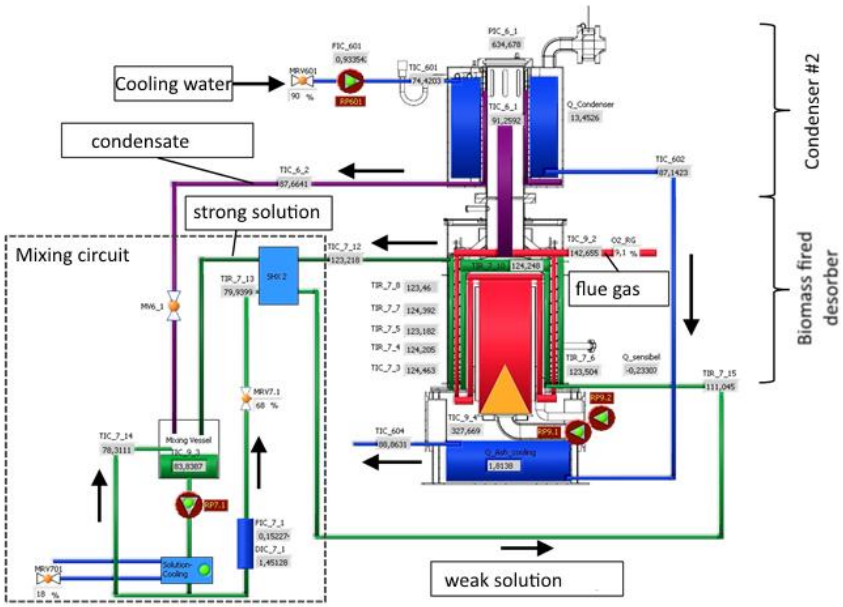

Figure 3.32. Interactive piping and instrumentation process view of the 14 kW biomass fired desorber, condenser and mixing circuit including representative measuring values.

Figure 3.3 Figure 3.33 shows a top view of the condenser towards the boiling lithium bromide solution in the biomass-fired tube-shell heat exchanger. Circumferential, the demister gates into the spiral condenser can be seen. A contamination of the condensate with lithium bromide decreases the overall system efficiency as well as capacity and therefore has to be avoided at all times. Below that figure, four different views of the biomass combustion plate at different firing capacities are shown. Combustion products are caught in a radiation cylinder where high turbulence and sufficient process temperature ensure a complete and low-emission combustion. Recirculation of flue gas helps to reduce maximum burning temperatures. Thus, a low nitrogen oxide output and ash discharge is achieved.

The footprint of the biomass fired desorber corresponds to standard wood pellet boilers. Only the above-mounted condenser increases the overall height of the machine to maximum 1.9 meters (Fig. 3.34). Due to safety reasons, an additional rupture disc and safety pressure switch limit the process pressure to 1.5 bar (absolute). Hence, no further special requirements and series of standards have to be considered in Germany.

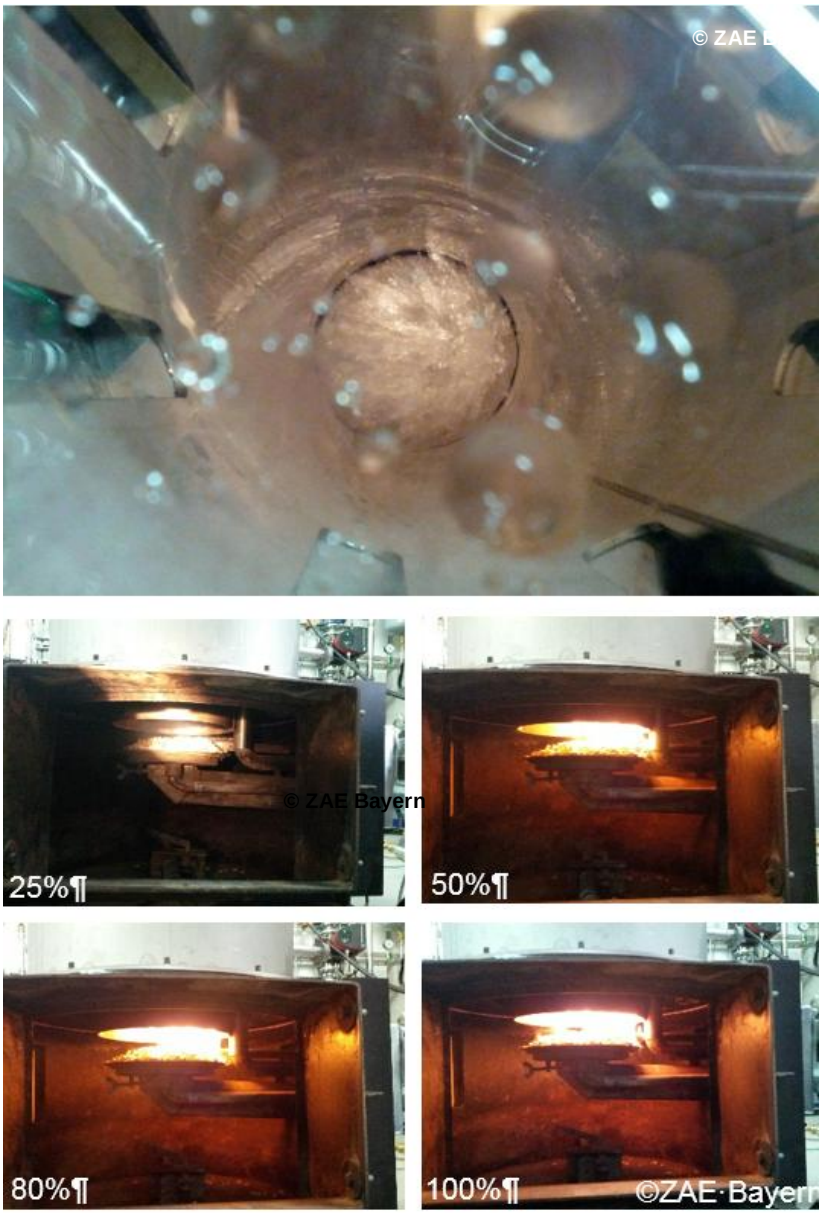

Figure 3.33. Boiling Lithium bromide solution in the biomass fired desorber (top left) and fire in pellet combustion chamber at 25 /50 /75 and 100% of nominal combustion capacity (bottom left).

Figure 3.34. Uninsulated second stage of a biomass driven absorption machine including piping of mixing circuit and control cabinet.

3.2.4 Results and outlook of biomass driven absorption chiller/heat pump development

Performance measurements of a full-scale functional model at the test-rig at ZAE Bayern in Munich prove an already competitive Coefficient of Performance COP_C of 1.2 compared to gas-fired absorption machines in cooling mode (Fig. 3.35). Applied as a heat pump this value increases to 2.2.

The boiler efficiency and fuel utilization respectively of the biomass desorber (conversion factor between chemical energy content of the wood pellets and heat absorbed in the desorber) is better than 0.74. Despite the increased system temperatures up to 160 °C required for desorption, this is already a competitive value compared to common standard pellet hot water boilers with moderate efficiency and it already fulfils all relevant harmonized standards. This could be improved easily with an optimized combustion chamber and exhaust gas recirculation in the future. Based on these values the machine achieves an overall

conversion factor from chemical fuel energy to cold output of 0.84 overall. This proves the general feasibility of the system concept. Furthermore, no degradation or corrosion of the heat exchanger surface has been detected. Load change ability is sufficiently fast for any building heating or cooling purpose.

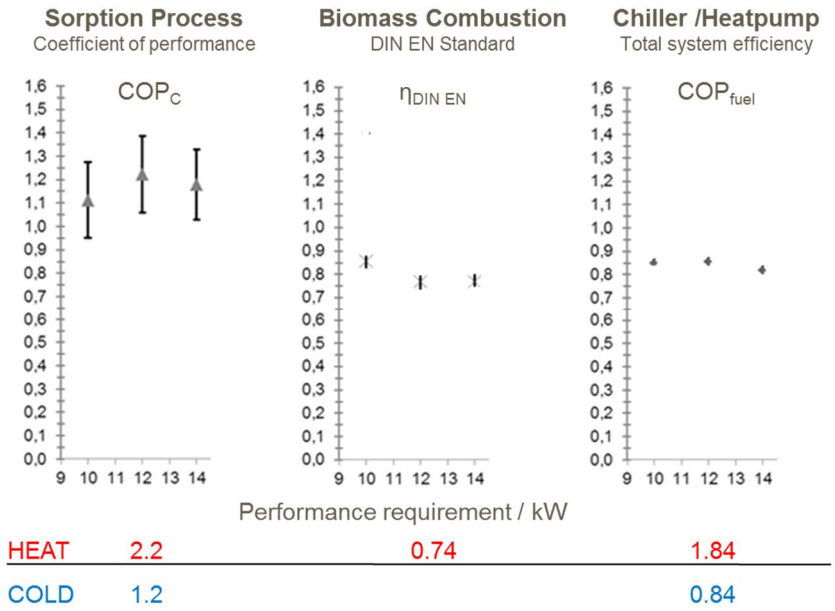

Figure 3.35. Performance figures of the sorption process, biomass combustion and the total system efficiency of the biomass-driven double-effect absorption chiller / heat pump in cooling and heating mode.

3.3 Forecasting of solar radiation and outdoor temperature fixed in place coordinates

Finnish Meteorological Institute (FMI) open data were utilized in a solar heat collector production forecasting algorithm. The FMI has decided to publish a major part of their meteorological and oceanographic datasets as open data using open standard web service interfaces for geospatial data (Finnish Meteorological institute, 2013). Weather forecasting from the FMI is based on the High Resolution Limited Area Model (HIRLAM) with a horizontal resolution of 7.5 kilometers. The vertical model has 65 levels, of which 20 are located in the lowest atmospheric level below 1000 meters. The HIRLAM weather forecast model is run four times a day (00, 06, 12 and 18 UTC) and it is a limited-range model, which covers Europe, the North Atlantic and part of the Arctic regions. Methods were developed to retrieve weather forecast and measurement data from the open data platform, analyse its accuracy, and to develop calculation model to forecast day-ahead solar

production. The data is available in XML schema and therefore some parsing of the data is required. Python programming language was used for data retrieval since calculations of the solar equations was also done using python.

To estimate the solar collector production, the azimuth and elevation angle of the sun should be accurately calculated. The production estimation algorithm calculates these angles for selected time steps during the day from coordinates and altitude of a selected location. Modelling of sun position angles is explained in [Bratu, 2008]. These angles are utilized to calculate the amount of solar radiation on a tilted surface and panel temperature. Solar radiation is divided into three components: direct, diffuse and reflected solar radiation. These components are illustrated in Figure 3.36.

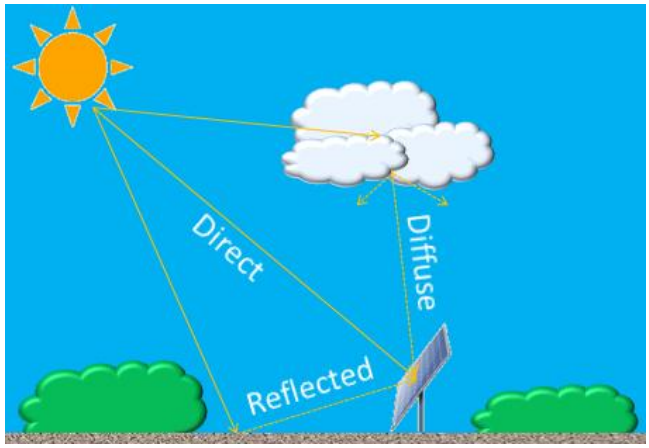

Figure 3.36. Radiation components on a tilted panel surface.

Of the three components, direct and diffuse parts are the most important for estimation of solar radiation on a tilted surface. The reflected part of the radiation depends on the place where the system is installed. The reflected part of the radiation is usually insignificant compared to the direct and diffuse radiation. Calculation of the radiation on a tilted collector/panel surface was done with the HDKR model [Duffie & Beckman, 2013]. The total radiation I_T on a tilted collector/panel surface is

$$I_T = (I_b - I_d A_i) R_b + I_d (1 - A_i) \left(\frac{1 + \cos\beta}{2}\right) \left[1 + f \sin^3\left(\frac{\beta}{2}\right)\right] + I_{\rho_g} \left(\frac{1 - \cos\beta}{2}\right) \quad (2)$$

Where I_T is the total radiation on the tilted surface, I_b is the beam radiation, I_d is the diffuse radiation, I_{ρ_g} is the ground reflectance (also called the albedo), R_b is the ratio of beam radiation on the tilted surface to beam radiation on the horizontal

surface, A_i is the anisotropy index, β is the slope surface and f is the final factor. The anisotropy index determines a portion of the horizontal diffuse and it is given by the following equation (3):

$$A_i = \frac{I_b}{I_0} \tag{3}$$

Where I_0 is the extraterrestrial horizontal radiation. The final factor is related to the cloudiness of the location and it is given by the following equation [Duffie & Beckman, 2013]:

$$f = \sqrt{\frac{I_b}{I}} \tag{4}$$

Where I is the global horizontal radiation on the earth's surface.

A database is used for storage of data on a local server. A PostgreSQL database solution was selected because of good experiences and performance on previous work [PostgreSQL, 2015]. A command library for connecting to a database is available for python, so integration was fairly smooth.

For ease of use, forecasts are saved in csv-format to an FTP-server, which is used to transfer to the Savosolar information system.

The server at the VTT end is a quite simple PC-machine (Fig. 3.37).

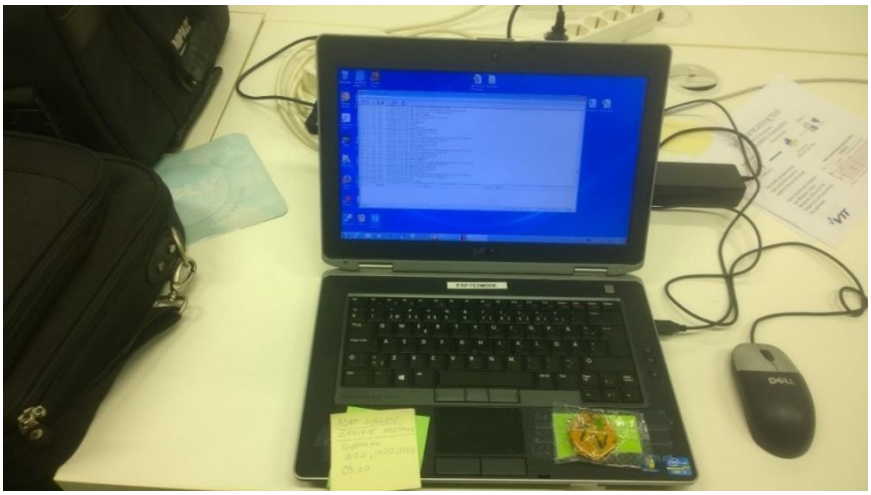

Figure 3.37. Forecast server at VTT.

The server is a standard laptop. We wanted to use the laptop because of natural backup power, which comes from a battery. Moreover, the server load is quite

small and is good enough for at least 1000 connections with an i7 processor and 8 GB of ram.

Some results from the radiation forecast system follows:

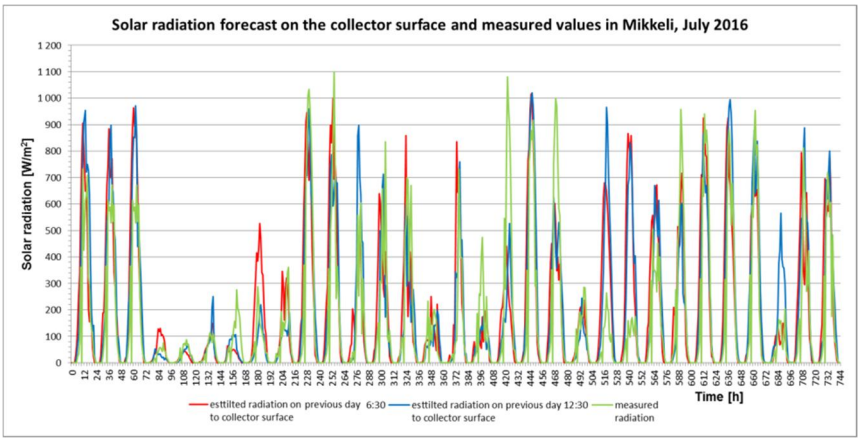

Figure 3.38. Solar radiation forecast compared to measurements in July 2016. Forecasts in red and blue and measurement in green.

The forecast in red is done at 6:30 in the morning and the forecast in blue at 12:30 midday the day before (Fig.3.38). Accuracy analysis is displayed in Figure 3.39, with results sorted from worst to best (durability curve). Only errors, when none zero radiation exist in days, are included.

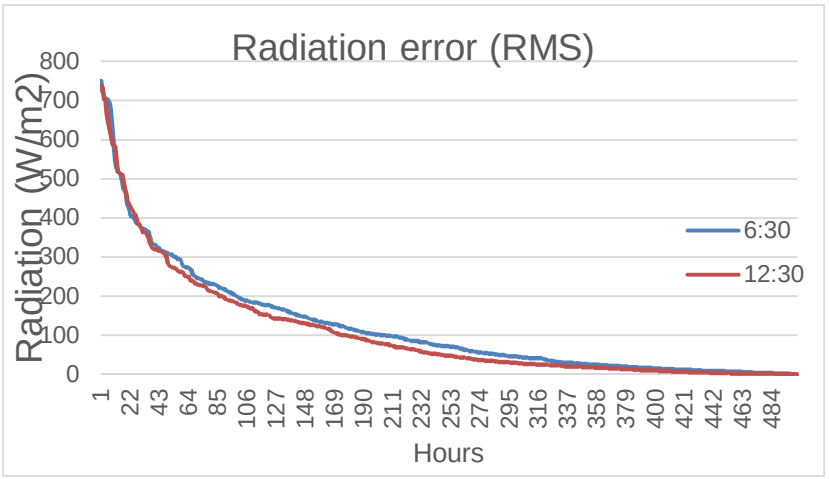

Figure 3.39. Durability curve of RMS error in radiation forecasts 6:30 forecast in blue and 12:30 in red.

Approximate threshold levels for accuracies are displayed in Table 3.11.

Table 3.11. Threshold levels for accuracy in the radiation forecast.

Error value W/m²	Percentage of errors under this value
300	91%
200	84%
100	66%

Although accuracy varies to some degree, this is enough for optimization purposes of the heating/cooling system. If for example optimization decides how to prepare for the next day, it just needs information on whether it is better to buffer more heat to the storage for the next day by let's say using solar heat, the heat pump or district heating, if there will be no sun. The heat pump can be operated optimally against electricity market price variation as well as SH and DH, using only electricity for pumping.

Figure 3.40 contains the results for the temperature forecast for the same period. The accuracy of the temperature forecast correlates with the radiation forecast quite well, meaning when the radiation forecast fails, so does the temperature forecast.

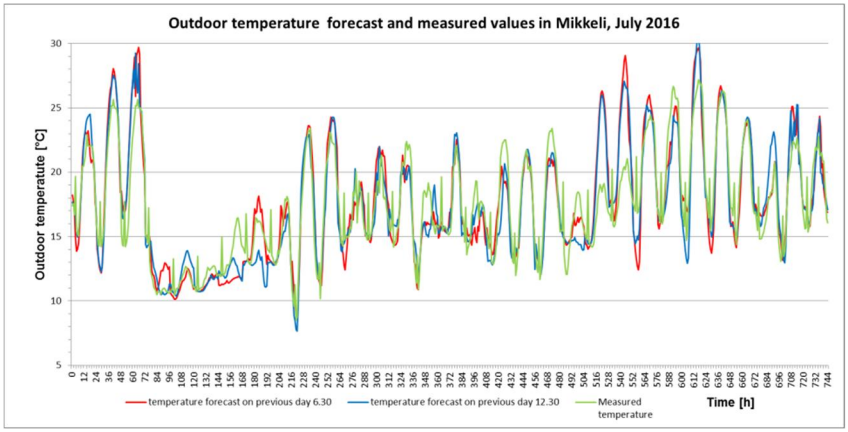

Figure 3.40. Forecast compared to measurements in July 2016. Forecasts in red and blue and measurement in green.

Here is temperature forecast accuracy analysis results in Figure 3.41.

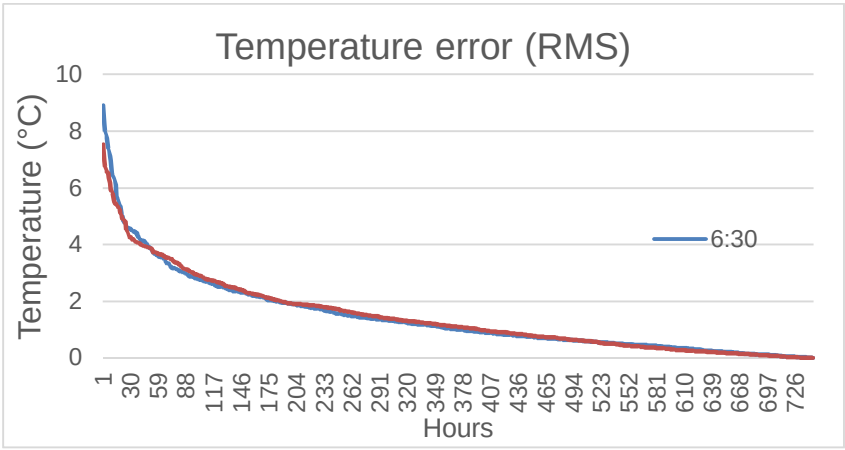

Figure 3.41. Durability curve of RMS error in temperature forecasts, 6:30 forecast in blue and 12:30 in red.

And threshold values for accuracy in the temperature forecast are given in Table 3.12

Table 3.12. Threshold levels for accuracy in three temperature forecast.

Error value °C	Percentage of errors under this value
3	87%
2	75%
1	47%

The temperature forecast is supplied directly by the Open Data service of the Finnish Meteorological Institute (FMI) and the global HILARM model. The development of HIRLAM was started in 1985, and has since been going in several phases. The first version of the model was completed in 1989 and introduced into operational use at the FMI in 1990. Presently, model version 7 is in use.

In addition to developing the model, the program participants use it operationally in weather forecasting. Since 2003, the FMI has had a special status in HIRLAM, acting as the so-called Lead Centre for the RCR (Regular Cycle with the Reference), which includes the special duty of running the official reference version of the HIRLAM model as its operational weather forecast model. The results and experiences thus gained are then utilized in model development. Internationally, HIRLAM has been found comparable to the models developed in larger countries, such as the United Kingdom, France, and Germany.' (Finnish Meteorological institute, 2015).

More on the HILARM model is described on the FMI website:
http://en.ilmatieteenlaitos.fi/weather-forecast-models

4. Simulation and planning of a solar heating and cooling system (SHC system)

4.1 Description of the building

The general data and thermal feature of the building are listed in Table 4.1. They refer to the Savo-Solar office building in Mikkeli (Figure 4.1). The building was built in 2012 as an extension on the side of the existing factory hall. The thermal properties of the building meet the requirements of the Finnish Building Energy Efficiency regulation of 2012 [Ministry of Environment, 2012a]. Data have been gathered onsite, from the technical construction report and, where information was missing, from the values of Meteonom [Meteonom, 2015].

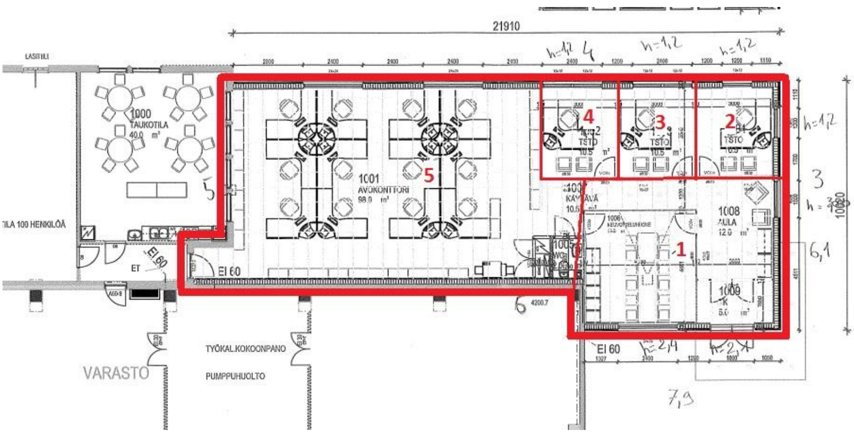

Figure 4.1. Map of the Savo-Solar office building.

The hourly building thermal loads were calculated with the program Dynamic Building Energy Simulation (DBES) [Viot et al., 2015]. The program developed on Matlab is based on the response factor theory for the transient analysis of the thermal heat transfer in building structures [Mitalas & Arseneault, 1972]. It was developed and verified as a task of the Finnish Tekes-founded project, Distributed Energy system [Sipilä et al., 2015].

Table 4.1. Thermal features of the building envelope elements: external wall, roof and window and main data of the building.

Building thermal features

	U Value W/m2K	g factor
Wooden structured external Wall		0.17 W/(m2K) -
Wooden structured roof	0.09 W/(m2K)	-
On-ground concrete floor slab	0.16 W/(m2K)	-
Triple glazed window	1.0 W/(m2K)	

Building general data

Location	Tampere, N 61° 29', E 27° 27'
Floor surface	170 m2
Internal - external superficial thermal resistances	0.2–0.07 m2K/W
Mechanical exhaust air ventilation rate	2.5–3.3 ac/h
Mechanical ventilation heat recovery	75%
Infiltration rate through the envelope at 50 Pa	2.0 m3/(m2h)
Mechanical ventilation supply air temperature	21°C (Outdoor air T < 7°C) 16°C (Outdoor air T > 8°C)
Cooling - heating set point temperatures	25°C - 21°C
DHW supply set point	55 °C
Water network temperature	5 °C
Ventilation heating water supply inlet temperature	50 °C
Ventilation heating water flow rate	582.02 kg/h
Radiant panels heating water supply inlet temperature	35°C
Radiant panels heating water flow rate	352.22 kg/h
Ventilation cooling water supply inlet temperature	10 °C
Ventilation cooling water flow rate	1018.53 kg/h
Radiant panels cooling water supply inlet temperature	16 °C
Radiant panels cooling water flow rate	322.14 kg/h
Hot storage tank set point	Accordingly to the requested load temperature
Average internal loads	7.2 W/m^2

For the simulation, the office was divided into five different rooms as described in Figure 4.1. Some small spaces/rooms were joined together as one room. The hourly profiles of the heating and cooling building energy requirements are

calculated for each room according to their own internal heat gains. In order to preserve the homogeneity between the building and the system models, the same weather file has been used in both simulations. In particular, the hourly building thermal loads have been processed in the system model as described in the introduction of Section 4.1.

Figure 4.2 shows the external air temperature and the solar radiation of Tampere. This information belongs to the weather data file used in the simulations. It refers to the Meteonorm database [Meteonorm, 2015].

The winter period is very cold, with severe external temperatures; in contrast, the summer period is quite mild.

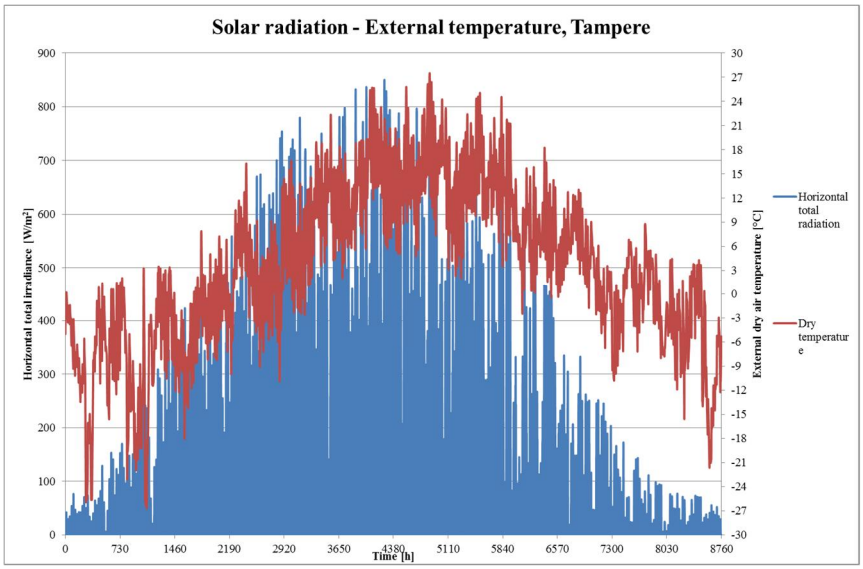

Figure 4.2. External air temperature and total horizontal solar radiation of Tampere.

4.2 Simulation and system sizing

The aim of the simulation is to assess the yearly and seasonal energy performance of two solar-cooling-driven system configurations: solar collectors, a tank and chiller connected in series or parallel, for an office building in northern Europe. TRNSYS software has been used to perform such an analysis. The building represents the office of Savo-Solar Oy Company in Mikkeli, Finland. A parametric analysis focusing on the influence of the storage tank volume and on the size of the solar thermal field has been conducted as well [Reda et al., 2016]. District heating has been considered as the heating source, in winter, and as hot

backup for the absorption chiller in summer. A simulation assessment has been carried out as preliminary activities to design the real control. Therefore, the system layout considered in the simulation slightly differs to the experimental system. However, the conclusion about the operating strategies found through this assessment is valid also for the experimental system, since changes were not so important as to affect them. Indeed, the main change between the simulation and experimental layout was in regard to the cold tank. Indeed, the simulation system layout did consider a cold storage tank. However, the effect of the cold storage tank was not so big, since the size was quite small compared to the application.

The building was built in 2012 as an extension to the side of the existing factory hall. The thermal properties of the building meet the requirement of the Finnish Building Energy Efficiency regulation of 2012. Data have been gathered onsite, from the technical construction report and missing information from [Ministry of Environment, 2012a].

The hourly building thermal loads were calculated with the program Dynamic Building Energy Simulation (DBES). The program developed on Matlab is based on the response factor theory for the transient analysis of the thermal heat transfer in the building structures. It was developed and verified as a task of the Finnish Tekes-founded project, Distributed Energy System [Sipilä et al., 2015].

The heat sources of the absorption chiller are the solar thermal collectors and the district heating system. In particular, a district heating system is used as a backup source whenever the temperature of the carrier fluid supplied to the desorber of the chiller is below the requested temperature. The district heating supply temperature varies throughout the year in Finland. Usually it goes from 115 °C, in winter, to 70 °C, in summer.

Solar thermal collectors supply energy through the hot tank to the building for covering part of the heating load. The Savo-Solar SF100-03 solar thermal collector has been considered in this study. Table 4.2 shows the main technical features of the solar thermal collector, the heat exchanger, between the solar primary and secondary sides, the cold and hot tanks, the circulation pumps and also the sizes of the considered solar thermal field and tank. It is important to notice that the cold tank has been considered only in the simulation. The experimental system does not include a cold tank. A very good practice for increasing the utilization rate of the solar thermal system, and in general system efficiency, is to adopt a variable speed pump as a solar circulator pump. This allows the achievement of higher solar thermal system temperatures when requested by the desorber. Therefore, a three speed controlled circulation pump has been considered in both primary and secondary solar loop. Decreasing the flow rate allows the achievement of higher temperature out of the solar thermal collectors, optimizing the use of available radiation.

Two system configurations, identified from now on as Case 1 (series) and Case 2 (parallel), have been assessed. Figure 4.3 shows the comprehensive scheme of the analysed solar cooling system in TRNSYS view. Actually Figure 4.3 refers to the Case 1 system. However, the figure gives an overview of the system, since only some connections change with regard to Case 2.

A key issue is the control of the desorber driving heat temperature. The choice of this temperature has been supposed only as a function of the external air temperature without considering the chilled capacity. Indeed, the principle of the implemented strategy is to guarantee that the chiller is always able to supply the maximum chilled capacity.

Table 4.2. Solar thermal system, hot and cold tanks main technical features. Note: It is important to notice that the cold tank has been considered only in the simulation. The experimental system does not include a cold tank.

Solar thermal filed			
Surface of one solar collector	2 m^2		
Tilt angle	50°		
	η_0 (Intercept efficiency)	a_1 $W/(m^2K)$ (Efficiency slope)	a_2 $W/(m^2K^2)$ (Efficiency curvature)
Solar thermal collector Efficiency η_{stc}	0.9	3.6	0.013
Total area	36 m^2; 24 m^2; 18 m^2 (All the panels have been connected in parallel)		
Storage tanks			
Hot tank capacity / solar surface [$lt_{,tank}/m^2_{,solar\ collectors}$]	27.8-41.7-55.6-69.4-83.3		
Cold tank capacity	0.35 m^3		
Loss coefficient	0.66 W/m^2K		
Solar heat exchangers			
Overall heat transfer coefficient of exchanger	5000 W/K		
Circulation pumps (Primary and secondary sides) [52]			
Flow rate (three speed pump)	66.6 – 46.6 – 23,35 l/(h, m^2 solar collectors)		
Power (2400l/h – 1200 l/h)	90 - 50 W		

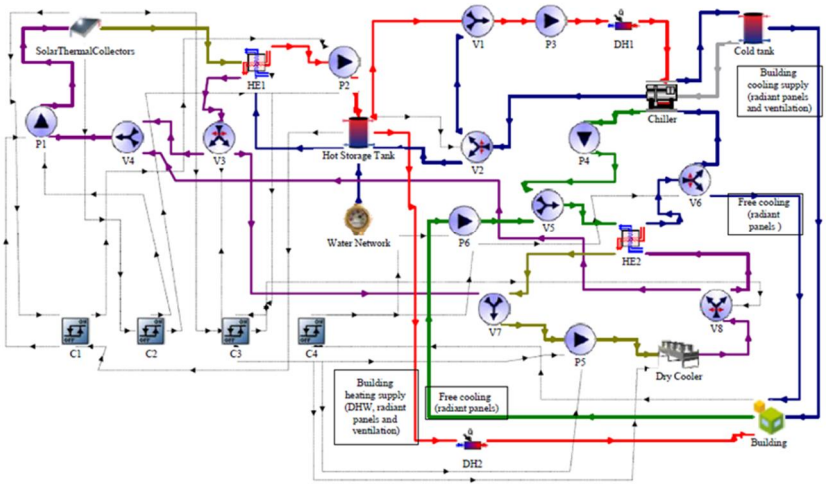

Figure 4.3. Solar cooling system comprehensive TRNSYS view of Case1.

The carrier fluid that circulates in the secondary side of the heat exchangers is water, while the carrier fluid that circulates in the primary side of the heat exchangers is mixture of water and propylene glycol at 40% (purple and gold connection in Figure 4.3). The heat capacity of this mixture has been assumed as 3.795 kJ $kg^{-1}K^{-1}$.

Figure 4.4 shows the correlation between the desorber driving heat temperature and the external temperature implemented in the simulations. This curve consists of 5 linear segments. They have been created considering the specification of the chiller manufacturer and the temperature drops in both solar and dry cooler heat exchangers (respectively HE1and HE2 Figure 4.3); both assumed to be 2 °C.

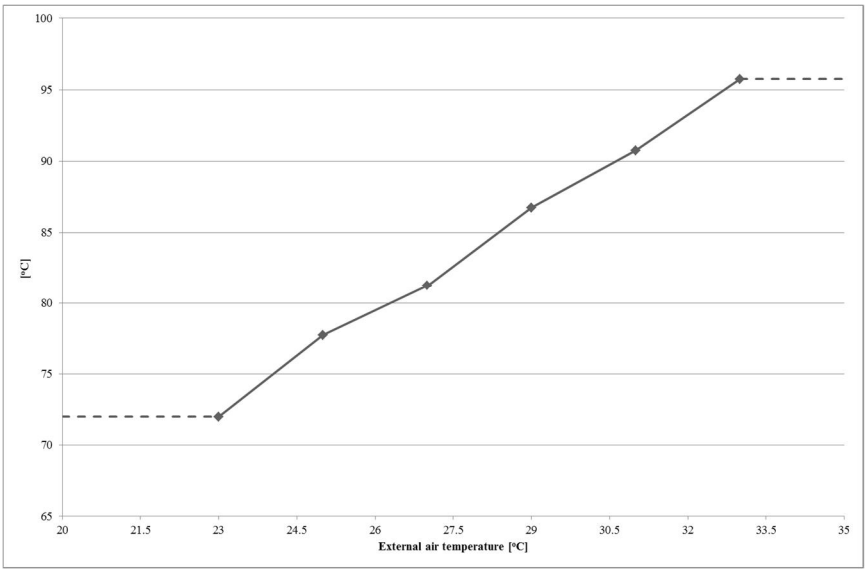

Figure 4.4. Driving heat set point temperature.

The cold tank (not realised in the pilot case) is instead used as a buffer; this allows a shaving of the cooling peaks. The green, red and blue connections in Figure 4.3 refer to water, while the remaining connections to a mixture of water and propylene glycol at 40%.

Case 1 (Reference case) - Solar collectors connected to the chiller via a hot storage tank

The Case 1 system has been considered as the reference case, since this system configuration has been identified as the most common. The Case 1 system configuration can be appreciated in Figure 4.5. It is important to notice that the HE1 (Fig. 4.3) is connected only to the hot storage tank and the tank to the absorption chiller, generating a series connection. The loading of the hot storage tank by means of the solar thermal collectors is regulated by C1 (Fig. 4.3). Indeed, it controls both P1 and P2 circulation pumps, triggering them when the outlet temperature of the solar thermal collectors is higher than 4 °C, if the pumps are not operating. Furthermore, in a continuous operation regime, C1 keeps the pump running when the aforementioned temperature difference is higher than 2 °C. In addition to this the working flow rate of the solar circulation pumps has been controlled. This is done by C2 (Fig. 4.3) and it has been set accordingly to the heat driving temperature required by the desorber. In particular, when the outlet temperature of the heat exchanger secondary side is lower than the driving heat set point temperature, the flow rate decreased to the lower value. Instead, when the outlet temperature is higher than 5 °C the flow rate increases to the maximum value. In the case of overheating of the solar thermal collectors, C3 (Fig. 4.3)

drives part of the flow rate of the solar thermal collectors, through V3, to the dry air cooler, in order to cool down the solar collectors. The last controller, C4 (Fig. 4.3), controls the FC supply. Indeed, when the external temperature is below the inlet temperature of the radiant panels the dry air cooler will be used to supply cooling energy. DH1 and DH2 (Fig. 4.3) are the backup heating sources respectively for the chiller and the building heating energy.

Case 2 - Solar collector connected in parallel with the tank and the chiller
Case 2 differs from the reference case for the hot storage tank connection. Figure 4.5 focuses on the hot storage tank connections of this specific case. In particular, HE1 (Figure 4.5) is connected to the hot storage tank and to the chiller desorber. The direct connection is triggered when the solar thermal collectors are able to supply directly the desorber of the chiller, accordingly to the driving heat set point temperature. When the direct connection is triggered, the hot storage tank can also be loaded. Only when the tank is used to supply the desorber can it not be loaded. Indeed, the tank has only one inlet and one outlet connection dedicated to chiller operations.

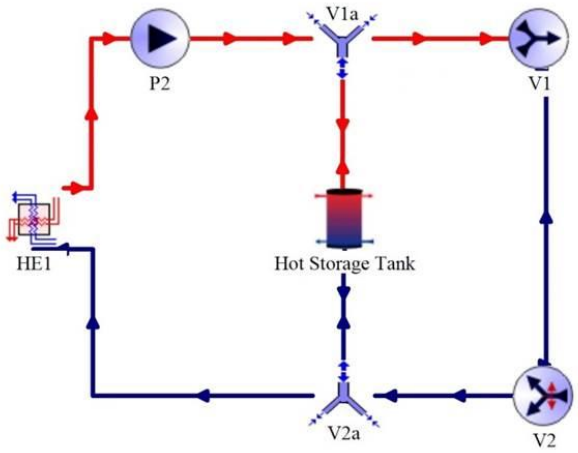

Figure 4.5. Case 2 hot storage tank connections.

Table 4.3 summarizes the analysed cases, giving a brief description of each case and showing also the sizes of the solar thermal system and the ratios between the hot tank capacity, with the solar surface taken into account. For each case, three solar thermal field sizes have been considered (S1, S2, S3; Table 4.3).

Table 4.3. Concise description of the analysed cases.

	Description	**Solar thermal system [m²]**		
Case1	Solar thermal collectors connected to the chiller via hot storage tank	**S1** 36	**S2** 24	**S3** 1
Case2	solar thermal collector connected in parallel with the tank and the chiller	**Hot tank capacity / solar surface [$l_{,tank}/m^2_{,solar\ collectors}$]**		
		27.8/41.7/55.6/69.4/83.3		

Results of the different cases are expressed as a function of the various ratios between the hot tank capacity and solar thermal field surface, as expressed in Table 4.3. The time step has been set to 0.25 h.

The considered performance indexes are stated below:

$$PER = \frac{\sum Q_{i,out}}{\sum\left(\frac{\sum E_{i,in}}{\varepsilon_{el}} + \frac{\sum Q_{i,in}}{\varepsilon_{DH}}\right)} = \frac{Q_{HD} + Q_{CD} + Q_{WD}}{\left(\frac{E_{P1} + E_{P2} + E_{P3} + E_{P4} + E_{P5} + E_{ch} + E_{dry}}{\varepsilon_{el}} + \frac{Q_{DH}}{\varepsilon_{DH}}\right)} \quad (5)$$

where:

$$Q_{DH} = Q_{DH,d} + Q_{DH,b}\ . \quad (6)$$

The electricity and district heating primary energy factors (ε_{el} and ε_{DH}) have been assumed respectively to be 1.7 and 0.7. PER gives more detailed information according to economic or environmental points of view. The authors have utilized the PER index due to the different quality ratings of the considered hot sources of the chiller (solar thermal collectors and district heating).

The building cooling, heating and DHW solar fractions of the different cases have also been presented, they are stated as:

$$SF_{,c} = \frac{Q_{sol,chiller}}{Q_d} \quad (7)$$

$$SF_{,h} = \frac{Q_{sol,building\ heating}}{Q_{HD}} \quad (8)$$

$$SF_{,DHW} = \frac{Q_{DHW}}{Q_{WD}} \quad (9)$$

and

$$SF_{,h+DHW} = \frac{Q_{sol,building\ heating+DHW}}{Q_{HD} + Q_{WD}} \quad (10)$$

Moreover, authors have referred to $SF_{,tot}$, which considers the whole solar contribution to the system. This is stated as:

$$SF_{,tot} = \frac{Q_{sol}}{Q_{HD} + Q_{WD} + Q_d} = \frac{Q_{sol,building\ heating+DHW} + Q_{sol,chiller}}{Q_{HD} + Q_{WD} + Q_d} \quad (11)$$

Figure 4.6 shows the energy supplied to the building, sorted by different sources, as a function of the V/S ratio (tank volume/ solar collectors' surface). Clearly the building loads are heating dominated and the solar contribution rises, increasing the V/S ratio, especially going from small ratios to medium. Furthermore, the solar contribution to the DHW is quite stable along the V/S ratios. Indeed, the $SF_{,DHW}$ is almost constant increasing the V/S ratio (Figure 4.6). Clearly, the tank size is not influenced by the DHW load, being quite small compared to the building heating requirement. On the other hand, the tank size influences the $SF_{,h}$, which varies from 15% to 28%, going from a small V/S ratio to a high ratio (Figure 4.6). Therefore, a system with a small tank is able to cover almost the same DHW demand of a system with large tank, but its $SF_{,h}$ (8) is considerably low compared to the system with a large tank. Thus, 55.6 l/m^2 can be considered a good V/S ratio. Indeed, there is no need to have a very large storage tank to increase the solar thermal collectors' capability of supplying heating energy.

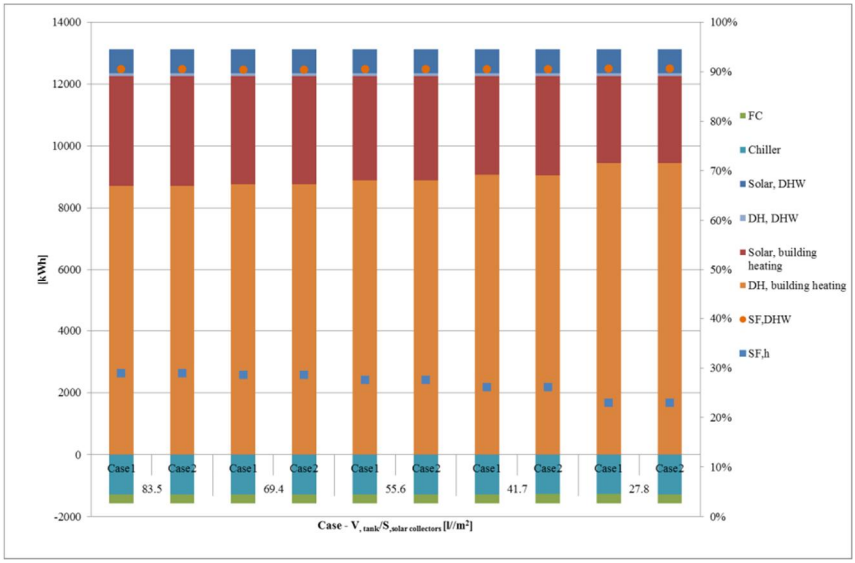

Figure 4.6. Energy supplied to the building by means of the different system components, $SF_{,DHW}$ (right axis) and $SF_{,h}$ (right axis) for the analysed solutions per various ratios between the volume of the hot storage tank and solar collector

surface. Note: DH (district heating), FRC (free cooling). Solar thermal system: S3 (Table 4.3).

Obviously, most of the building heating energy is supplied by means of the DH. As specified in Figure 4.6, the role of FRC is minor compared to the chiller. Indeed, FC covers the 47% of the radiant panels cooling load, which represents the 19% of the total building cooling load.

Figure 4.7 shows the delivered energy to the desorber from DH, the hot storage tank and directly from the solar collectors via the heat exchanger, in the case of Case 2 systems only, as a function of the V/S ratio (tank volume/ solar collectors' surface). Moreover, the $SF_{,c}$ (7) is also depicted. This figure sheds light on the different performance of Case 1 and Case 2, emphasizing the solar thermal energy contributions to the desorber. Case2 systems show higher $SF_{,c}$ than Case1 systems for all the considered V/S ratios. The $SF_{,c}$ of both cases (Case1 and Case2) rises increasing the V/S ratio, reaching a plateau at 55.6 l/m^2. This means that the solar thermal system has been pushed to its operational limit. At this point, for increasing the $SF_{,c}$ a bigger solar thermal system size would be needed. Interesting to notice is that the difference in $SF_{,c}$ between Case 2 and Case 1 is significantly higher than for higher V/S ratios when the V/S ratio is small. Indeed, a small tank has limited ability to store heat rather than a large tank. Basically, it does not store enough energy during periods with high solar irradiance, failing to supply heat to the desorber during hot cloudy days. Instead, Case 2 system solutions benefit also from the direct connection between the solar thermal collectors and the chiller (blue bar in Figure 4.7). This is due to the priority given to the direct connection over the tank for supplying the chiller. The direct connection is used when solar irradiance levels are high enough, allowing the tank to stay loaded.

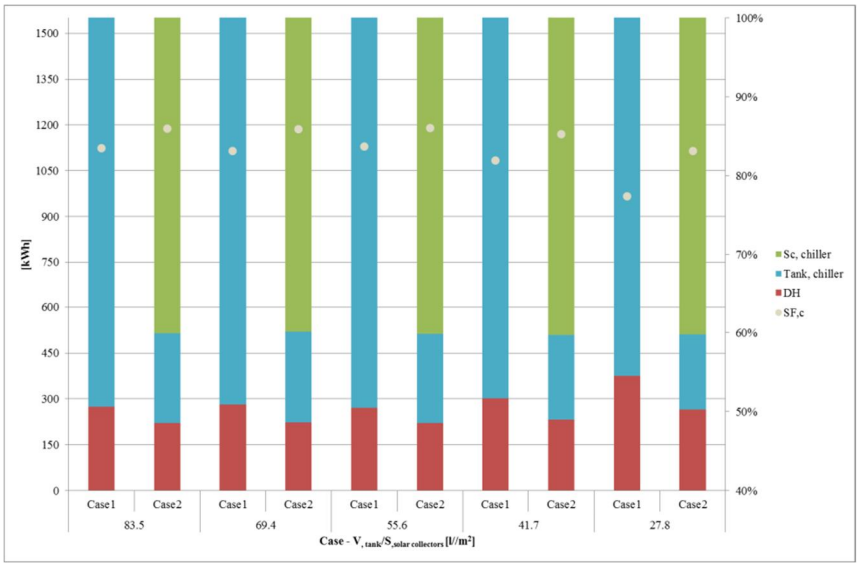

Figure 4.7. Energy delivered to the desorber from the DH, the hot storage tank and directly from the solar collectors via the heat exchanger (Sc) and $SF_{,c}$ (right axis) for the analysed case per various ratios between the volume of the hot storage tank and solar collector surface. Solar thermal system: S3 (Table 4.3).

Practically, when the solar irradiance is abundant both cases effectively use the produced solar thermal energy to run the cooling system. In this situation there is even a surplus of the produced solar thermal energy, which is stored in the tank. Indeed, the temperature in the tank increases, even though it is used to supply the desorber. This is possible because of the large solar collector area and the relatively low external temperature, which allows for keeping the desorber driving temperature low. Instead, when the solar irradiance is moderate Case2 solutions perform far better than Case1 solutions.

4.3 Result of solar configurations

Results of the solar configurations: S1 and S2 (Table 4.3) are now presented. In particular, a comparison, in terms of PER indexes (summer, winter and annual), between all the solar configurations (S1, S2 and S3, Table 4.3) has been elaborated. Figure 4.6 and Figure 4.7 offer a comparison between Case 1 and Case 2 with different solar configurations in terms of PER and SF as a function of the V/S ratio. The first figure refers to $PER_{,win}$ and $SF_{,h+DHW}$ (8), while the second to $PER_{,sum}$ and $SF_{,c}$. In both figures the reddish points indicate the SF, while the other the PER. Case 2 and Case 1 system (Table 4.3), which adopt the same solar thermal system size, perform similarly in winter ($PER_{,win}$). Indeed, the $SF_{,h+DHW}$ points from both cases overlap. As expected, $PER_{,win}$ and $SF_{,h+DHW}$ are

strictly connected. They have a similar trend for the same solar thermal system size. Furthermore, the solar contribution rapidly rises increasing the V/S ratio, especially going from a small V/S ratio (13.8 l/m^2) to a medium one. As for the S3 configuration, as discussed in the previous section, 69.4 l/m^2 is an effective ratio also for S2 and S3. In particular the $SF_{,h+DHW}$ corresponding to this ratio are 33%, 25% and 21% respectively for S3, S2 and S1.

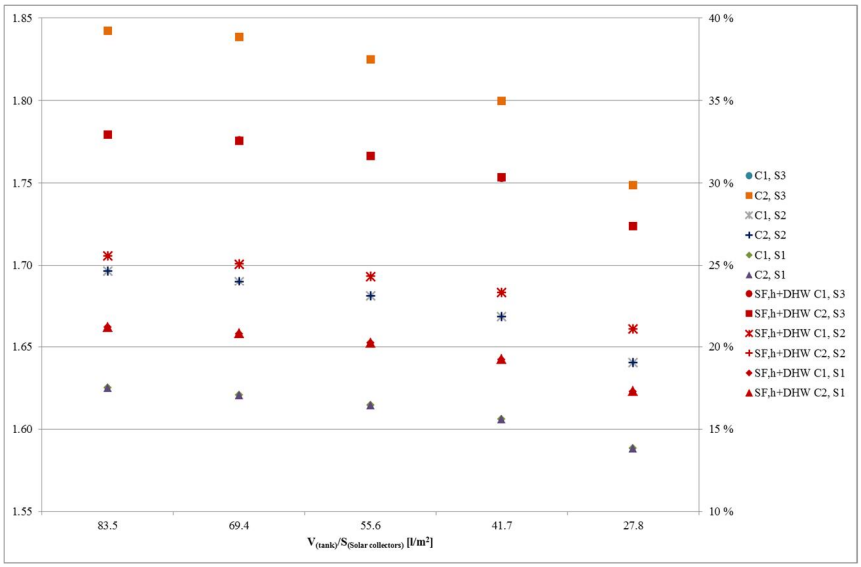

Figure 4.8. $PER_{,win}$ and $SF_{,h+DHW}$ of Case1 and Case2 configurations per various ratios between the volume of the hot storage tank and solar collector surface and different solar configurations: S1, S2 and S3 (Table 4.3). Note: only the $SF_{,h+DHW}$ refer to the right axis.

During summer operations, Case2 solutions show better performance than Case1 solutions also for the solar configurations S1 and S2 (Figure 4.9). In particular, the same conclusions can be drawn for S2 and S1 solar configurations as were done for S3 previously. 69.4.l/m^2 and 55.6 l/m^2 can be considered the most suitable tank configuration respectively for S3-S2 and S1 for summer operations. Interesting to notice that, with regard to S2 and S1 (Figure 4.9), the $SF_{,c}$ decreases for a very high V/S ratio. This is due to the fact that the solar thermal system is very much down-sized; therefore it is not able to keep a big tank at a high temperature.

Moreover, cooling operations of S2 and S1 Case 2 systems ($SF_{,c}$,Figure 4.9) with the smallest tank (27.8 l/m^2) are higher than Case1 systems with the biggest tank (83.5 l/m^2). This emphasizes that systems with a small solar thermal field, where bringing the tank up to high temperatures is difficult, particularly benefit from Case2 configuration brings.

It is important to mention that PER values are strongly influenced by the primary energy factors of the considered location. Indeed, making a direct comparison with similar systems located in different localities could be misleading. For instance, considering another system that is located in Germany, the most similar location to Finland, the estimated value of $PER_{,sum}$ is about 2.2, if a heating burner is used as an auxiliary system. This result refers to a $SF_{,c}$ of 88%; it falls near the $SF_{,c}$ of Case1 system with an S3 and V/S ratio of 69.4 l/m^2 (83%,Figure 4.9). Case1 $PER_{,sum}$ is 3.38, which is considerably higher than the value achieved by the German system. This is due to the primary factors considered in this other study, which are 2.7 and 1.1 respectively for electricity and the gas burner. They are far higher than the Finnish ones, which are respectively 1.7 and 0.7.

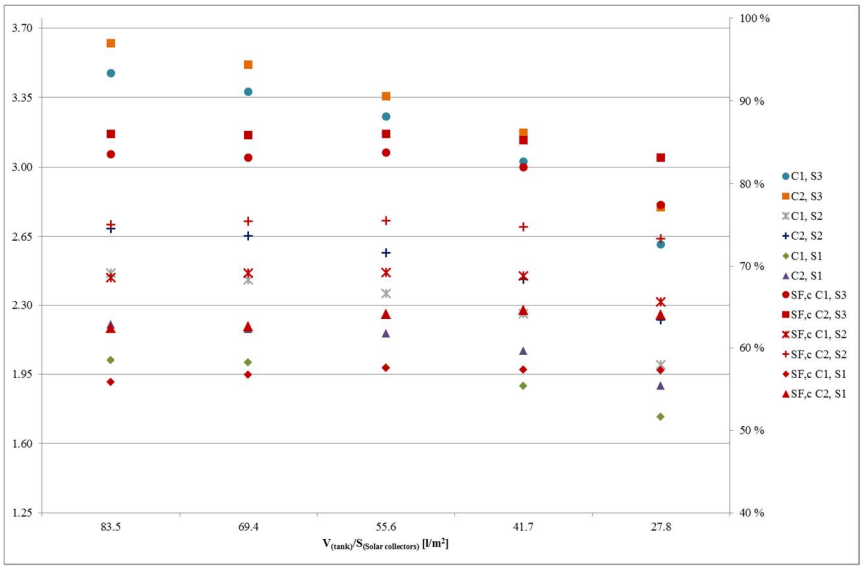

Figure 4.9. $PER_{,sum}$ and $SF_{,c}$ of Case1 and Case2 configurations per various ratios between the volume of the hot storage tank and solar collector surface and different solar configurations: S1, S2 and S3 (Table 4.3). Note: only the $SF_{,c}$ refer to the right axis.

Figure 4.10 shows $PER_{,annual}$ and $SF_{,tot}$ (11) of Case1 and Case2 configurations. It is obvious that the largest considered solar thermal field (S3) has higher performances than the others and that $PER_{,annual}$ is connected to $SF_{,tot}$. As expected, Case 2 solutions have slightly higher $PER_{,annual}$ than Case 1 (Figure 4.10), because of the summer system operations (Figure 4.9). Finally, it can be concluded that the most suitable V/S for all the cases is 55.6 l/m^2 (Figure 4.10), since adopting a bigger tank is not worth the investment; indeed the $PER_{,annual}$ does not considerably grow.

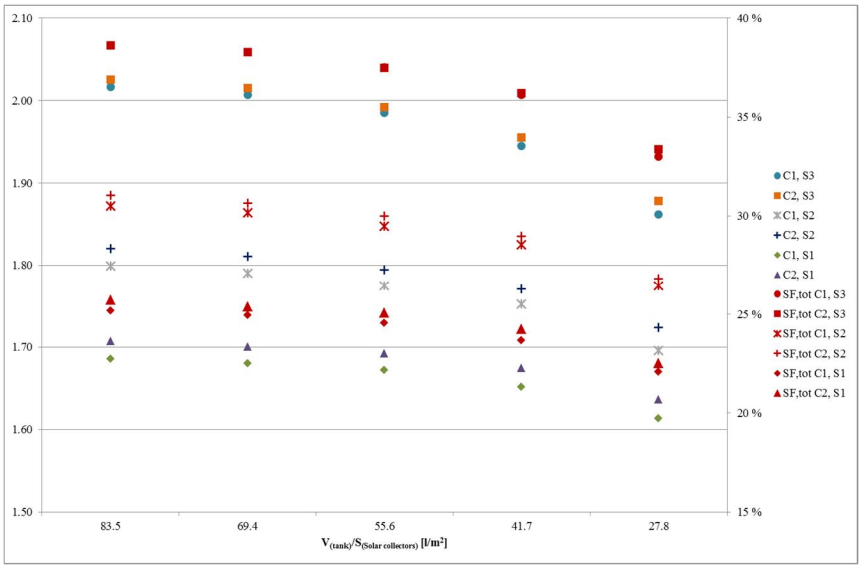

Figure 4.10. $PER_{,annual}$ and $SF_{,tot}$ of Case1 and Case2 configurations per various ratios between the volume of the hot storage tank and solar collector surface and different solar configurations: S1, S2 and S3 (Table 4.3) Note: only the $SF_{,tot}$ refer to the right axis.

4.4 System concept, operation modes and control of the SHC-system

The SHC-system pilot plant is located in Mikkeli, Finland and supplies heat and cold to the Savo-Solar Oy office building. As the biomass-driven desorber is still in a prelaminar test status, the available district heating network serves as a backup heat source to ensure a reliable energy supply.

The commissioning the pilot plant was done in January 2016 with a following optimization of the system from March to June 2016 in cooling mode and from October to November 2016 in heating mode. Furthermore, the measuring data transfer to VTT and ZAE Bayern was automated and the control strategy of all operation modes are already tested and adjusted to the building needs. The absorption chiller has a nominal cooling capacity of 10 kW and in heat pump mode a heating capacity of 24 kW. The nominal inlet and outlet temperature of the extern water flows in the different numbered subsystems of the hydraulic installation, as shown in Figure 4.11, are:

#1XX	Solar primary glycol circuit	95-82 °C by a volume flow of 1.4 $m^3 \cdot h^{-1}$

#2XX	Solar secondary water circuit	92-80 °C by a volume flow of 1.2 $m^3 \cdot h^{-1}$
#3XX	Driving water circuit	90-80 °C by a volume flow of 1.0 $m^3 \cdot h^{-1}$
#4XX	Reject heat/heating water circuit	37-45 °C by a volume flow of 2.5 $m^3 \cdot h^{-1}$
#5XX	Chilled water circuit	15-10 °C by a volume flow of 1.7 $m^3 \cdot h^{-1}$
#6XX	Dry air cooler glycol circuit	35-43 °C by a volume flow of 2.8 $m^3 \cdot h^{-1}$

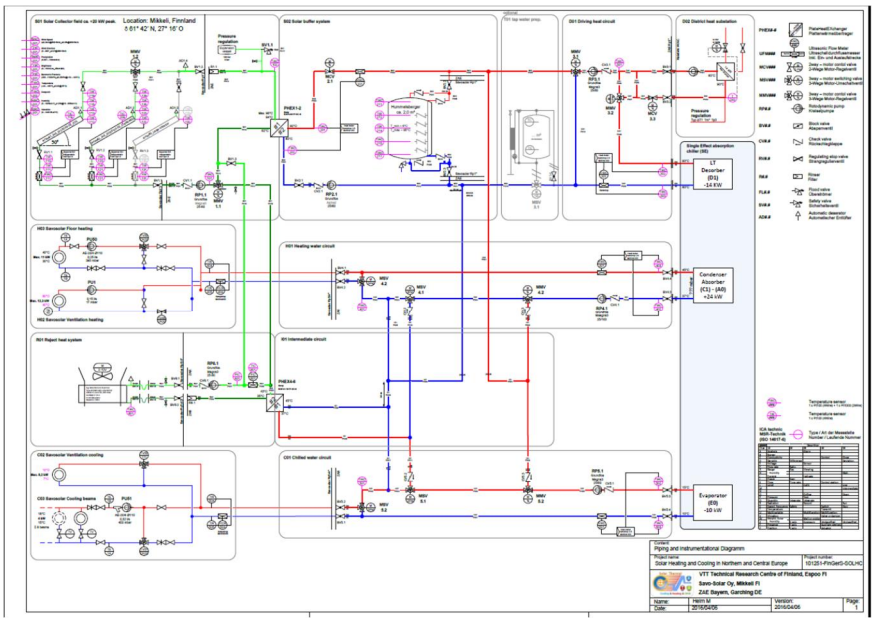

Figure 4.11. Piping and Instrumentational diagram (P&ID) of the pilot installation at Savo-Solar, Mikkeli.

For real-time visualization and scientific analysis of the system key figures and operation modes, the software ‘Labview’ from National Instruments is used. All signals of the sensors, pumps, valves and so on are transferred to ‘Labview’ and processed, logged and finally transferred to the databases at VTT and ZAE Bayern.

For the control purposes of the solar heating and cooling system, an affordable freely programmable universal control from the company ‘Technische Alternative Elektronische Steuerungsgerätegesellschaft m.b.H’ is used. The system provides 128 optional combinable function blocks and thus allows a simple programming via drag and drop and logical wiring. Additionally, it is possible to control and manually set all switching states by means of a graphical touch interface. The

control strategy includes the following operation modes. Further simplified operation modes schemes are provided in the annex! The numbers indicate the preferred operation modes in sequence for heating and cooling separately. But, the system is designed to operate in a mixed mode as well. In the case of simultaneous heat and cold demand, the dominating energy consumption defines the operation mode.
#C1_Free Cooling
#C2_Solar Cooling
#C3_Backup Cooling
#H1_Solar Heating
#H2_HeatPump(Air)
#H3_HeatPump(Solar)
#H4_BackupDistrictHeating

Some control functions work independently of the chosen operation mode. These are internal control of the absorption chiller, all safety criterial, the solar collector field and the loading of the buffer tank, where only the set point temperature varies. All devices are labelled according to Standard ISO 14617-6 and ANSI/ISA S5.1 respectively, as shown in Figure 4.11.

4.5 Control of absorption chiller/heat pump internally

Before starting the chiller the two external hydraulic circuits chilled water and cooling/heating water have to be activated first. The chilled water pump (RP5.1) runs IF the internal evaporator temperature (TIC01) is greater than 2 °C (+0.1/-0). Here, values in brackets indicate the switching hysteresis, which are mandatory for stable operation. Subsequently, the cooling/heating water pump (RP4.1) operates IF the internal temperature of the weak solution (TIC03) is greater than the calculated crystallisation temperature of the lithium bromide solution. Then, when the absorption chiller/heat pump is required, the internal solution and refrigerant pump are switched on in sequence. Solution Pump (RP02) runs WHEN Cooling pump (RP4.1) AND chilled water pump (RP5.1) are running AND all safety criteria are fulfilled. An internal ball valve of the absorption machine then regulates the aqueous lithium bromide solution flow from the absorber to the Desorber proportionally with reference to the current chilled water capacity. Thus, a good thermal Coefficient of Performance COP even in part load is achieved. Refrigerant pump (RP01) runs WHEN Chilled water pump (RP5.1) AND the internal evaporator temperature (TIC01) are greater than 2 °C. Finally, the driving heat pump (RP3.1) runs IF all other pumps (internal and external) are in operation AND the internal temperature of the strong solution leaving the Desorber (TIC04) is below the calculated crystallisation temperature. WHEN the absorption chiller is not required any more, the shutdown routine with demand-actuated dilution begins. In a first step, the driving heat pump (RP3.1) stops operating immediately.

Then, the cooling AND chilled water pump (RP4.1 /RP5.1), solution AND refrigerant pump (RP01 /RP02) follow up until the temperature difference between the condenser (TIC02) and the strong solution (TIC04) drops below 45 K. A follow-up time of at least 60 s guarantees the whole mixture of the solution in the absorption chiller. In addition to that, a magnetic bleed valve in the refrigerant loop pours a certain amount of refrigerant into the solution in order to reach uncritical concentrations, but only when necessary AND pumps RP01 AND RP02 are circulating. The overall goal of the dilution is to lower the concentration of the lithium bromide solution to 58% before standstill, but not less. Any further dilution does not increase safety level any more, but increases start-up time and in particular lowers the overall thermal COP. In addition, a small amount of solar energy can be 'stored' in the concentrated solution for the proximate start-up.

Besides the crystallisation of the aqueous lithium bromide solution, the freezing of the refrigerant has to be avoided at all times. Thus, IF the internal evaporator temperature (TIC01) drops below 4°C (+0.1/0) the bleed valve is activated and refrigerant is directly pumped to the absorber in order to reduce solution concentration and therefore the ability to absorb refrigerant vapour. By doing so, the absorption machine loses evaporator capacity and increasingly the fed-in heat to the desorber is emitted via the Condenser only. Thus, a smooth transition to #4BackupDistrictHeating mode is obtained.

4.6 Control of the solar collector and buffer tank circuit

The main objective is to gain as much solar heat as possible at the right temperature level. Here, the weather forecast helps to manage buffer charging according to the daily prediction of energy consumption, ambient air temperature and solar irradiation.

Depending on the weather forecast and operation modes, the required solar heat temperature level at sensor TIC201 is set. The solar pump (RP1.1) can only run at times between sunrise and sunset. This inherently precludes any unwanted operation during night-time. Due to safety reasons, three different sensors might activate the solar pump. IF the maximum of the aperture area sensor of the foil (TIC119) OR the standard (TIC129) collector climbs above the set temperature level of TIC201 (+5/+2 K) OR at more than 85 °C (+0/-5 K) the solar pump (RP1.1) starts circulating. Additionally, the pump starts WHEN the solar radiation (RIC001 / $W \cdot m^{-2}$) in the collector plain fulfils the following linearized equation

$$RIC001 > Set\_criterium\_solarfield \cdot 10 \cdot (TIC201\_Set - TIC001) \quad (12)$$

where (TIC201_set – TIC001) gives the minimal required temperature difference between the collector and ambient temperature according to the collector

efficiency curves in Figure 3.27. This helps to expedite the warm up of the entire collector circuit in the morning. Anyhow, the solar pump has a follow-up time of 5 minutes to avoid staccato runtimes. In any case the pump stops working IF the collector outlet temperature (TIC102) drops below 0 °C (0/+5 K) to prevent the plate heat exchanger (PHEX1-2) from freezing on the water side. Additionally, the collector inlet temperature (TIC101) must be lower than 110 °C (+0/-5 K) at any time. In the event of these two safety cases the follow-up time is neglected and the pump (RP1.1) stops immediately. During operation the flow in the solar collector circuit is adjusted by the proportional speed control of pump RP1.1 according to the solar irradiation in the collector plain (0 $W \cdot m^{-2}$ = 0% /1000 $W \cdot m^{-2}$ = 100%). This ensures an adequate temperature difference between the supply and return pipe and saves auxiliary electricity for pumping.

In order to prevent the solar collectors from stagnation, an emergency cooling via the dry air cooler in hydraulic circuit #6XX is activated WHEN the collector inlet temperature (TIC101) rockets above 85 °C (+0/-5 K) AND the solar collector pump (RP1.1) is running. THEN mixing valve MMV1.1 opens the bypass from the solar collector circuit to the dry air cooler and controls the supply temperature TIC101 to 88 °C. The simultaneously activated reject heat pump RP6.1 then transfers the heat through the bypass with about 2 $m^3 \cdot h^{-1}$. Meanwhile, fan speed is adjusted to a constant outlet temperature (TIC601) of 40 °C by means of a PID controller.
On the secondary side of the plate heat exchanger (PHEX1-2) heat is fed into the buffer tank by means of buffer tank pump RP2.1. IF the solar pump (RP1.1) is running AND the temperature (TIC102) of the solar collector system is 2 K above the TIC201_Set temperature, the pump starts to provide a constant head at flow control valve MCV2.1. THEN this valve adjusts the volume flow to the buffer tank in order to reach the required set temperature at TIC201. WHEN the buffer maximum temperature of 95 °C at the bottom of the tank (TIC217) is reached further charging is prohibited and MCV2.1 closes instantaneously, while RP2.1 stops only after 5 Minutes. There is also an anti-freeze protection which is set to 2 °C. If the collector outlet temperature TIC102 drops below this set value, the valve and pump are not allowed to operate.

Mode#C1: Free Cooling and Mode#C2: Solar Cooling

During summertime the SHC system is expected to operate in mode#C2 mainly as depicted in Figure 4.12. The absorption chiller provides chilled water with 10 °C to the Savo-Solar Office Cooling system by means of heat from the 18 standard and 18 improved foil solar collector panels at an adequate temperature level, which is defined by the lift to thrust correlation and moreover, the requested cooling capacity. A dry air cooler dissipates the rejected heat to the ambient air. Thus, the cooling water return temperature to the chiller correlates directly with the changing ambient air temperature. But, in contrast to wet cooling towers, no additional effort for water makeup, bacteria contamination etc. is needed.

IF the ultrasonic flow meter in the chilled water circuit of the building detects a certain volume flow (FIC504 > 0.25 $m^3 \cdot h^{-1}$ (+0/-0.1)) AND ambient temperature TIC001 is less than 15 °C (+0/+2 K), free cooling (see Figure 4.12) via the dry air cooler in hydraulic circuit #6 is possible. Therefore, the switching valve MMV5.2 connects reject heat circuit #6XX and chilled water circuit #5XX via the plate heat exchanger in the intermediate circuit and pump RP6.1 is started. Fan speed of the dry air cooler regulates TIC601 to 16 °C and the flow of FIC601 is proportionally adjusted to the chilled water flowrate measured at flowmeter FIC501. OTHERWISE the absorption chiller is requested.

IF the chiller signals availability, THEN the chilled water pump RP5.1 starts with variable speed adjusted to the chilled water inlet temperature (TIC502). Temperatures greater than 15 °C demand full speed, while the speed is linearly reduced until the temperature reaches 10 °C. The volume flow through the other pumps (RP4.1 /RP3.1 and RP6.1) are proportionally adjusted to the volume flow of the chilled water pump (RP5.1) in order to improve part load auxiliary energy efficiency (e.g. EER).

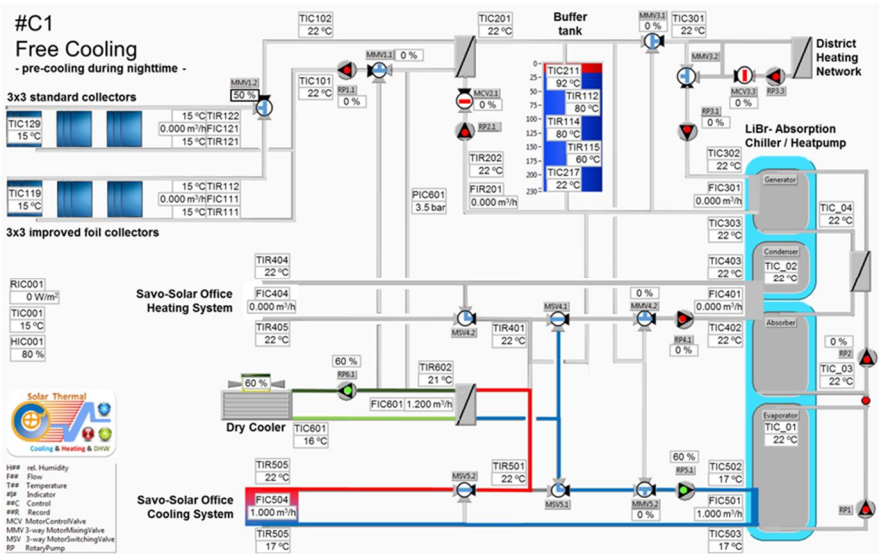

Figure 4.12. Schematic view of operation mode #C2 Solar Cooling.

Mode#C2: Backup Cooling

For reliable cold supply to the building, backup heat is needed (Fig. 4.13). The driving heat can be supplied by the buffer tank (MRV3.1) and/or the district heating network (MCV3.2). Due to reduced system temperatures in the district heating

network during summertime of about 70 °C, this backup system can only operate when the buffer tank temperature (TIC211) drops below that temperature.

Depending on the available temperature level of the buffer tank (TIC211), the cooling water outlet temperature of the dry air cooler TIC601 is set with respect to critical process parameters such as the crystallisation line of lithium bromide. The chilled water capacity of the chiller is adjusted by means of MMV3.1, in combination with the inlet temperature to the desorber (TIC302). If the buffer tank drops below 70 °C, the backup is required and supplies the absorption chiller with heat. Then the buffer tank is loaded again by the solar field.

If TIC211 exceeds 70 °C (+2/0), the backup is shut down and the buffer supplies the absorption chiller again. Due to the switching hysteresis, greater tactfulness is avoided. So the chiller minimum runtime in solar or backup cooling mode is around 60 min.

If the chiller is running by the buffer tank the set temperature TIC201 is the required temperature to achieve the cooling capacity.

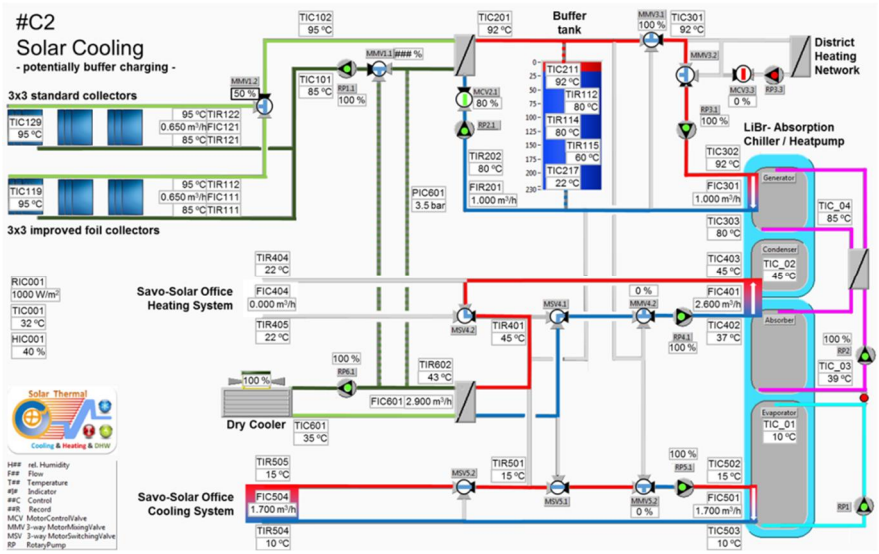

Figure 4.13. Schematic view of the operation mode #C2 Backup Cooling.

Mode#H1: Solar Heating

If the heating demand of the office is detected (FIC404 > 0.05 m³/h) and the buffer tank temperature (TIC211) is high enough, the solar heating is activated (Fig. 4.14). The pump RP.4.1 is started and the valve MMV4.2 adjusts the heating temperature depending on the heating curves of the office.

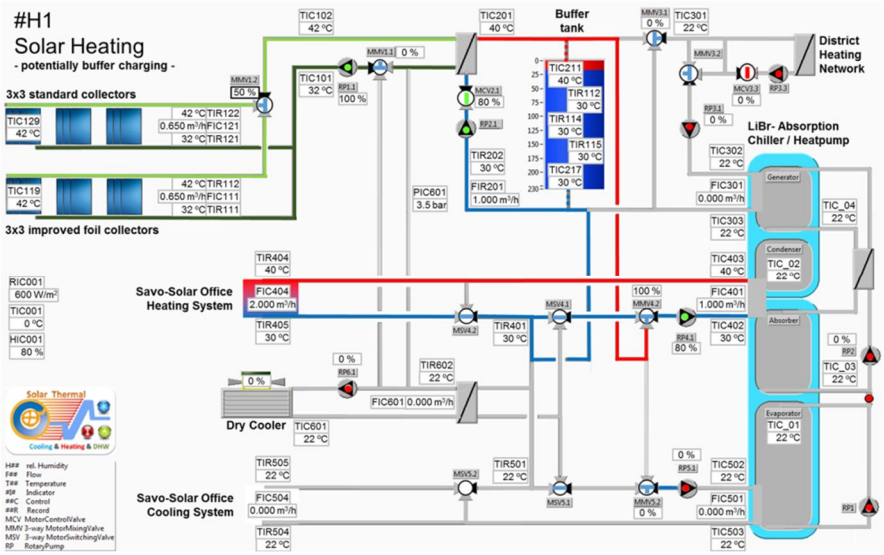

Figure 4.14. Schematic view of operation mode #H1 Solar Heating.

Mode#H2: Heat pump (Air) and Mode#H3: Heat pump (Solar)

If the heating demand of the office is detected (FIC404 > 0.05 m³/h) and the buffer tank temperature is too low for solar heating, the heat pump is required (Fig. 4.15). A check is made if the air can work as a low temperature heat source (ambient temperature > 8 °C). If not, the valve MMV5.2 supplies the heat source for the evaporator from the buffer tank (15°C to 5°C). The driving heat temperature depends on the required heating temperature of the office and is supplied by the backup system. The volume flow of the driving heat pump (RP3.1) and cooling water pump (RP4.1) are coupled to the volume flow of the chilled water pump (RP5.1).

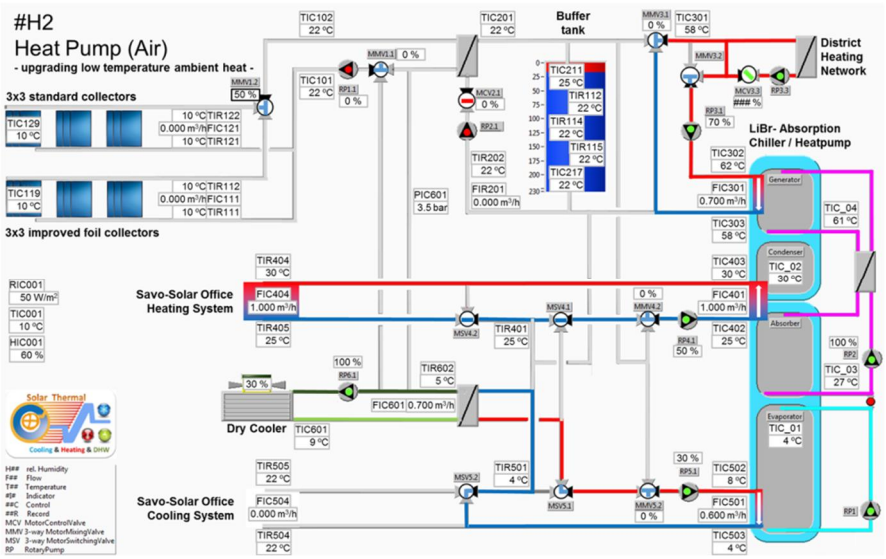

Figure 4.15. Schematic view of operation mode #H2 Heat pump (Solar).

If the air can supply a low heat source, valve MSV5.1 is active. The heat reject system is activated (RP6.1 and fan) and supplies a temperature from 15 °C to 5°C. The driving heat temperature depends on the required heating temperature of the office and is supplied by the backup system. The volume flow of the driving heat pump (RP3.1), the cooling water pump (RP4.1) and the heat reject system (RP6.1) are coupled to the volume flow of the chilled water pump (RP5.1).

Mode#H4: Backup district heating

If heating demand for the office is detected (FIC404 > 0.05 m³/h) and no solar heating or heat pump (air or solar) is possible the backup directly heats the office (Fig. 4.16). In this case the absorption chiller works as a ‘heat exchanger’. Therefore the backup is activated. The driving heat pump (RP3.1) is coupled to the heating pump (RP4.1). The solution pump (RP02) and refrigerant pump (RP01) are running at a fix speed. The driving heat is transferred to the solution in the desorber. There the refrigerant is desorbed and condenses in the condenser and delivers the heat to the heating circuit. The refrigerant runs down to the evaporator and is pumped back via the bleed valve to the solution from the desorber. The solution is than pumped to the desorber again and the circle is closed. Due to the effect as ‘heat exchanger’, no further low temperature heat source is used.

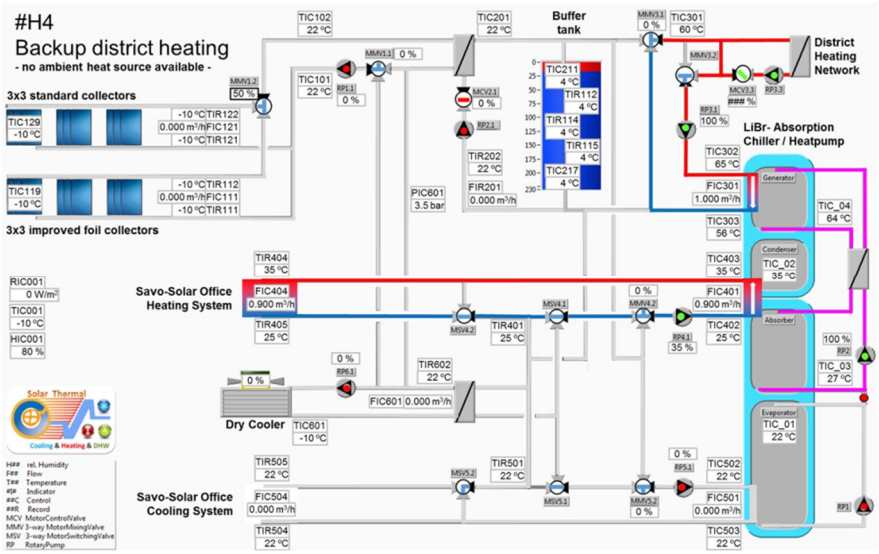

Figure 4.16. Figure 42: Schematic view of operation mode #H4 Backup district heating.

5. Subsystems and main components

The construction of the pilot plant in Finland, Mikkeli, was done between July 2015 and January 2016 in several phases. A flat-plate collector field with a 36 m² aperture area on the rooftop of the office building provides hot water for heating and cooling. The hot water buffer tank with a filling volume of around 2 m³ has been installed to store excess solar energy and comes with an optimized stratification system. By means of the compact absorption chiller/heat pump this heat is transformed to meet the building needs. During cooling mode, a dry air cooler on the office roof dissipates waste heat to the ambient air. In times with insufficient solar gain a connection to the district heating system is used as a backup heat source. The following chapter gives an overview of the different subsystems and their detailed technical design data.

5.1 Solar collector field

The solar field is located on the flat roof top of the office building (Fig. 5.1). The field is made of two rows of nine solar collectors at a distance apart of 3.45 m, facing south. On the back row are installed the standard SF100-03-DS collectors and on the front row are installed the proto version of the same collector with a foil as a second front cover. Each row is made of three parallel arrays of three collectors connected in series. The collector tilt angle is 50°.

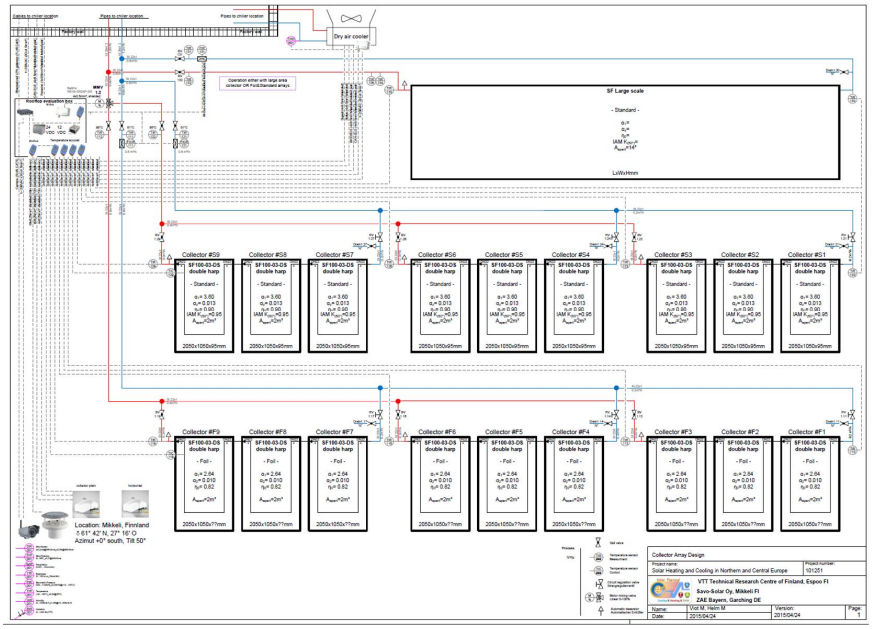

Figure 5.1. Piping and Instrumentational diagram (P&ID) of the solar collector field at Savo-Solar pilot installation.

The energy output of each collector array is measured separately by high accuracy temperature sensors and flow meters. The volume flow in the two collector rows is balanced with a 3-way motor mixing valve in order to maintain the same output temperature from both. Within each row the volume flow rate of each array is balanced by manual flow regulation valves. The pump and heat exchanger station for the solar field is located inside the factory building next to the rest of the solar heating & cooling system.

5.2 Buffer tank with an improved stratification device

Storing heat at the right temperature level is essential for matching volatile solar radiation and fluctuating building energy consumption in both operation modes of cooling and heating. In this respect, important key values (see Table 5.1) are, among others, the specific storage volume per square meter of collector aperture area, total storage volume, surface-to-volume ratio, insulation type, and the corresponding heat loss coefficient, as well as the hydraulic connection and temperature levels of the connected system.

Table 5.1. Key design values of buffer tank subsystem.

unit	Design criteria	SHC system value	Standard range
$dm^3 \cdot m^{-2}$	Specific storage volume per square meter of aperture area	55.5	40 - 100
$m^2 \cdot m^{-3}$	Surface-to-volume-ratio	4.15	Minimum 3
mm	Insulation inner layer	20	
$W \cdot m^{-1} \cdot K^{-1}$	Heat conductivity coefficient	0.040	Armaflex
mm	Insulation outer layer	200	
$W \cdot m^{-1} \cdot K^{-1}$	Heat conductivity coefficient	0.043	Mineral wool
°C	Temperature range	5 - 95 °C	0 - 110 °C
kWh	Maximum storage capacity	~ 210	N/A

The hot water storage tank used in this project has a height of 2 m and an outer diameter of 1.2 m, both measured without insulation. It has a volume of 2 m^3 and is equipped with an improved internal stratification device with five outlets, which are evenly distributed over the height of the tank. The functional principal of the stratification unit is based on the fact that the density of water is temperature dependent. If hot water with a low density enters the tank (e. g. at T = 80 °C, it has a density of 972 kg/m^3), it leaves the stratification device at an upper outlet, because the entering water is lighter than the cooler water volume already stored in the tank. Cold water with a higher density (e. g. at T = 20 °C, the density is 998 kg/m^3) sinks down in the stratification device and therefore leaves it at a lower outlet. As can be seen, the density difference between hot and cold water is not very high, but sufficient to use this effect to generate a good stratification.

The use of such a stratification device increases the stored exergy remarkably because entropy generation via mixing processes is mostly prevented. Moreover, in the present case, the operating time of the absorption chiller in combination with the solar thermal system can be extended with such a stratified storage tank. For example, if the return flow coming from the chiller is at 70 °C and the bottom temperature of the storage tank is 40 °C, the temperature would be mixed up to about 55 °C in a tank without a stratification device. This mixing temperature cannot any longer be used as a driving temperature for the generator of the absorption chiller for cooling. But, if the return flow with a temperature of 70 °C enters above the existing 40 °C layer, this temperature still suffices to drive the chiller, e. g. in the evening at decreased ambient temperatures below 30 °C. Thus, a stepwise cooling down of the buffer tank is achieved leading to a higher share of

solar fraction for cold production because the heat from the solar system can be used for a longer time.

Experiments from TU Chemnitz on stratification devices with open outlets show two negative effects, called sucking effects, which reduce the stratification efficiency significantly. The first effect describes the scenario when a storage, which is cold at the beginning, is loaded. Hot water entering the stratification device sucks cold water into the device from the storage through the open outlets of the stratification device. The water mixes and the temperature finally entering the tank is reduced.

The second effect occurs when a stratified storage tank is loaded by water with a temperature between the highest and the lowest temperature of the storage. The water in the stratification device sucks hot water from the existing layers at the top and partly destroys those layers. Thus, the exergy of the storage is reduced.

In a former project at ZAE Bayern a new stratification device with a flap mechanism was invented to get rid of those two effects. Flaps seal the outlets of the stratification device whereby no fluid can be sucked into the stratification unit. The density of the flap material is close to the density of water and can be lifted easily by the fluid streaming into the stratification device.

The outlet pipes of the storage are situated at the very top and bottom of the tank and are connected to the solar collector system and the absorption chiller, respectively. All four inlet and outlet pipes are equipped with check valves to prevent any unwanted circulation or maldistribution. In addition, each external circuit is closed by a valve (MCV2.1 and MMV3.1) during standstill. Heat from the buffer tank can be transferred to either the heating system of the building directly or the evaporator of the absorption machine via the intermediate hydraulic circuit IO1 and MMV4.2 or MMV5.2 (see Figure 4.11).

Figure 5.2 shows a cross-sectional view of the installed buffer tank with its two inlets and two outlets, the advanced stratification device, and the position of the five temperature sensors (length 1000 mm each). The tank also serves as a hydraulic separator between the different subsystems. Furthermore, the attached expansion vessel ensures a constant system pressure in the entire SHC system over the temperature range of 5 to 95 °C.

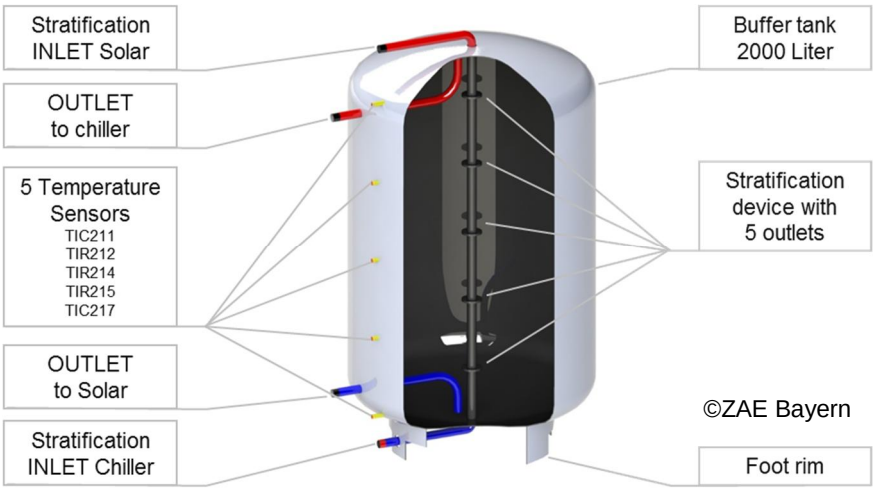

Figure 5.2. Cross-section-view of the 2000 Litre buffer tank with improved stratification device.

The company Hummelsberger, Germany [http://vacuum-storage.com/] normally manufactures such a storage tank with the improved stratification device from ZAE Bayern in combination with a vacuum super insulation (VSI). It is sold for volumes between 5000 and 40 000 liters. In this project the buffer tank is situated next to the absorption chiller in the temperature controlled factory hall. Due to that fact and for economic reasons, the vacuum super insulation option has been omitted.

An ideal stratification is explained in the example of loading a storage tank. The aim is to keep clearly separated layers. The tank has a stratification device with nine outlets to illustrate the example with a good resolution. At the beginning it has a temperature of 20 °C. In the time frame from 20 to 80 minutes it is loaded with a high temperature of 80 °C. The hot water leaves the stratification device at first at the top outlet until the first layer has a temperature of 80 °C completely. Now the second outlet and after 40 minutes the third outlet is used. The sharp rising edge characterizes the 'ideal' stratification, as no mixing of fluids and therefore temperatures takes place. After 80 minutes, the inlet temperature is reduced to 50 °C and now leaves at the outlets in the middle part of the tank. During this time, the upper layers stay untouched and thus keep their high temperature. The three layers at the bottom also keep their low temperature and do not cool down any layers above. In reality, there will be transition zones between the layers with a mix temperature, as can be seen in Figure 5.3 at the bottom right.

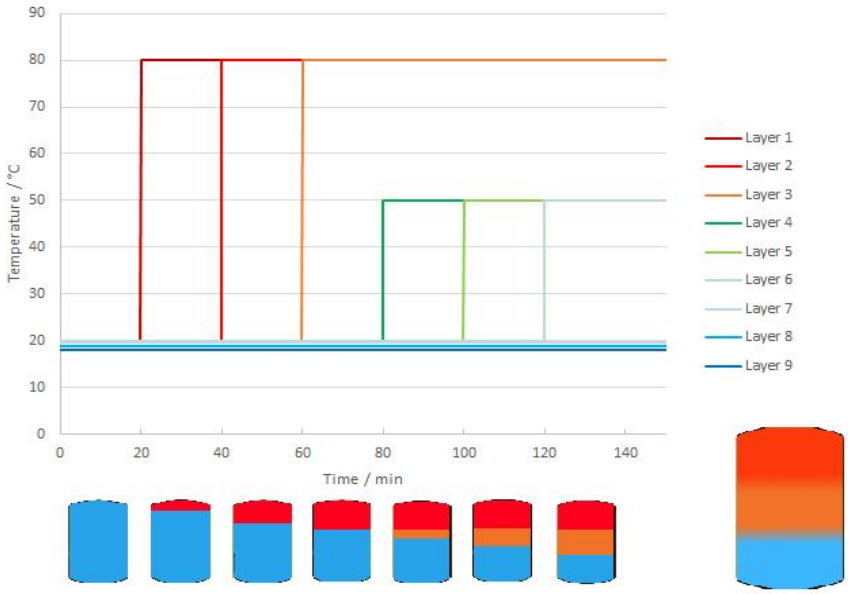

Figure 5.3. Ideal loading of a stratified storage tank with a stratification device of nine outlets. Start temperature: 20 °C, inlet temperature (20–80 min): 80 °C, inlet temperature (80–140 min): 50 °C. Bottom right: Stratified storage tank in reality with transition zones between temperature layers.

5.3 Absorption chiller / heat pump

The absorption chiller / heat pump design is based on the current status of research on the horizontal tube falling film heat exchanger technology. Adequately alloyed stainless steel thin-walled laser welded tubes and housing facilitate lightweight and reliable heat exchanger design and good specific performance. Figure 5.4 indicates the average temperature thrust (driving heat to cooling water) needed for a certain lift (chilled water to cooling water average) and capacity. It is calculated for cooling water temperatures of 15 °C return and 10 °C supply, but the uncertainty within the temperature range of 21 to 6 °C is less than ± 1 K. The red line with 0 kW indicates the theoretical limit to maintain the sorption process. Compared to other chillers, the required thrust is nearly halved, which allows for lower chilled water temperature at dry heat rejection and a low district heating temperatures of 75 °C.

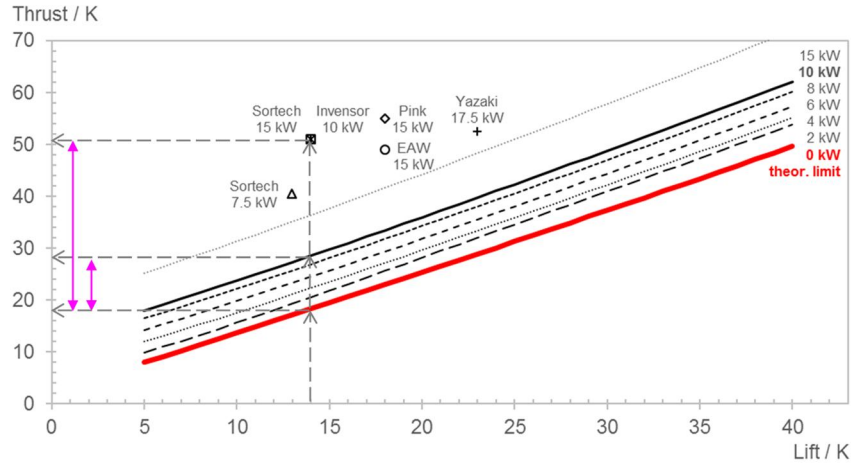

Figure 5.4. Average temperature lift versus thrust correlation of the improved absorption machine compared to available small scale COTS-products in Europe.

Figure 5.5 shows the compact absorption chiller with a cooling capacity of 10 kW and the integrated hydraulic module and measuring module on the right-side. The whole system is installed in a drain tray with a ground area of 0.8 to 1.2 meter. Through high pre-fabrication the onsite installation effort /costs are reduced by about 25%. Its agility and variability in various operation modes makes it attractive for many applications.

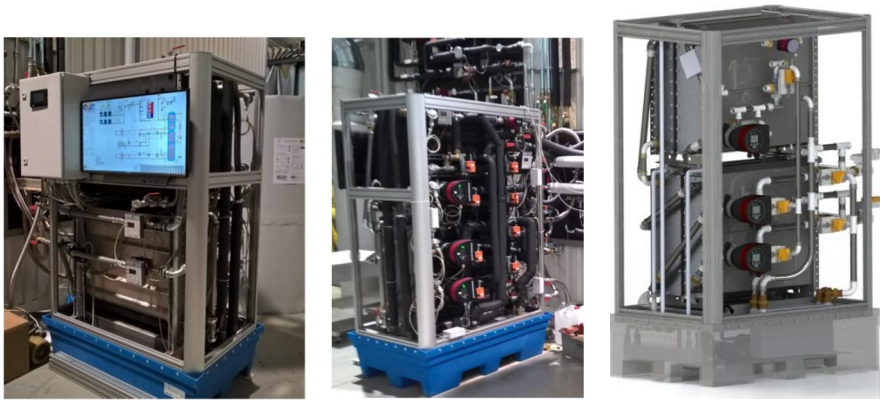

Figure 5.5. Sorption heat transformer with process visualization (left), integrated hydraulic module (middle) and rendered 3D-CAD model (right).

5.4 The reject heat circuit and dry air cooler

In order to get rid of the waste heat of the absorption cooling process during summertime, a dry air cooler is installed on the roof of the Savo-Solar office building. The secondary reject heat circuit #6, filled with propylene glycol mixture (50%), transfers the heat from the plate heat exchanger PHEX4-6 (Table 5.2) in the cooling water circuit #4 to the dry air cooler. A single pipe length is about 20 meters and the inner diameter of 32 mm correlates to the nominal flow rate of 2.8 $m^3 \cdot h^{-1}$. The closest approach temperature of 1.5 K (37.02–35.5 °C) between the plate heat exchanger inlet and outlet on both sides is a good compromise between system efficiency and investment costs.

Table 5.2. Main design data for the plate heat exchanger PHEX4-6 SWEP_B80ASx101/2P).

SWEP B80ASx101/2P		**Water**	**Propylene glycol** $50\%_{mass}$	
Heat load	kW		23.94	
Inlet temperature	°C	45.00		35.50
Outlet temperature	°C	37.02		43.48
Flow rate	$kg \cdot s^{-1}$	0.7179		0.8312
Max. pressure drop	kPa	20.0		20.0
Thermal length		5.25		5.25
Total heat transfer area	m^2		5.94	
O.H.T.C. (available/required)	$W \cdot m^{-2} \cdot K^{-1}$		2660/2650	
Total weight (mainly stainless steel)	kg		18.9	

The dry air cooler (Tab. 5.3) performance is full duty rated according to the local maximum ambient conditions during summertime. Its position on the black painted flat roof on the eastern side of the building is not ideal, but acceptable. The more favourable location on the northern side with greened ground was not available. A temperature approach of 5.5 K demands a relatively high total heat transfer area of 244.8 m^2 when an electricity consumption of not more than 100 Watts is targeted. But, considering all costs for transportation and installation, the slightly increased costs are overcompensated by increased system performance. Additionally, a streamer diffusor is installed at the outlet of the fan. On the one hand, this avoids any recirculation of outgoing air and on the other hand the electricity consumption decreases by 10%.

Table 5.3. Main design parameter of the dry air cooler.

Güntner **GFH 090.2A/1-L(S)-F6/12P**		**Air**		**Propylene glycol** $50\%_{mass}$
Capacity	kW		24.7	
Inlet temperature	°C	30.0		43.5
Outlet temperature	°C	39.2		35.5
Flow rate	$m^3 \cdot h^{-1}$	8600		2.85
Max. pressure drop	kPa			19.0
Total heat transfer area	m^2		244.8	
O.H.T.C.	$W \cdot m^{-2} \cdot K^{-1}$		21.03	
Fan VT03104U capacity (el.)	kW		0.100	
Total weight	kg		312	

5.5 District heating as backup for the system

When the solar heat is not available to run the absorption process, heat from the local district heat network can be used. A substation has been installed specially for the installation in order to be able to provide water at a higher temperature than is available from the existing substation (for space heating and DHW). The technical specifications of the substation are given in Table 5.4 below.

The volume flow rate on the primary side is adjusted automatically so that the outflow on the secondary side is at the temperature of 90 °C. The valve is shut totally when the absorption process does not need the backup heat. A thermal energy meter is installed on the primary side to measure the energy used by the substation (Fig. 5.6). The substation is located on the other side of the factory building next to the main connection to the district heating network. Therefore, there are long pipelines on the secondary side between the substation and the system.

Table 5.4. Main parameter of the DH-substation.

	Primary	Secondary Heating
PN class	16	6
Min./Max. temperature (°C)	10/120	10/95
Max. use pressure (bar)	14,5	5,6
Power (kW)	14	14
Temperature setting (°C)	115-82	80-95
Volume flow rate (l/s)		0,11/0,23
Heat exchanger pressure loss (kPa)		3/8

Figure 5.6. District heating substation.

5.6 Connection to the heating and cooling system of the building

The system has been connected to the existing heating and cooling systems of the building (Fig. 5.7). The two connections are done in the same way as described in the simple figure below. The system supplies heat/cold to the air handling unit and the space heating/cooling. The heating and cooling equipment and their set points are described in part 4.1 description of the building.

Two energy meters are installed on the heating and cooling circuit of the building to measure the real demand. The connection to the existing heat and cold supply: used before the system was installed and is still there, but is no longer in use.

Main parameters of floor heating, activated ceilings and HVAC unit (m2, flows, effectiveness of heat exchanger etc.) and common temperature levels etc. can be found in Chapter 4.1, Table 4.1.

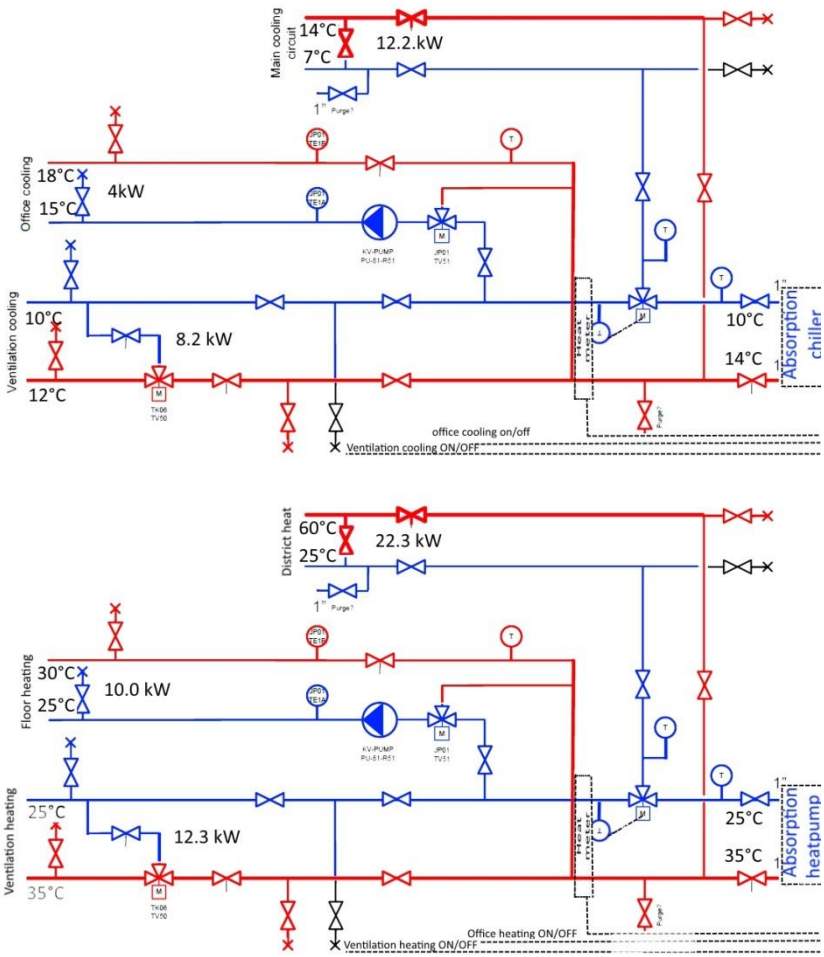

Figure 5.7. Principle scheme of the connection of the absorption system to the existing heating and cooling systems of the building.

5.7 Auxiliary electricity consumption

The system design comprises the latest results and outcomes from IEA TASK38 and TASK48 [Helm, 2015] to reduce auxiliary electricity consumption for cold and heat production with sorption machines.

Table 5.5 lists all installed electricity consumers and their minimal and maximal power demand. The different variable speed circulators RP#.# from Grundfos transfer heat and cold between the components. The affinity laws describe the

theoretical dependency of rotation speed, head, and power consumption of the rotary pumps for an ideal, frictionless and incompressible flow. Their overall power consumptions P1 theoretically correlate with the power of three to the volume flow and further is slightly dependent on the temperature and heat carrier medium viscosity (e.g. Glycol vs. water). A simplified correlation given in equation (13) predicts electricity consumption P1 in Watt if the flow Q in m³/h, pressure loss in the system p in millibar, and overall pump efficiency η is known.

$$P1 = \frac{Q \cdot p}{36 \cdot \eta} \quad (13)$$

For medium-scale highly efficient circulators the overall pump efficiency is about 0.5, depending on the operation point. In order to reduce pressure drops in the pipelines, a maximum flow velocity of around 1 $m \cdot s^{-1}$ is targeted in all hydraulic circuits at nominal capacity. RP01 and 02 from the manufacturer Lowara provide a constant pressure head to circulate the solution and refrigerant inside the absorption chiller. The fan speed of Guentner dry air cooler is adjusted according to required cooling water temperature and ambient air temperature.

Table 5.5. Electricity consuming devices in the SHC System.

Device	Medium	P1 Min W	P1 Max W	Type
RP1.1 solar collector pump	Glycol	10.5	96.4	Magna3 25-80
RP2.1 buffer tank pump	Glycol	15.4	49.5	Alpha2 25-80
RP3.1 driving heat pump	Water	11.1	114.6	Magna3 25-80
RP4.1 heating water pump	Water	11.7	155	Magna3 25-100
RP5.1 chilled water pump	Water	10.5	104.5	Magna3 25-80
RP6.1 cooling glycol pump	Glycol	26.9	118	Magna3 25-80
RP01 refrigerant pump	R718	20	20	Ecocirc 25-6
RP02 solution pump	LiBr	30	30	Ecocirc 25-6
Fan of dry cooler	Air	6	100	EBM Papst
Control	-	1.5	3.5	UVR16x2
Total		**143.6**	**791.5**	

With reference to the nominal chilled water capacity of 10 kW, the EER_C for solar cooling is computed to 12.6 and in 20% part load to 13.9 respectively. Thus, the energy efficiency ratio EER_H for heating is around 30 at a nominal capacity of 24 kW and 33.4 at minimum operating conditions. Between minimal and maximum operating conditions the efficiency values increase. As in that case, the reduction in the hydraulics and fan speed still exceeds the remaining constant power consumption of refrigerant and solution pump, as well as the control.

6. Ecological benefits of solar heating and cooling system

6.1 CO_2 emissions reduction of solar-assisted cooling and heating systems

Solar radiation penetrates almost all greenhouse gas (GHG), but the gas absorbs most of the heat radiation coming back from the earth surface, creating greenhouse effect. Due to greenhouse gases the temperature of the earth rises higher than without those gases. The most remarkable greenhouse gases are water steam (36–70% of GHG effect, clouds are not included), carbon dioxide (CO_2, 9–26% of GHG effect), methane (CH_4, 4–9% of GHG effect), ozone (O_3, 3–7% of GHG effect) and nitrogen oxidule (N_2O, 6% of GHG effect). The lag-time of greenhouse gases vary from some days (steam) to hundreds of years (CO_2).

The SOLCH absorption chiller system is planned to be operated in both a cooling and heating mode as a function of indoor and outdoor temperature.

Using solar energy as a source for producing cooling and heating is aimed at saving fossil fuel energy source and reducing emissions. Fabrication of a solar collector, PV-panels, chillers and other auxiliaries also generate CO_2 emissions.

A chiller's output is 10 kW cooling and 15 kW heating and they are supposed to be driven as shown in Table 6.1 producing cold energy 10 MWh and heat 30 MWh a year. Absorption, adsorption and compressor chillers utilise solar energy for 60% of necessary driving energy in the cooling season, with the rest of the driving energy coming from district heating. In heat pump mode they use DH-energy. The compressor chiller uses electricity in heating mode and 60% solar energy in cooling mode.

Average fuel mixture in summer and winter for electricity and district heat production are shown in Figure 6.1 and CO_2 emissions in Table 6.2. These fuel mixtures are expected to continue for the next 15 years.

Table 6.1. Chillers used in cooling and heating modes.

technology	cooling kWh	COP -	peak time h/a	heating kWh	COP -	peak time h/a	aperture m²	cooling kWh	heating kWh
compressor	10	2.5	1000	15	3.5	2000	36	10 000	30 000
absorption	10	0.7	1000	15	1.2	2000	18	10 000	30 000
adsorption	10	0.6	1000	15	1.1	2000	21	10 000	30 000

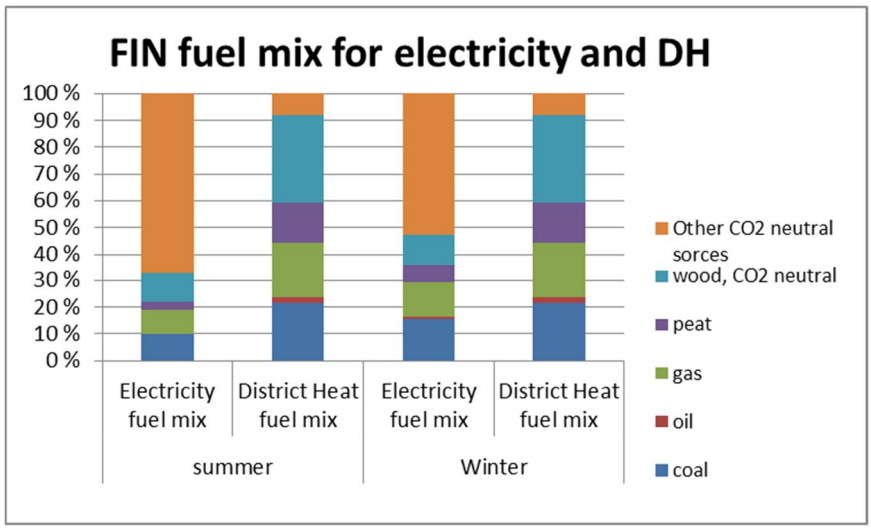

Figure 6.1. Summer and winter average fuel mix of electricity and district heating production in Finland (Sipilä et al., 2015 [electricity] and Finnish energy industry [heat], 2015).

Annual CO_2 emissions of the chillers driven and components (storage tank, solar collectors, panels (mono-Si), batteries (NiCd), inverters, etc.) manufacturing material emissions of the system are shown in Table 6.3. Driven emissions are divided in summer and winter parts. Only components, which are different in chiller types, are included to see the difference in starting point (year 0).

Table 6.2. CO_2 emissions of fuels (Statistic Finland).

Fuel	CO_2 kg·kWh^{-1} (fuel[(1)])
Coal	0.341
Oil	0.279
Gas	0.202
Peat	0.381
Wood CO2 neutral	0.000
Other CO2 neutral	0.000

(1) Statistic Finland

Table 6.3. Annual CO_2 emissions (kg/a) of chillers with and without solar support in cooling and heating production mode as well as the components' material emissions [Vares & Shemeikka, 2016].

Item		Compressor with solar	Compressor without solar	Absorption with solar	Absorption without solar	Adsorption with solar	Adsorption without solar
energy	summer	375	664	1 330	2 862	1 552	3 339
	winter	2 368	2 368	5 369	5 369	5 857	5 857
	sum	2 743	3 032	6 699	8 231	7 409	9 196
material	chiller	161.5		277.4		277.4	
	storage tank	128.3		712.8		712.8	
	collectors/panels	777.8		1 440		1 680	
	DH station			60.0	60.0	60.0	60.0
	battery storage+inverter	593.8					
	sum	1661.4	0	2.490.2	60.0	2 730.2	60.0
	total	4 405	3 032	9 190	8 291	10 139	9 256
collectors m²				36		42	
Si-PV panels m²		22					
heat storage m³				2.00		2.00	
cold storage m³		0.36					

6.2 Life-cycle CO_2 emissions

Life-cycle CO_2 emissions of the chillers' production are shown with and without solar support in Figure 6.2. The life-cycle emissions of the solar supported absorption (103 tn) and adsorption (114 tn) chiller are more than double compared to the compressor (44 tn) chiller over 15 years. If non-solar-supported systems are used, emissions increase 2% (4.6 tn) for the compressor, 20% (20 tn) for the absorption and 21% (24 tn) for the adsorption chiller.

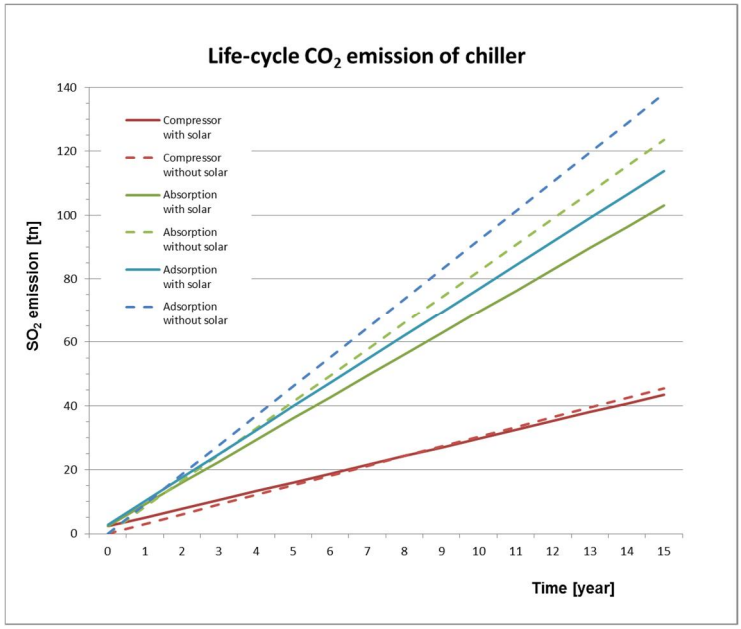

Figure 6.2. Life-cycle CO_2 emissions (ton) of chillers with and without solar support in cooling production mode.

7. Operational experience and measurements of the subsystem

The internal measuring equipment and a data uplink to ZAE Bayern and VTT ensure real-time monitoring. All the data from the system are transferred via the data uplink into the data measurement analysis program 'MEDVIEW2', from ZAE Bayern. After programming and testing of the different control strategies, several optimizations have been carried out. The overall goal is a high solar share of renewables and low auxiliary electricity consumption.

7.1 Solar collectors

Two kinds of solar collector are installed on the roof of the Savo-solar office. At the first stage, nine collectors (2 m^2) of the Savo-Solar SF100-03 type are installed in row two and six of the same collectors with foil under the face glass in row 1. Later, three more collectors with foil were installed in row 1. The total number of installed collectors was 18 (36 m^2) as of the middle of September, 2016. An example of the temperatures in the solar collector row 1 and 2 are shown in Figure 7.1. At this point, only six collectors had been installed in row 1.

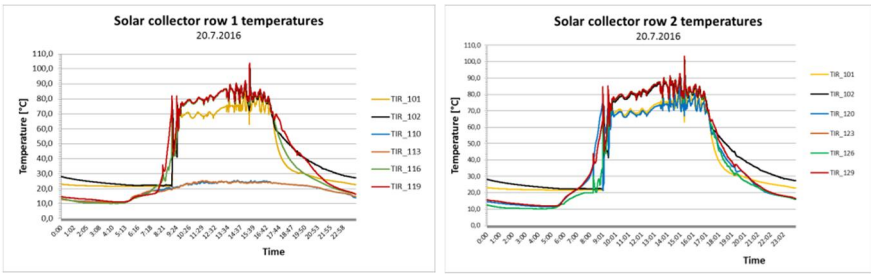

Figure 7.1. Temperatures in collector row 1 and 2. T101 and T102 are temperatures in and out of the collector rows. Row 1: in T110, out T113, T116, T119; Row 2: in T120, out T123, T126, T129 (look at Fig. 4.11).

Solar radiation in the same day on the horizontal and collector surfaces (50^{o} from horizon) are shown in Figure 7.2. Brightness from four compass directions is shown in Figure 7.3.

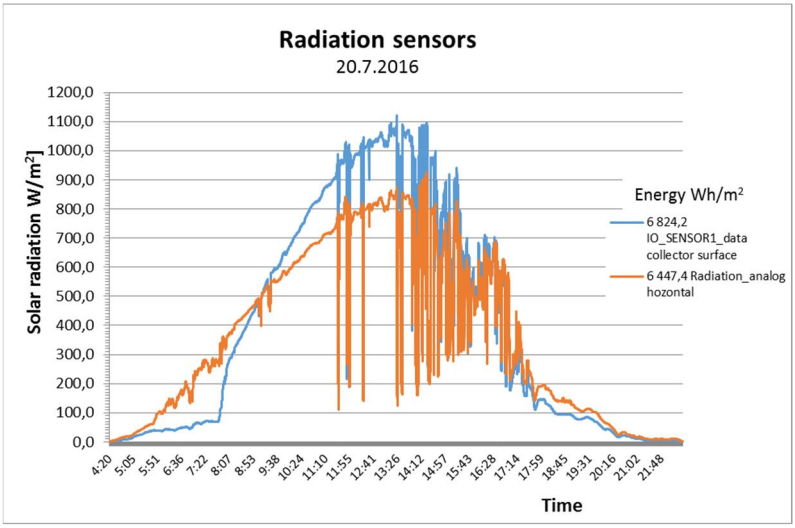

Figure 7.2. Solar radiation over the course of a single day on the horizontal and collector surfaces.

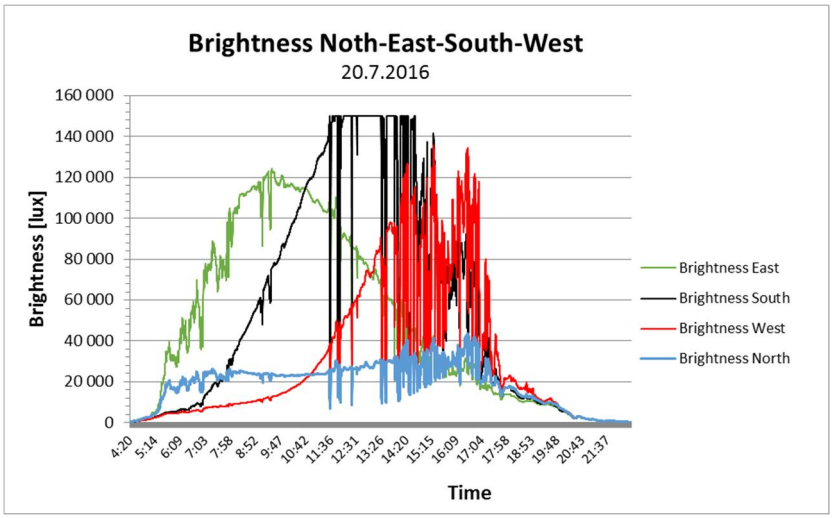

Figure 7.3. Brightness over the course of a single day from four compass directions.

Solar energy output from collector rows 1 and 2 are shown in Figure 7.4 in the range of solar irradiation 40–250 kWh/day. The output of solar row 1 (collectors with foil) is on average 3.6% higher compared to solar row 2 (collector without foil).

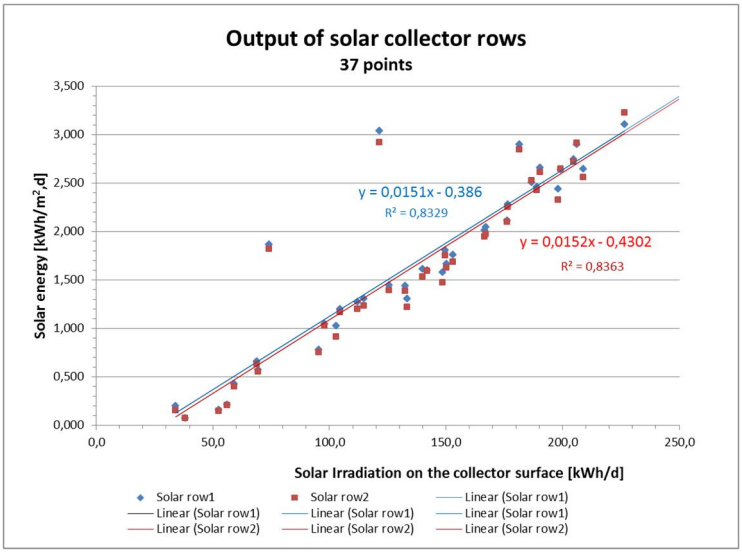

Figure 7.4. Solar collector output as a function of solar irradiation on the surface of collector row 1 and row 2 per day.

The monthly comparison between foil and MPE collectors are presented in Table 7.1.

Table 7.1. Comparison of monthly efficiency values of new foil collectors and the standard MPE collectors.

Month 2016	Foil collector efficiency	MPE collector efficiency	Relative efficiency enhancement of foil
June	0.33	0.31	+5 %
July	0.31	0.31	+1 %
August	0.31	0.30	+4 %
September	0.28	0.25	+11 %
October	0.34	0.31	+9 %

.

7.2 Buffer tank with a improved stratification device

Another important issue is the storage efficiency of the buffer tank. In the system, a hot water storage tank with a volume of around 2000 l and an improved

stratification system is installed. To evaluate the stratification of the buffer tank five temperature sensors are installed: one at the top and one at the bottom of the tank, which are used for control and three sensors at different heights. The storage capacity is 200 kWh with a temperature spread of 90 K (5 °C to 95 °C). In the cooling mode only temperatures from 95 °C to 60 °C are sufficient to drive the chiller. Thus, the storage capacity for cooling is around 82 kWh. By a maximum driving heat of around 14 kWh, the ideally loaded storage can meet the heat demand for around 6 hours. As mentioned previously, the maximum required cooling capacity is 5 kW, so the maximum driving heat is only 7 kW. In this case the maximum loaded buffer can provide the driving heat for around 11 hours. It must be mentioned that these values are theoretical. Firstly, due to safety issues, the buffer cannot be loaded completely to a temperature of 95 °C. Secondly, the buffer tank has thermal losses. To reduce the thermal losses and avoid condensation the buffer tank is isolated with 10 cm mineral wool and 2 cm of Armaflex. The thermal losses per hour of the buffer tank and the storage mean temperature over 4 days are shown in Figure 7.5. Average losses are around 0.35 kWh/h. As expected the thermal losses correlate with the storage temperature.

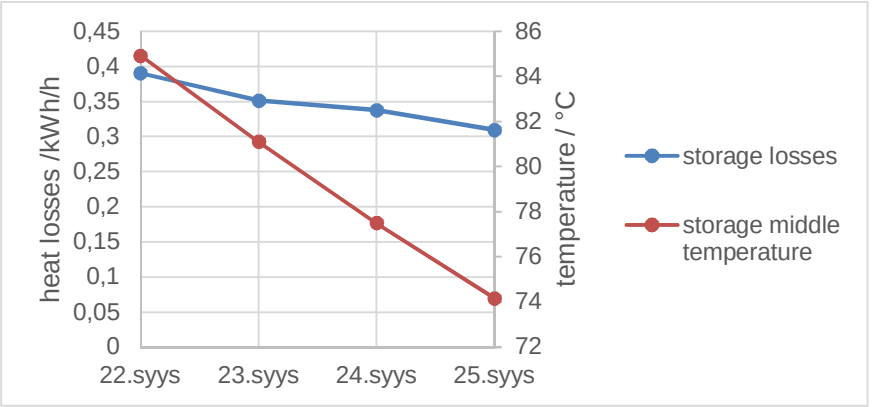

Figure 7.5. Thermal heat losses of the buffer tank.

In Figure 7.6 a single day at the beginning of September is analysed where the storage tank supplies heat to the desorber of the absorption chiller. In the morning, the storage tank is not used and the slow decrease of the temperatures of the storage tank (TIC_211 (top), TIR_212, TIR_214, TIR_215, TIC_217 (bottom)) show its thermal losses.

At 12:30 a.m. the absorption chiller is requested due to the cooling demand of the building (light blue curve, pump RP3.1). Now, the top layer of the storage supplies hot water to the chiller. As the cooling demand is only 2 kW in the evaporator of the absorption chiller (nominal power: 10 kW) the desorber inlet temperature,

coming from the storage tank, is mixed down to about 78 °C (TIR_302) by a mixing valve. This temperature is sufficient to supply the 2 kW for cooling. The chiller return temperature (TIR_303) is in the range of 72–68 °C.

This temperature is entering the storage tank at the bottom and is pushed through it up to the top layer over the 6.5 hours of the chiller operation time. The four lower layers drop to the return temperature (72–68 °C) one after the other, starting from the lowest one. The time offset between the layers shows that there is no large mixing between two subsequent layers during unloading of the tank. The top layer follows the same temperature drop curve as the other ones. When the absorption chiller is turned off at 7 p.m., its temperature drops quickly to below 80 °C. At that point, a stratification between the top and the four bottom layers can still be seen. In general, the storage tank shows good stratification behaviour, slightly deviating from the ‘ideal’ behaviour. But some mixing is inevitable, the ‘ideal’ stratification is only achievable in theory.

In Figure 7.7 one day at the beginning of October is analysed where the storage tank supplies heat to the space heating. In the late afternoon, the solar thermal system reheats the lower part of the storage tank for a short time. Let’s first have a look at the space heating mode. The light blue curve shows when the pump of the space heating is running (RP4.1). The return temperature of the space heating into the bottom of the storage tank is at 25–28 °C. In the first two short-space heating intervals, it can be seen that the temperature of the bottom layer (TIC_217) drops a little bit each time. As the layer is at 75 °C at the beginning and the water volume entering is not very large due to the short time, the temperature drop is not very large. After the start of the third period a steeper drop can be seen (30–29 °C), almost down to the temperature of the return water. The second layer from the bottom drops as well after some time, but there is always a temperature difference between both layers. The two top layers stay untouched. In the fourth period a similar behaviour can be seen.

At about 3 p.m. the temperature of the solar system (TIR_201) rises over the temperature of the bottom storage layer and the solar pump (RP2.1) is switched on. The solar temperature mainly affects the temperature of the bottom layer, the other layers do not see a large change. This shows that the stratification device works quite well for the given volume flow.

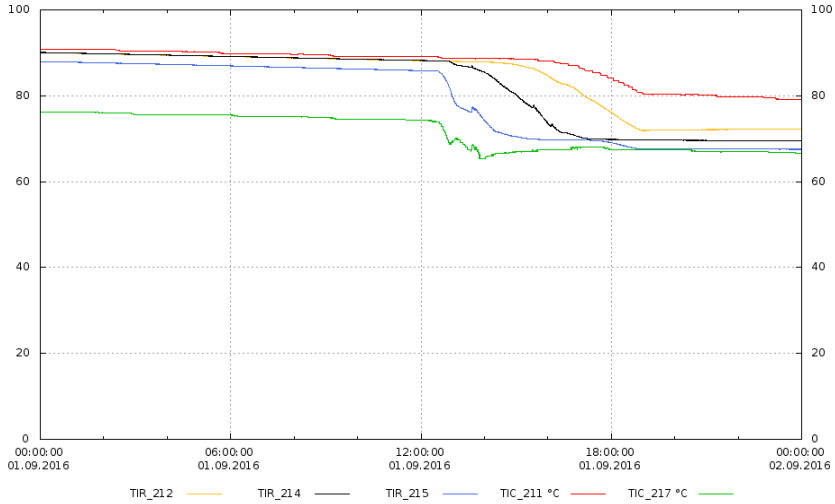

Figure 7.6. Unloading profile of storage tank while supplying heat to the absorption chiller.

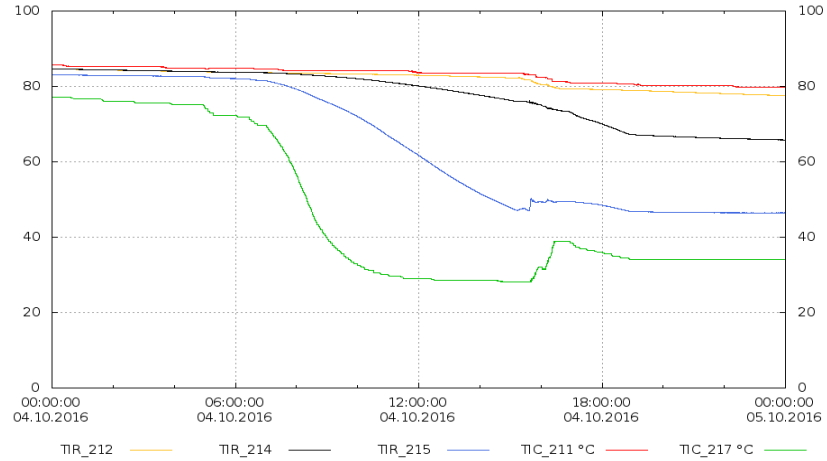

Figure 7.7. Unloading profile of storage tank while supplying heat to space heating of SavoSolar office.

In Figure 7.8, the following day in October can be seen. As in Figure 7.7, it is a mixture of space heating and the solar thermal system that interacts with the storage tank. In contrast to the day before, the solar collectors supply heat to the system over more than seven hours. The storage tank works quite reliably apart from the temperature drop of the top layer, starting from 9:30 a.m. to about 12:00 a.m. The stratification results are better when only the space heating is turned on. The poorer result can be explained with the higher volume flow entering the storage tank due to the solar pump which is on average 1 m³/h compared to the space heating volume flow, which is only about 0.2 m³/h. The smaller volume flow

is due to the fact that the space heating only needs a temperature of 40 °C whereas the top layer supplies 80 °C. So the temperature is mixed down, resulting in a small volume flow. There are two possibilities that result in the temperature drop of the top layer. Either the entering water not only leaves the stratify at the outlets in the middle, but the volume flow is so high that the flap of the outlet at the top layer is forced to open as well. Or the water leaving at the outlets in the middle has such a high impulse, that it is mixed up with the layers above. This behaviour is unwanted and has to be addressed in further research work.

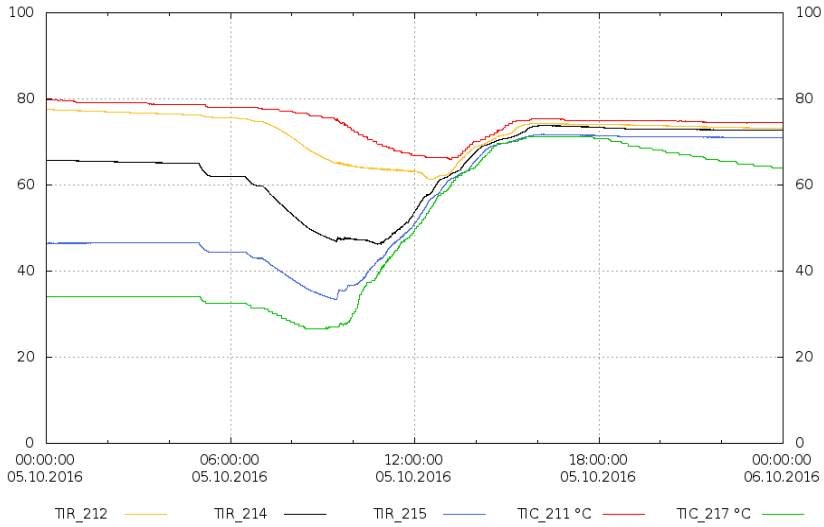

Figure 7.8. The loading and unloading profile of the storage tank during a typical heating day in October.

In Figure 7.9, a day in mid-October is visualized. The unloading of the storage tank in combination with the absorption heat pump can be seen. It is an example of a good stratification as the layers drop to the return temperature, starting from the bottom layer, finishing with the top layer. The time offset shows that the different layers are loaded separately and no mixing of the whole storage tank takes place.

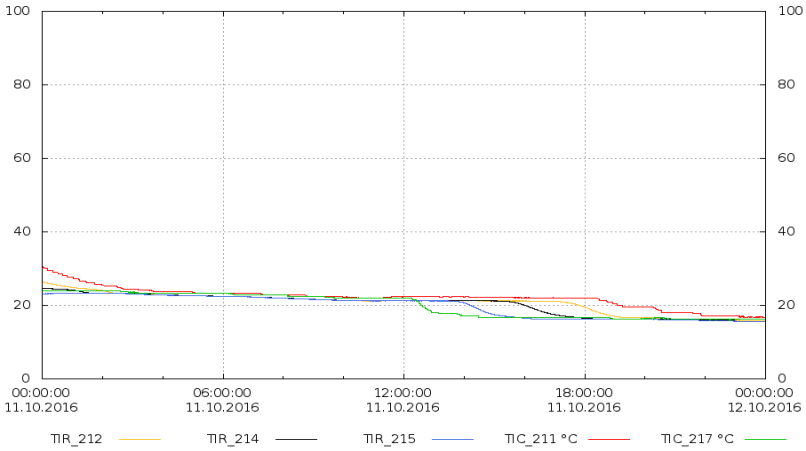

Figure 7.9. Unloading profile of the storage tank while supplying heat to the evaporator of the heat pump.

7.3 Absorption chiller / heat pump

In Figure 7.10 the temperature profile of the inlet and outlet of the absorption chiller and the COP over the course of a single day in cooling mode is shown.

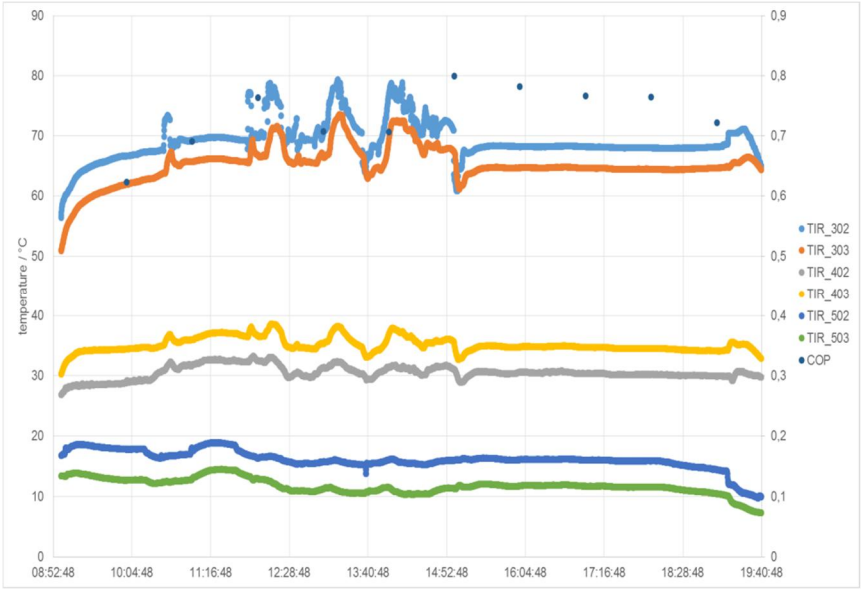

Figure 7.10. Temperature profile and COP over a day.

Heating circuit: TIR_302 inlet; TIR_303 outlet
Cooling circuit: TIR_402 inlet; TIR_403 outlet
Chilled circuit: TIR_502 inlet; TIR_503 outlet

In the morning, the absorption chiller driving heat is supplied by the buffer tank. During the starting process of the system and the heat up of the absorption chiller, the COP is 0.62. Between 11:30 am and 3:00 pm the absorption chiller driving heat is supplied by the solar field and/or buffer tank. The inlet temperature of the driving circuit follows the solar output. The cooling temperatures also follow this progress in the lower wave. If the temperature of the driving heat circuit increases the cooling temperature can also be increased to achieve the same chilled water capacity. As seen, due to the fluctuation, the COP is between 0.69 and 0.76.

At 3:00 pm the solar output is low and the buffer tank is discharged under 70 °C. Now the absorption chiller is driven by the district heat substation. The temperature can be delivered constantly at around 70 °C and consequential the other temperatures become constant. The COP is now between 0.76 and 0.80.

Only at 7 p.m., at lower cooling demand and shutdown of the system, does the COP decreases to 0.72.

Following the influence of the driving heat, the inlet temperature and the cooling power on the COP_{Cold} and EER_{Cold} are analysed (Fig. 7.11, Fig. 7.12). Therefore measurement data are analysed with a constant driving inlet temperature and cooling power over several hours. So the influences of the fluctuations are reduced.

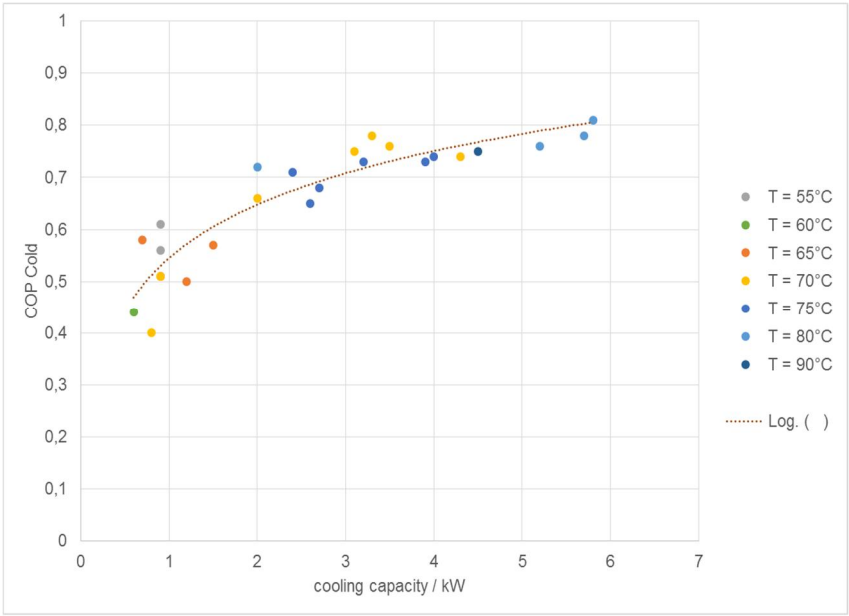

Figure 7.11. COP_{Cold} depending on driving heat inlet temperature and cooling power.

Figure 7.11 shows the COP_{Cold} depending on the driving heat inlet temperature of the desorber and the cooling power. The COP_{Cold} approximates to a value of 0.81 by the highest cooling power and a high driving temperature. If the cooling power and therefore the required driving temperature fall the COP_{Cold} also fall to lower values (0.4-0.6). This is because the heat loss of the system does not fall in the same manner as the cooling power. Over a cooling power of 3 kW the COP_{Cold} is greater than 0.7 regardless of driving heat temperature. To achieve a cooling power above 2 kW a driving temperature of 70 °C or higher is required. A higher driving temperature does not guarantee a high COP_{Cold} (first two yellow points). If the ambient temperature is higher, the heat reject system cannot provide low temperatures and is compensated by a higher driving temperature to achieve the

required cooling power. Because the volume flow of the solution is not adjusted, the indicated progress of the measurements follows as expected in Figure 7.11.

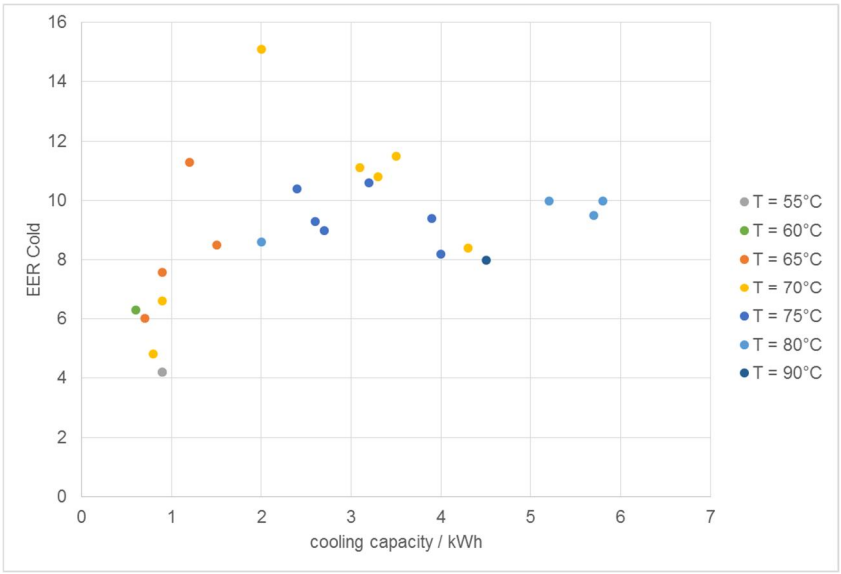

Figure 7.12. EER_{Cold} depending on driving heat inlet temperature and cooling power.

The EER_{Cold} has a similar progress as the COP_{Cold} (Fig. 7.12). At low cooling power (<1 kW) the EER fall sharply. The pumps are running on the lowest speed level and the electrical consumption increases compared to the cooling power. The great distribution of the EER_{Cold} is due to the running system parts. If only the chiller runs for cooling with heat from the storage tank, the EER_{Cold} is higher as also the storage tank is loaded by the solar field or the chiller is driven from the district heat substation. If the cooling power is over 1 kW the EER_{Cold} is greater than eight, regardless of which system parts are running.

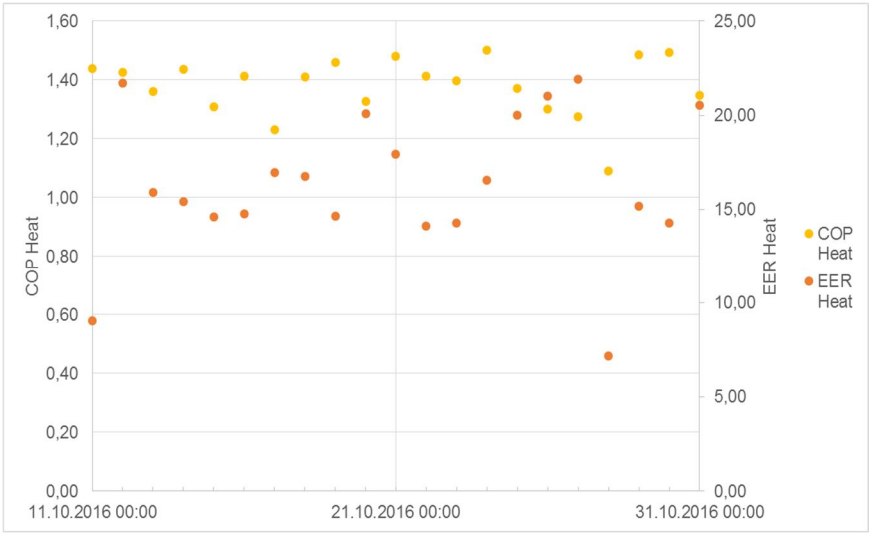

Figure 7.13. COP_{Heat} and EER_{Heat} of heating period.

The heat pump modus begins on the 11.10.2016. Before this date the building was directly heated by the buffer tank. The COP_{Heat} for the heat pump is continuously above 1.2 in Figure 7.13. Only on the 28.10.2016 is the COP_{Heat} 1.1. On this day only a small amount of heat was required and so the heat up and shutdown losses are some percentage higher. Also the EER_{Heat} is low on this day due to the low required heat. Otherwise the EER_{Heat} is greater than 13, up to 22. During the analysed heating period until 31.10.2016, the heat pump satisfied the heat demand and the collectors harvest enough solar heat to load the buffer tank over the course of the day. The total amount of heat from the heat pump is 1215 kWh from 11.10.2016 to 31.10.2016. The delivered driving heat from the district heat substation is 896 kWh. The overall COP_{Heat} for the heat pump mode from 11.10.2016 to 31.10.2016 is 1.36 and the EER_{Heat} is 13.91. The COP_{Heat} of the heat pump is almost independent of the driving heat inlet temperature and the heating capacity and varies between 1.4 and 1.6 (Fig. 7.14).

-

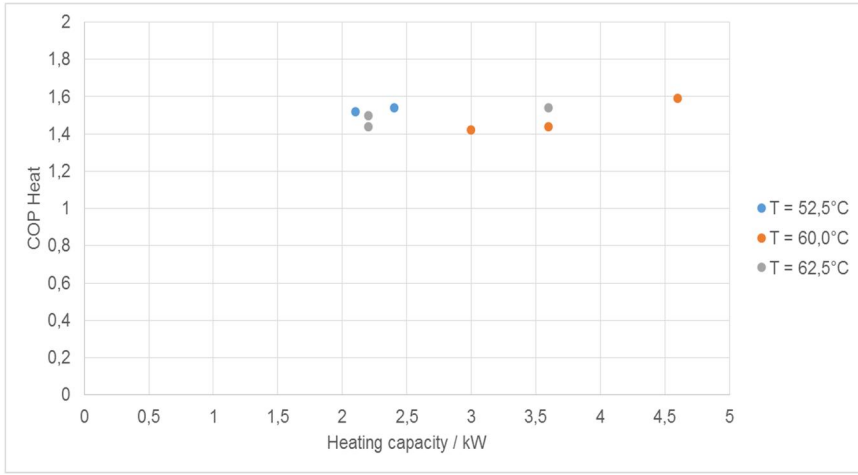

Figure 7.14. COP_{Heat} as a function of the heating capacity and the driving heat inlet temperature.

8. Seasonal energy balance and savings from the system

The seasonal, daily and hourly evaluation of the entire system has been done from June till the end of October. The cooling period runs from June till the end of August. Afterwards the heating period started. During the cooling period the whole cooling demand of the building was covered by the absorption chiller. In September the heating demand was satisfied by solar heating directly by the buffer tank. In October the solar irradiance is too low to heat up the buffer tank for direct solar heating. But the irradiance is enough to heat up the buffer tank to around 10–15 °C. The heating of the building is supplied with the absorption heat pump. In this case the district heat substation serves as the driving heat source and the buffer tank is the low-temperature heat source.

The seasonal solar coverage during cooling is around 65%. The seasonal available solar irradiance and the harvested solar heat are shown in Table 8.1.

Table 8.1. Performance of the solar collector field between June and October 2016.

Month 2016	**Total solar irradiance in collector plain** kWh	**Harvested solar heat** kWh	**Conversion factor** %
June	4635	1482	0.32
July	3634	1128	0.31
August	2972	893	0.30
September	2826	748	0.27
October	1186	460	0.39

The harvested solar heat is around 31% of the available solar irradiance and the storage efficiency of the harvested solar heat is 75%. The total amount of stored solar heat is 2625 kWh. Table 8.2 gives difference between the driving heat and

the amount of solar heat and backup heat of 94 kWh is due to heat losses of the system and measurement errors.

Table 8.2. Comparison of monthly efficiency values of new foil collectors and the standard collectors.

Month 2016	Foil collector efficiency	Standard collector efficiency	Relative efficiency enhancement of foil
June	0.33	0.31	+5%
July	0.31	0.31	+1%
August	0.31	0.30	+4%
September	0.28	0.25	+11%
October	0.34	0.31	+9%

Table 8.3. Seasonal energy balance of absorption chiller.

Source of energy	Useful energy kWh
Solar heat to chiller	1968
Backup heat to chiller	1269
Driving heat to chiller	3143
Heat from chiller	4360
Cold from chiller	1871

The seasonal COP for cooling is 0.60 and the seasonal EER 7.60 roughly. These values contain also the starting and shutdown procedure and standing losses and the time before the optimization. After optimization, July and August, the average COP is 0.61 and the average EER is 8.70.

The COP_c and EER_c of the chiller is shown in Figure 8.1 based on 446 measurement points. A power line equation of COP_c and EER_c is also shown in the same figure. The average values for COP_c and EER_c is 0.53 and 6.2 as a function of the cooling output in the range of 0–7.5 hourly kW_c. The typically used range of cooling capacity is 3–10 kW_c. The average COP_c and EER_c is then 0.7 ± 20% and 9.1 ± 30%, reaching the average maximum values of 0.8 and 14.0 when cooling capacity is at maximum 10 kW_c. The COP_c and EER_c target of the project for the chiller was 0.7 and 15.0, so they are reachable in the range of average, including variation around the average. In further developing the control of the

whole process, it is possible to decrease variation round the regression equation and higher the COP_c and EER_c values on the chiller.

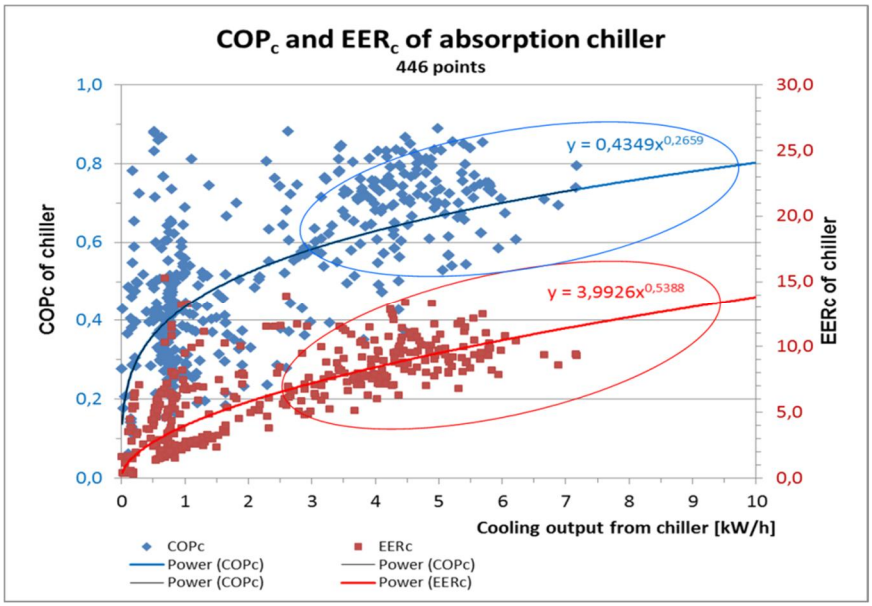

Figure 8.1. COPc and EERc of the chiller in the range of 0–10 kWc and regression equations.

Cooling and ejected heat from the chiller is shown as a function of the heat input to the desorber of the chiller based on 452 measurements in Figure 8.2. Linear estimation gives cooling of 9.5 kW_c when heat input to the desober is 15 kW_h.

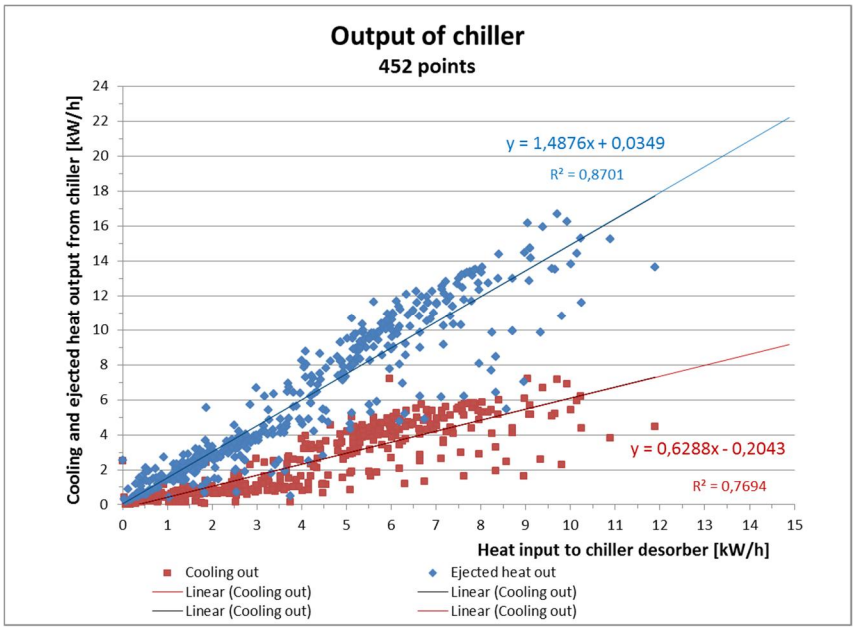

Figure 8.2. Cooling output and ejected heat from the chiller as a function of the heat input to the chiller desorber.

Also the COP_{Cold} contain the starting and shut down processes. Another reason for the low EER_{Cold} and COP_{Cold} is the backup system. In the summer time the backup system only supplies a driving temperature of around 70 °C. To achieve the required cooling power of the building, the heat reject system must provide a lower cooling temperature for the absorption chiller. The electrical energy consumption of the heat reject system increases.

Also the low driving temperature leads to a worst COP_{Cold}. Also around 50% of time the cooling requirement of the building is very low (< 2 kW). The losses of the system are increasing compared to the delivered cooling capacity and the COP_{Cold} decreases. Also the electrical consumption of the system can only be reduced to a certain point. In the case of a cooling requirement lower than 2 kW the pumps are running at the lowest level. But the electrical consumption increases compared to the delivered cooling capacity. If only the time with a cooling capacity over 3 kW is considered, the COP_{Cold} is around 0.72.

Figure 8.3 shows the COP_{Cold} and the EER_{Cold} for a typical day with a cooling capacity over 3 kW, that is, July 1st. The average COP_{Cold} of the whole day is 0.68. As seen the COP_{Cold} between 9:30 to 17:00 o'clock is continuously over 0.70 and the EER_{Cold} over 10.

Table 8.4. Percentage of monthly cooling with a cooling capacity over 3 kW.

Month	cooling capacity over 3 kW
June	24%
July	31%
August	34%

In June the solar coverage is 74% and in July and August the solar coverage is around 55% of the cooling demand in Table 8.5. If there is no solar coverage, the backup system supplies driving heat for the absorption chiller.

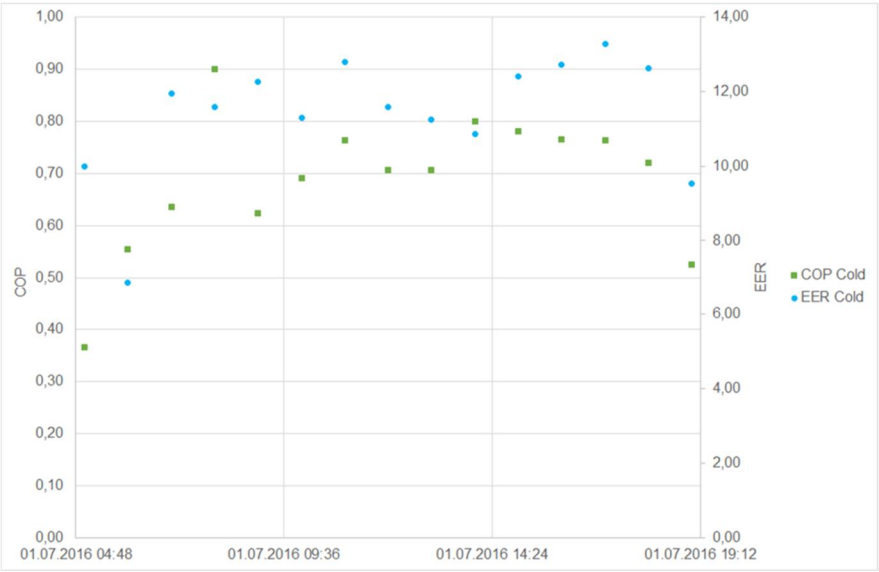

Figure 8.3. COP_{Cold} and EER_{Cold} by a cooling capacity over 3 kW.

Table 8.5. Operating hours of the cooling system and solar coverage.

Month	Cooling demand hours	Solar cooling hours	Backup cooling hours	Solar coverage
June	474.58	350.34	124.24	74%
July	282.78	155.20	127.58	55%
August	186.28	105.91	80.37	57%
September	61.27	58.65	2.61	96%

The following parameters are adjusted for the cooling mode:

- speed factor for the chilled water pump to achieve a temperature spread of 5 K between the external evaporator inlet and outlet (TIC502-TIC503)

- speed factor for the coolant pump and driving heat pump in comparison to the speed of the chilled water pump
- speed factor between the chilled water pump and heat reject pump
- curve for the cooling temperature depending on the available driving temperature
- required driving temperature depending on required chilled water power and the temperature of the external evaporator outlet (TIC503)
- temperature set point for running the backup system

The following parameters are adjusted for the solar field:

- calculation if solar irradiation is great enough to load the buffer
- volume flow of the solar field to achieve a temperature spread in the collectors of around 10 K

Due to adjustment of the speed factors, the energy consumption of the pumps is reduced by 50% and so the EER_{Cold} increases by around 100%. In July and August, after optimization, the average EER_{Cold} is around 9 and the COP_{Cold} is around 0.63.

Table 8.6 Monthly average of COPCold and EERCold.

Month	COP Cold	EER Cold
June	0.57	5.41
July	0.62	8.72
August	0.60	8.66
September	0.54	4.91

The EER_{Cold} contains the electrical energy consumption of the solar heating and cooling system:

- standby energy consumption
- solar harvest and buffer tank loading without a cooling requirement
- emergency cooling of the solar field

The efficiencies of Savo-Solar normal SF100-03 and foil collector are calculated based on measurement in 10 minutes average values (July 1st ,2016) as a function of temperature difference between collector and outdoor temperatures and solar irradiation as tested (1000 W/m^2) in chapter 3. Maximum solar irradiation in that day was more than 1000 W/m^2. Foil collector area is 12 m^2 in that day, but standard collector area is 18 m^2 and the auxiliaries and pipelines are about same to both of them.

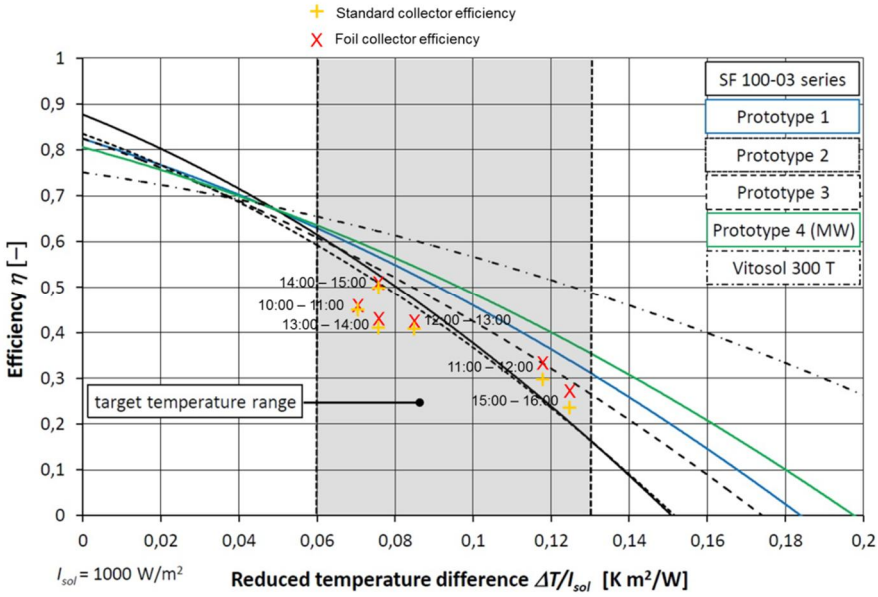

Figure 8.4. Efficiency of the foil and standard collectors as a function of ΔT and solar irradiation.

9. Economy of the solar heating and cooling system

9.1 Investment cost of the pilot plant

The installation cost of the solar cooling project consists of a chiller, a heat storage tank, solar collectors (18 x 2 m^2= 36 m^2), a district heat substation, measurements, data collection, pipelines, wirelines, etc.. The total cost divided across the main items was EUR 69 549 (EUR 6955/kW_c), as shown in Table 9.1. Labour cost is also included in the main items. The cost is higher in the pilot investment because of the additional instrumentation and data collection system compared to the commercial version of the solar cooling system. The HVAC system of the office building is a standard system and no additional investments are made.

Table 9.1. Cost of the main parts in the solar cooling pilot project.

Item	cost [EUR]	%	obs! Vat = 0
Solar field	16 805	24,2	9 x 2 m^2 (standard)+ 9 x 2 m^2 (foil) = 36 m^2
Solar field development	3 076	4,4	
Chiler & Hydraulics	10 618	15,3	10 kW
Heat storage	4 912	7,1	2 m^3
Dry air cooling unit	6 975	10,0	25 kW
DH back-up	13 943	20,0	15 kW
Measurements	9 942	14,3	
Data acquisition	3 278	4,7	
	69 549	100	initial investment 6955 €/kWcold

The share of cost across the main items is presented in Figure 9.1.

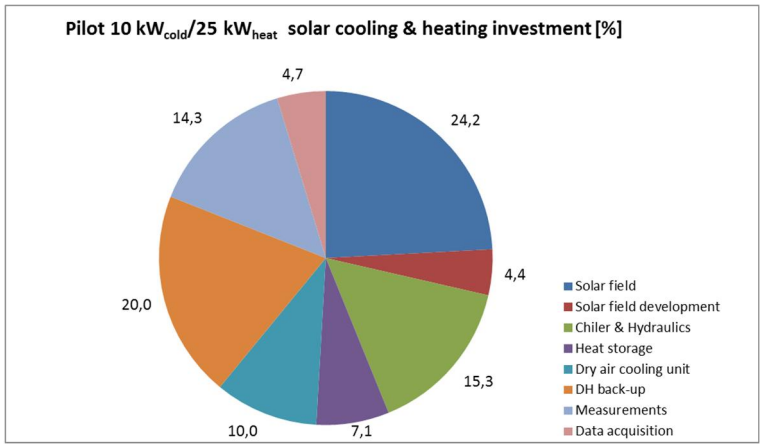

Figure 9.1. Share of solar cooling investment cost in the main items.

For a commercial solar-driven Chiller/heat pump we have to take out the additional equipment needed for data collection and research. Table 9.2 shows the estimated investment cost for 10 kW_c solar-driven chiller with DH backup. The investment price of the commercial version is EUR 46 281 EUR (EUR 4628/kW_c) and it is 33.5% cheaper compared to the price of the pilot plant. The cost is divided across the main items in Table 9.2, with the deviation of cost in Figure 9.2.

Table 9.2. Cost of the main parts of the commercial solar cooling project.

Item	cost [EUR]	%
Solar field	16 805	36,3
Chiller & Hydraulics	10 618	22,9
Heat storage	4 912	10,6
Dry air cooling unit	6 975	15,1
DH back-up	6 971	15,1
	46 281	100

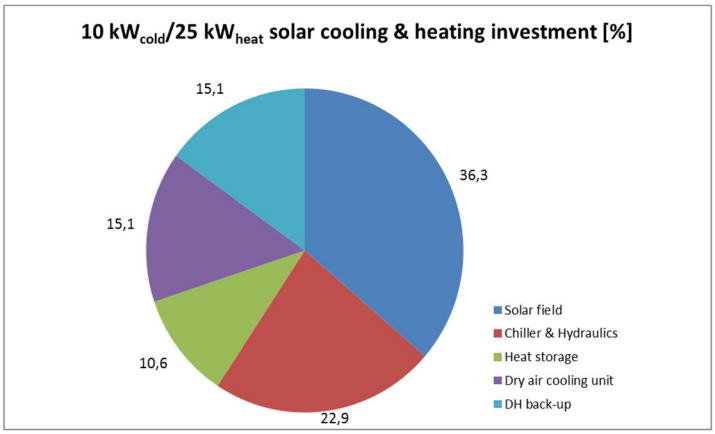

Figure 9.2. Share of commercial solar cooling investment cost in main items.

9.2 Operating cost of the pilot plant

The operating cost consists of used electricity of auxiliary devices and district heat. The produced daily cooling energy and auxiliary energy for driving the chiller is shown May to September 2016 in Table 9.3. Zero in the cooling column means that the chiller is not in use and – means, the data was not available. The total use of electricity was 360 kWh and the district heating 1081 kWh, which generates 2392 kWh cooling energy.

The driving cost is shown in Table 9.4, where any taxis are not included in electricity and district heating prices. The share of needed solar and district heating energy was 70/30 to drive the chiller.

The total driving cost was EUR 120.09, which means 4.7% interest and a 15-year lifetime, the total price of 4.7 EURcent per kWh for the cooling energy. If we include investment cost of the pilot project, the price of cooling energy is EUR 2.34 per kWh$_c$. A commercial project price is also evaluated EUR 1.50/kW$_c$ in Table 9.4.

Table 9.3. Produced daily cooling energy and auxiliary energy for driving the chiller.

Day	May			June			July			August			September		
	Cooling kWh	Electricity kWh	District heating kWh	Cooling kWh	Electricity kWh	District heating kWh	Cooling kWh	Electricity kWh	District heating kWh	Cooling kWh	Electricity kWh	District heating kWh	Cooling kWh	Electricity kWh	District heating kWh
1	0,0	0,8	0,0	19,2	5,3	0,0	58,0	5,2	52,9	48,9	4,9	30,0	14,2	1,3	0,0
2	0,0	0,0	0,0	45,6	7,5	18,6	13,8	2,3	11,9	41,3	4,2	21,9	12,0	1,3	7,4
3	0,0	0,0	0,0	29,5	5,8	18,9	17,3	2,9	28,5	34,9	3,2	28,7	7,1	1,5	0,0
4	0,0	0,0	0,0	2,4	5,4	0,0	0,0	0,0	0,0	21,6	1,6	34,1	0,0	0,0	0,0
5	33,9	7,8	0,0	0,0	0,0	0,0	0,0	0,0	0,0	37,3	3,6	44,2	13,3	1,6	0,0
6	29,9	3,3	0,0	0,0	0,0	0,0	0,0	0,0	0,0	12,2	1,9	16,2	8,3	1,4	0,0
7	17,0	3,2	0,0	28,9	7,4	0,0	0,0	0,0	0,0	11,3	2,0	0,2	10,6	1,1	0,0
8	22,9	3,1	0,0	6,3	2,1	0,0	7,6	1,0	16,5	50,1	5,0	34,3	8,5	1,0	0,0
9	36,9	3,1	0,0	0,0	0,5	0,0	0,0	0,3	0,0	33,0	3,1	29,8	7,4	1,2	0,0
10	36,2	3,2	0,0	1,5	0,6	0,0	9,8	2,2	10,1	5,8	0,6	5,1	0,0	0,0	0,0
11	1,8	0,7	0,0	6,9	2,2	0,0	53,2	4,6	3,7	0,0	0,0	0,0	0,0	0,3	0,0
12	13,0	3,3	0,0	8,3	4,8	0,0	13,3	1,9	28,9	-	-	-	7,7	1,1	0,0
13	17,8	3,3	0,0	12,1	4,4	0,0	17,2	2,3	7,5	-	-	-	7,1	1,5	0,0
14	12,1	2,0	0,0	18,6	4,6	4,3	22,7	3,3	9,6	-	-	-	9,2	1,7	0,0
15	12,6	1,9	0,0	53,3	7,6	17,2	6,9	1,1	17,9	-	-	-	0,0	0,1	0,0
16	13,1	1,8	0,0	43,3	7,8	35,8	0,0	0,5	0,0	-	-	-	0,0	0,1	0,0
17	13,0	0,6	0,0	43,3	7,8	58,0	0,0	0,3	0,0	4,5	0,7	0,0	0,0	0,0	0,0
18	9,3	2,1	0,0	16,2	7,4	25,1	17,3	2,5	0,0	5,6	0,8	0,0	0,0	0,0	0,0
19	2,6	1,4	0,0	7,1	2,9	24,7	33,1	3,9	0,0	23,6	2,9	0,0	0,0	0,6	0,0
20	16,1	0,6	0,0	22,1	6,6	47,3	45,1	5,1	0,0	0,0	0,5	0,0	0,0	0,0	0,0
21	0,0	0,0	0,0	54,7	7,4	47,4	0,0	0,0	0,0	5,0	1,1	0,0	0,0	0,3	0,0
22	12,8	2,6	0,0	52,2	8,5	18,6	0,0	0,0	0,0	41,2	3,6	10,0	0,0	0,0	0,0
23	27,2	2,7	0,0	54,8	7,0	37,7	0,0	0,0	0,0	23,6	2,4	9,1	0,0	0,0	0,0
24	26,8	3,6	0,0	43,5	7,7	10,7	0,0	0,5	0,0	23,0	2,7	0,2	0,0	0,0	0,0
25	7,9	2,9	0,0	14,5	3,5	0,0	60,4	6,7	40,5	0,0	0,0	0,0	0,0	0,0	0,0
26	3,5	1,4	5,1	16,5	3,6	0,0	69,3	7,3	30,4	27,8	2,8	0,0	0,0	0,0	0,0
27	0,0	0,5	0,0	45,9	6,0	0,0	66,8	7,2	39,1	0,0	0,5	0,0	0,0	0,9	0,0
28	0,0	0,0	0,0	24,1	2,9	0,0	61,0	6,4	22,1	4,6	1,6	0,0	0,0	0,0	0,0
29	5,4	4,0	0,0	46,7	4,9	39,1	19,5	2,1	13,7	0,0	0,0	0,0	0,0	0,0	0,0
30	22,6	4,9	0,0	59,3	5,4	37,6	12,8	2,4	17,2	0,0	0,0	0,0	0,0	0,0	0,0
31	22,9	4,5	0,0				15,2	2,6	13,0	17,2	2,1	0,0			
sum	417,3	69,1	5,1	776,8	147,6	441,0	620,3	74,7	363,5	472,5	51,8	263,8	105,4	17,0	7,4

Table 9.4. Monthly driving cost of the solar cooling system (any taxis are not included).

		Electricity EUR·kWh^{-1}	DH EUR·MWh^{-1}
Specific prices		0.073	47.32
Month	Cooling kWh	Electricity kWh	District heating kWh
April	-	-	-
May	417.3	69.1	5.1
June	794.6	197.0	502.0
July	604.2	98.3	430.6
August	437.2	67.9	336.5
September	100.5	26.0	8.2
October	186.3	65.4	447.6
sum	2540.1	523.7	1730
Cost [EUR]	120.09	38.23	81.86
Cost EUR·kWh^{-1}	0.047	driving cost	
Tot cost EUR*kWh^{-1}	2.34 1.50	Investment + Driving cost, pilot plant Investment + Driving cost, commercial plant	

9.3 Life-cycle cost of the solar system and comparison to traditional systems

Annual cost divided into investment and driving cost can be used for a comparison of different cooling production systems. Investment can be divided into annual cost, when the expected life-time in years and interest-bearing for the investment are required. A better understanding can be achieved when the life-cycle cost is calculated.

Basic data on energy prices, expected life-time, and interest for the calculation in Mikkeli case, as well as the cooling requirements of Office building (10 kW, t_{peak} = 1000 h·a^{-1}) are shown in Table 9.5. Energy prices are the same as in the case of the Mikkeli office.

Table 9.5. Input data for comparison of cooling alternatives.

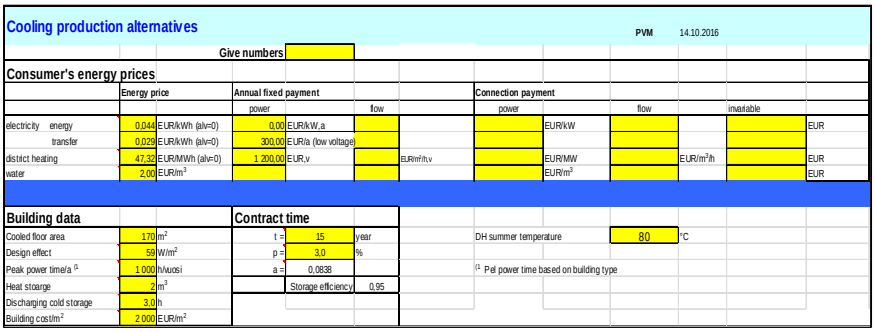

Cooling production alternatives — PVM 14.10.2016

Give numbers

Consumer's energy prices

	Energy price		Annual fixed payment power		Annual fixed payment flow		Connection payment power		Connection payment flow		Connection payment invariable	
electricity energy	0,044	EUR/kWh (alv=0)	0,00	EUR/kW,a				EUR/kW				EUR
transfer	0,029	EUR/kWh (alv=0)	300,00	EUR/a (low voltage)								
district heating	47,32	EUR/MWh (alv=0)	1 200,00	EUR,v		EUR/m³/h,v		EUR/MW		EUR/m³/h		EUR
water	2,00	EUR/m³						EUR/m³				EUR

Building data

Cooled floor area	170	m²
Design effect	59	W/m²
Peak power time/a [1]	1 000	h/vuosi
Heat storage	2	m³
Discharging cold storage	3,0	h
Building cost/m²	2 000	EUR/m²

Contract time

t =	15	year
p =	3,0	%
a =	0,0838	
	Storage efficiency	0,95

DH summer temperature 80 °C

[1] Pel power time based on building type

Absorption, adsorption and compressor chillers are compared more or less commercial side in Table 9.6. The total investment cost of absorption /adsorption /compressor chillers are EUR 4625/5016/2745·kW_c^{-1}. Additional investments in the absorption and adsorption chillers compared to the compressor chiller are solar collectors and heat storage tank (abs. 36 m^2 and ads. 40 m^2; storage 2 m^3). The compressor is supported with solar panels, an inverter, accumulator (22 m^2, 3 kW, 1250 Ah) and cold storage tank (0.36 m^3). Annual driving cost are EUR 2268 /EUR 2367/EUR 3046 to abs./ads./comp. The cooling energy prices are 55.5 EURcent per kWh_c for absorption, 59.2 EURcent per kWh_c for adsorption and 50.2 EURcent per kWh_c for compressor chiller divided into fixed and variable prices as shown in Figure 9.3.

When looking at life-cycle cost for those three chiller types (Figure.9.3) we notice that the break-point of life of absorption compared to the compressor chiller is about 17.5 years and adsorption to compressor chiller more than 30 years.

Investment cost of absorption, adsorption and compressor chiller without solar support is EUR 3006, 3267 and 2547 ·kW_c and annual driving cost 2841, 3117 and 3143 EUR/a. The cooling energy price of absorption, adsorption and compressor chiller is 53.6, 58.5 and 55.5 EURcent/kWhc. Absorption and adsorption chiller should have a higher capacity of at least 50 kW_c or more.

Table 9.6. Comparison of absorption. adsorption and compressor chillers.

BUILDING		Savosolar office	/	Mikkeli				
peak capacity	10,0	kW	cold energy	10,0	MWh/a	peak time	1000	h
cooled area	170	m²				peak time storage	5	h
Building cooling								

Compressor cooling

Technical properties		unit	amount	
Max cooling power		kW	10,0	
Cooling temp.	suply	°C	8	
	return	°C	15	
COP			3,60	3,77
Design power chiller		kW	10	
Condensed power		kW	13	
Power		kW	3	
Cold storage capacity		MWh	0,016	
Give cooling media			R-407C	
Cold media amount		kg	5	
Give outdoor cooling tower type			1	
Give cooling water T_{in}		°C	10	
Cooling media cost.		EUR/kg	33,64	
Lubrication oli cost	naime 1	EUR/lt	10,00	

Compressor cooling

Investment (vat=0)		Time [y]	Inv.cost [EUR]	Cost/year [EUR/a]
Connection price	electricity	15	0	0,00
	DH	15		0,00
	DC	15		0,00
Chiller	1 pc	15	7 003	586,65
Amount of cold media		5	168	36,73
Cooling tower	1 pc	15	5 038	422,01
electricity work		30	2 500	127,55
Pipe lines		30	2 000	102,04
Pumps		15	1 000	83,77
Liquid circle filling		10		0,00
Free cooling		15		0,00
Room for chiller				
Room		30	2 096	106,92
Bed for chiller		15	161	13,53
sound insolation		30	2 000	102,04
Others		1		0,00
Cold storage 0,36 m³		15	2 000	167,53
Outdoor investment		15		0,00
Cooling tower shelter		15		0,00
Cooling tower sound insolation		15		0,00
Architect extra construction		15		0,00
Others		15	1 500	125,65
		Investment cost	25 467	1 874,41

Solar collector		Compressor		
Technical facts		amount	unit	Obs.
Solar radiation on the surface		600	W/m2/vuosi	
Light aperture		2,0	m2	
effciency		0,7		
collector vertical angle		50	°	45-58 °
max. mass flow		0,0228	kg/s --> kg/h	82,08
pressure loss in collector		0,91	kPa	
liquid volume in collector		1,9	lt	glykol+water
Investment cost	solar panel 22 m2 + accumulato		15 500	
Investment cost sum			**40 967**	**1 298**

Compressor cooling

Driving cost		unit	Quantity	Annual cost [EUR/a]
Fixed cost				
Annual payment	electricity	kW	2,8	203,49
	DH	kW		
Variable cost				
Cooling energy		MWh	10,0	
Cooling circle pumping		MWh	2,47	180,76
Chiller, electricity		MWh	2,7	194,26
Blowers, electricity		MWh	3	195,25
Condense circle pumps, electricity		MWh	0,85	61,97
Gas consumption		MWh		
Cold media adding	R-407C	kg/a	1,0	33,64
Chiller, oil consumptio		lt/a	10,0	100,00
Water comsumption		m³/a	0	0,00
Stoarage loss		MWh	0,0	0,00
Service contract	5 years			200,00
Spare parts				200,00
Service contract		h	4,0	1 473,34
Others				300,00
		Driving cost		3 142,70
		Annual cost total		**4 441,08**

Compressor cooling

Driving cost		unit	Quantity	Annual cost [EUR/a]
Solar circle electricity		kWh		
Solar energy repayment		MWh	1,3	-97,13
		Driving cost		**-97,13**
Annual cost total				**4 343,95**
		Investment cost [EUR/kW]		**2544,74**
		Investment cost[EUR/m²]		**149,80**
		Investment cost [EUR/m³]		**49,93**
		Cooling energy cost. [EUR/MWh,a]		**443,53**
			%	EUR/MWh
		Fixed cost	46,8	207,520
		Variable cost	66,2	293,540

Absorption cooling

Technical properties		unit	amount	
Max cooling power		kW	10,0	
Cooling ter	suply	°C	8	
	return	°C	15	
COP			0,80	0,85
Design power chiller		kW	10	
Condensed th power		kW	23	
DH th power		kW	12	
Heat storage capacity		MWh	0,016	
Give cooling media			LiBr+H2O	
Cold media amount		kg	10	
Give outdoor cooling tower type			1	
Give cooling water T_{in}		°C	10	
Cooling media cost.		EUR/kg	20,00	
Lubrication	naime 1	EUR/lt	10,00	

Absorption cooling

Investment (vat=0)		Time [y]	Inv.cost [EUR]	Cost/year [EUR/a]
Connection	electricity	15		0,00
	DH	15	0	0,00
	DC	15		0,00
Chiller	1 pc	20	11 672	784,57
Amount of cold media		8	200	28,49
Cooling towe	1 pc	15	5 726	479,62
	electricity work	30	1 000	51,02
	Pipe lines	30	2 000	102,04
	Pumps	15	1 000	83,77
	Liquid circle filling	10		0,00
Free cooling		15		0,00
Room for chiller				
	Room	30	2 234	114,00
	Bed for chiller	15	161	13,53
	sound insolation	30	0	0,00
	Others	1		0,00
Heat storage 2 m³		15	5 000	418,83
Outdoor investment		15		0,00
	Cooling tower shelter	15		0,00
	Cooling tower sound insolation	15		0,00
	Architect extra construction	15		0,00
	Others	15	1 069	89,55
		Investment cost	30 063	2 165,41

Absorptiojäähdytys				
Investments (vat=0)		time [y]	Inv.cost [EUR]	Annual cost [EUR/a]
18 pc collector		20	8 059	541,70
pipeline		20	7 065	474,88
Pumps		15	1 000	83,77
filled liquid		5	94	20,48
other		15		0,00
		Investment cost	16 218	1 121
			46 281	**3 286**

Absorption cooling

Driving cost		unit	Quantity	Annual cost [EUR/a]
Fixed cost				
Annual payment	electricity	kW		
	DH	kW	11,8	
Variable cost				
Cooling energy		MWh	10,0	
Cooling circle pumping		MWh	2,47	180,76
Chiller, electricity		MWh		
		MWh	12,5	592,27
Blowers, electricity		MWh	3	204,66
Condense circle pumps, electr.		MWh	0,92	67,58
Gas consumption		MWh		
Cold media	LiBr+H2O	kg/a	1,2	24,00
Chiller, oil consumptio		lt/a	2,0	20,00
Water comsumption		m³/a	0	0,00
Stoarage loss		MWh	0,0	0,00
Service co	5 vuotta			150,00
Spare parts				200,00
Service contract		h	4,0	1 101,89
Others				300,00
		Driving cost		2 841,17
		Annual cost total		**6 127,39**

Absorption cooling

Driving cost		unit	Quantity	Annual cost [EUR/a]
Solar circle electricity		kWh	267,1	19,55
Solar energy repayment		MWh	12,5	-592,27
		Driving cost		**-572,72**
		annual cost total		**5 554,67**
		Investment cost [EUR/kW]		**4624,57**
		Investment cost[EUR/m²]		**272,24**
		Investment cost [EUR/m³]		**90,75**
		Cooling energy cost. [EUR/MWh,a]		**554,75**
			%	EUR/MWh
		Fixed cost	59,2	328,196
		Variable cost	40,8	226,550

Adsorption coolings

Technical properties		unit	amount	
Max cooling power		kW	10,0	
Cooling tem	suply	°C	14	
	return	°C	18	
COP			0,60	0,85
Design power chiller		kW	10	
Condensed th power		kW	27	
DH th power		kW	12	
Heat storage capacity		MWh	0,009	
Give cooling media			H_2O+Silicagel	
Cold media amount		kg	10	
Give outdoor cooling tower type			1	
Give cooling water T_{in}		°C	10	
Cooling media cost.		EUR/kg	20,00	
Lubrication o	naime 1	EUR/lt	10,00	

Adsorption coolings

Investment (vat=0)		Time [y]	Inv.cost [EUR]	Cost/year [EUR/a]
Connection p	electricity	15		0,00
	DH	15	0	0,00
	DC	15		0,00
Chiller	1 pc	20	13 676	919,25
Amount of cold media		8	200	28,49
Cooling tower	1 pc	15	6 324	529,76
	electricity work	30	1 000	51,02
	Pipe lines	30	2 000	102,04
	Pumps	15	1 000	83,77
	Liquid circle filling	10		0,00
Free cooling		15		0,00
Room for chiller				
	Room	30	2 234	114,00
	Bed for chiller	15	161	13,53
	sound insolation	30	0	0,00
	Others	1		0,00
Heat storage 2 m³		15	5 000	418,83
Outdoor investment		15		0,00
	Cooling tower shelter	15		0,00
	Cooling tower sound insolation	15		0,00
	Architect extra construction	15		0,00
	Others	15	1 069	89,55
		Investment cost	32 665	2 350,22

Adsorptiojäähdytys				
Investments (vat=0)		time [y]	Inv.cost [EUR]	Annual cost [EUR/a]
20 pc collector		20	9 366	629,54
pipeline		20	7 065	474,88
Pumps		15	1 000	83,77
filled liquid		5	103	22,55
other		15		0,00
		Investment cost	17 534	1 211
			50 199	**3 561**

Adsorption coolings

Driving cost		unit	Quantity	Annual cost [EUR/a]
Fixed cost				
Annual payment	electricity	kW		
	DH	kW	11,8	
Variable cost				
Cooling energy		MWh	10,0	
Cooling circle pumping		MWh	2,47	180,76
Chiller, electricity		MWh		
		MWh	16,7	789,69
Blowers, electricity		MWh	3	204,66
Condense circle pumps, electr.		MWh	0,92	67,58
Gas consumption		MWh		
Cold media	H2O+Silicagel	kg/a	1,2	24,00
Chiller, oil consumptio		lt/a	2,0	20,00
Water comsumption		m³/a	0	0,00
Stoarage loss		MWh	0,0	0,00
Service cont	5 vuotta			150,00
Spare parts				200,00
Service contract		h	4,0	1 179,95
Others				300,00
		Driving cost		3 116,66
		Annual cost total		**6 677,62**

Adsorption coolings

Driving cost		unit	Quantity	Annual cost [EUR/a]
Solar circle electricity		kWh	551,5	40,37
Solar energy repayment		MWh	16,7	-789,69
		Driving cost		**-749,32**
		annual cost total		**5 928,30**
		Investment cost [EUR/kW]		**5016,14**
		Investment cost[EUR/m²]		**295,29**
		Investment cost [EUR/m³]		**98,43**
		Cooling energy cost. [EUR/MWh,a]		**592,06**
			%	EUR/MWh
		Fixed cost	60,1	355,634
		Variable cost	39,9	236,426

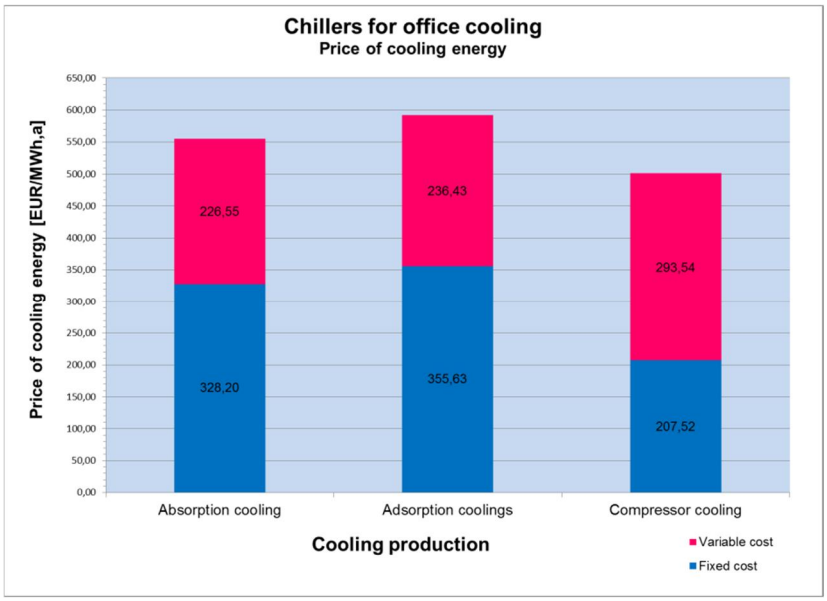

Figure 9.3. Annual cost of cooling production alternatives.

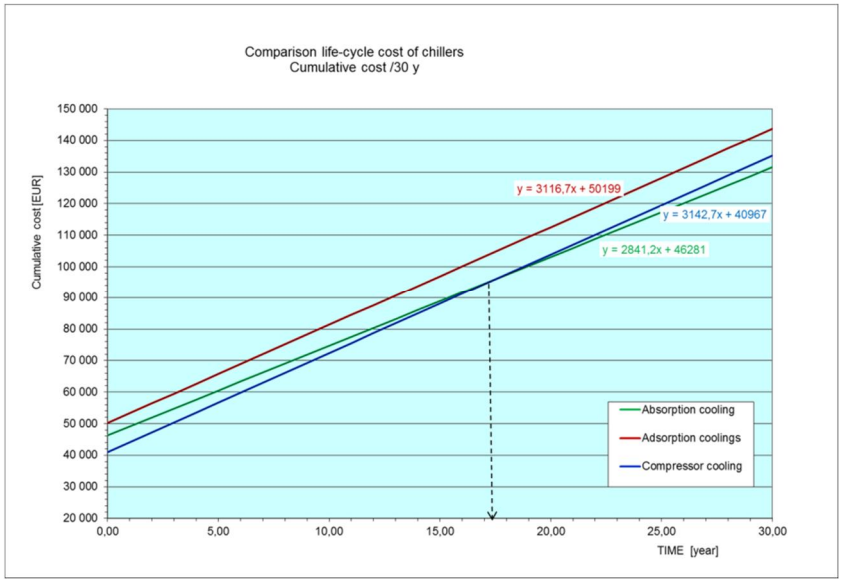

Figure 9.4. Life-cycle cost of cooling production alternatives.

10. Conclusion and recommendations

In this Finnish–German joint research project, a small scale (10 kW) solar cooling and heating (25 kW) system with a compact absorption chiller/heat pump and improved foil collectors has been developed and successfully demonstrated at Savo-Solar office building in Mikkeli, Finland. By use of thermally-driven absorption instead of electrically-driven compressor heat pump technology, no additional grid stress or reserve capacity, either in summer or in winter is caused. The demonstration consists of a solar/heat driven (36 m^2 collectors) absorption chiller, heat storage and district heating or biomass boiler backup (15 kW) for the chiller. The absorption machine can be operated as a chiller or heat pump. Based on simulation the most suitable V/S (heat storage volume/collector surface) is 55.6 l/m^2, so it means 2 m^3 in Savo-Solar case.

Besides the improvement of the absorption machine with regard to the required temperature thrust and overall efficiency of the flat-plate solar thermal foil collectors, a practical feasibility study of a biomass-driven double stage absorption machine was conducted at ZAE Bayern labs in Munich, Germany. Despite challenging corrosion phenomena's, the results of the Biomass fired double-effect chiller/heat pump are quite satisfying. Thus, it will be commercialized in a follow-up project with the German company HDG Bavaria in 2017/2018, based on wood chip combustion. In combination with ground heat exchangers and solar collectors ,it appears as a very promising alternative for a low-carbon heat and cold supply for buildings and industrial processes in the temperature range between 4 and 110 °C for Finland as well.

Regretfully, no economically satisfying solution was found for replacing the well-insulating but non-friendly mineral wool inside the 2 m^2 collector. But, by adding a foil between the glass and aperture area, the front-side heat losses were reduced on average by 6% from June–October 2016 and significantly up to 11% in September, especially at higher temperatures, which are required to drive the absorption chiller during summertime. As the future of the solar thermal collector industry is stated in large scale applications the developed techniques are suggested for transfer to bigger scales as well.

Right now, the system itself shows adequate key performance results, but there is still a high optimization potential by adopting the control strategy for the special requirements and peculiarities of the building. The system size of 10 kW cooling capacity was chosen in order to cover the office needs. From an economic point of view, the targeted size of the system is 50 kW chilled water capacity and up. As renewable heat from the collectors is very rare in wintertime, an additional ground heat exchanger or the use of low temperature waste heat (e.g. from the coating machine) would increase the annual share of renewables for cooling and heating to more than 50% in total.

The total investment cost of the solar-driven chiller pilot project was EUR 69 550 (6955 EUR/kW_c), which consists of a solar field (35.0%), chiller & hydraulics (21.5%), heat storage (10.6%), dry air cooling (17.7%) and district heating backup 15.1%. The driving cost of the pilot project was 4.7 EURcent per kWh of cooling energy. If we include investment cost of the pilot project, the price of cooling energy is 2.34 EUR/kWh_c. A commercial project price is evaluated to be about 1.50 EUR/kWh_c.

Advantages

- Simultaneous cooling/heating possibility, high driving hours/a
- High EER, more than 9
- COP of at least 0.7 or more
- Compact package, two pieces: chiller and heat storage in addition to solar heating system, DH or biofuel boiler
- Large range of working modes
- Solar cooling meets demand
- DH-based cooling and heating meets demand as well as Biofuel-based cooling and heating meets demand
- Foil collector up to 11% more efficiency. Collector field has at least 3% higher efficiency compared to standard version

Items for solving or developing later

- Provide sufficient temperature and power to the chiller (district &solar)
- EER_C of more than 15 is favourable
- COP_C of more than 0.8 is favourable
- Lower heat loss in the collector and especially the piping
- Control system development according to the building needs and peculiarities
- Improvement of weather forecast and control interaction
- Humidity prevention of collector
- Multi-stage version of abs. chiller

11. Acknowledgments

The work described in this publication is a Finnish–German collaboration and was funded by the Federal Ministry of Economics and Technology (BMWi) and was managed by the Project Management Organization Jülich (PTJ) in Germany and by Tekes – the Finnish Funding Agency for Innovation in Finland. The project was carried out in the time frame 10/2013–12/2016.

Two solar driven cooling/heating cases have been built, one in the office building of Savo-Solar Oy in Mikkeli, Finland, and one in the test hall of ZAE-Bayern in Münich, Germany.

12. Publications and disseminations in the project

Reda Francesco, Viot Maxime, Sipilä Kari, Helm Martin, 2016, Energy assessment of solar cooling thermally driven system configurations for an office building in a Nordic country, Applied Energy, Volume 166, 15 March 2016, Pages 27-43, ISSN 0306-2619.
http://dx.doi.org/10.1016/j.apenergy.2015.12.119.

Helm, M., Reuss M., Riepl M., 2016. Solar thermal cooling. District heating days. August 24-25, 2016. Mikkeli. Finnish energy industry. 19 p.
http://energia.fi/sites/default/files/images/solar_cooling_-_reuss_-_mikkeli_25.08.2016.pdf

Bundesministerium für Wirtschaft und Energie (BMWi), Innovation durch Forschung; Erneuerbare Energien und Energieeffizienz: Projekte und Ergebnisse der Forschungsförderung 2014; April 2015, p. 126,
http://bmwi.de/DE/Mediathek/publikationen,did=703846.html

Bundesministerium für Wirtschaft und Energie (BMWi); Solar Heating and Cooling in Northern and Central Europe – Deutsch-finnisches Kooperationsprojekt; Forschungsjahrbuch Energie 2015; August 2016; p. 299
http://www.forschungsjahrbuch-energie.de/projekt/2067

Innovation durch Forschung; Erneuerbare Energien und Energieeffizienz: Projekte und Ergebnisse der Forschungsförderung 2014; Bundesministerium für Wirtschaft und Energie (BMWi), April 2015, p. 126
http://bmwi.de/DE/Mediathek/publikationen,did=703846.html

Solar Heating and Cooling in Northern and Central Europe – Deutsch-finnisches Kooperationsprojekt; Forschungsjahrbuch Energie 2015; Bundesministerium für Wirtschaft und Energie (BMWi); August 2016; p. 299
http://www.forschungsjahrbuch-energie.de/projekt/2067

Helm, M., 2015, Solarthermisches Heiz- und Kühlsystem; Presentation at Ökoprofit Working group, Munich 2015

References

Beikircher, T. 2010. Abschlussbericht - Hocheffizienter Flachkollektor mit Foliendämmung und Überhitzungsschutz für Temperaturen zwischen 70-100 °C. Technical report, Zentrum für angewandte Energieforschung in Bayern (ZAE Bayern), 2010. German document available under http://www.tib-hannover.de/ - Förderkennzeichen 0329280A; Last access: 03.02.2015.

Bin Gadhi, S., Agarwal, R. & Kaushik, S. 1987. Nucleate Pool Boiling Heat Transfer Coefficient for Methanol-Salt Mixture (LiBr.ZnBr2) Solutions: Experimental Studies. s.l., Solar and Wind Technology 431-441.

Bratu, C. 2008. Evaluation of solar irradiance to a flat surface arbitrary oriented. *Electrical Engineering series. No.32. 2008*. 1842-4805.

Deutsches Institut für Normung (DIN): Thermische Solaranlagen und ihre Bauteile - Kollektoren - Teil 2: Prüfverfahren; Deutsche Fassung EN 12975-2:2006, 2006.

Duffie, J.A. & Beckman, W.A. 2013. Solar Engineering of Thermal Processes. 4th Edition. Wiley. May 2013. 936p.

Duffie, J.A. & Beckman, W.A. 2006. Solar Engineering of Thermal Processes. John Wiley & Sons, 2006.

DuPont AG: Tefzel (ETFE) Fluoropolymer Properties Handbook. 1999. Available under http://www.cable-ties.com/catalog/pdfs/tefzel.pdf; Last access: 03.02.2015

EU. 2007. EU's 'Energy and Transport Trends 2007: Business as usual Scenario'.

IEA. 2012. Technology Roadmap Solar Heating and Cooling. International Energy Agency. 2012. https://www.iea-shc.org/data/sites/1/publications/2012_SolarHeatingCooling_Roadmap.pdf

Finnish Meteorological Institute. 2013. December. *Open Data Manual*. Retrieved from http://en.ilmatieteenlaitos.fi/open-data-manual

Finnish Meteorological Institute. 2015. December. *Weather forecast models.* Retrieved from http://en.ilmatieteenlaitos.fi/weather-forecast-models

Giovanetti, F., Kirchner, M., Rockendorf, G. & Kehl, O. 2011. Cellulose Triacetate Honeycomb Compounds for improved Flat-Plate Collectors: Performance and Reliability. In: Proceedings ISES Solar World Congress, 2011.

Giovanetti, F. et al. 2013. Abschlussbericht - Hocheffiziente Flachkollektoren mit selektiv beschichteten Zweischeibenverglasungen. Technical report, Institut für Solarenergieforschung GmbH (ISFH), 2013. German document available under http://www.tib-hannover.de/ - Förderkennzeichen 0325973 A-D; Last access: 03.02.2015

Helm, M. 2015. Pumps Efficiency and Adaptability. [Online]
Available at: https://www.iea-shc.org/data/sites/1/publications/Task48%20A4%20-%20Pump%20Efficiency%20and%20Adaptability_Final%20%20%20report.pdf

Helm, M., Reuß, M. & Riepl, M. 2016. Solar thermal cooling, Mikkeli distric heating days. [Online] Available at:
http://energia.fi/sites/default/files/images/solar_cooling_-_reuss_-_mikkeli_25.08.2016.pdf

Henning, H-M. & Motta, M. 2013. Solar Cooling Handbook, 3rd Completely revised editi3on, Solar heating and cooling programme, IEA, Ambra V, 2013, 367 p.

Hummelsberger GmbH. 2017. Vacuum storage. [Online]
Available at: http://vacuum-storage.com/ [Zugriff am 16 01 2017].

IEA. 2012. Technology Roadmap Solar Heating and Cooling.. http://www.iea-shc.org/data/sites/1/publications/2012_SolarHeatingCooling_Roadmap.pdf Hrsg. s.l.: International Energy Agency (IEA).

Keith, E.H., Radermacher, R. & Klein, S.A. 1996. Absorption Chillers and Heat Pumps. ISBN 9780849394270, CRC Press (Taylor & Francis Group).

Koponen, P., Pasonen, R. & Löf, A. 2016. Analysis of optimal dynamic price control of heat pump houses with solar power, CIRED Workshop, 14–15 June 2016, Helsinki, Finland, CIRED (2016), Paper 0038.

Kren, C. 2009. Flue gas fired absorption chillers. s.l.: Dissertation, Fakultät für Physik, Technische Universität München.

Meteonorm. 2015. METEOTEST, Bern, Switzerland
http://meteonorm.com/products/meteonorm/database/

Ministry of Environment. 2012. D3 Energy Management in Buildings Regulations and Guidelines 2012. Available at: http://www.finlex.fi/data/normit/37188-D3-2012_Suomi.pdf (in Finnish).

Mitalas, G. & Arseneault, J. 1972. Fortran IV program to calculate z-transfer functions for the calculation of transient heat transfer through walls and roofs, National Research Council of Canada, Ottawa, 1972.

Moretti, E., Bonamente, E., Buratti, C. & Cotana, F. 2013. Development of Innovative Heating and Cooling Systems Using Renewable Energy Sources for Non-Residential Buildings. Energies, 9 11, Issue 6, pp. 5114–5129.

Obernberger, I. 2008. Industrial combustion of solid biomass fuels – state-of-the-art and relevant future developments (keynote lecture). Milano, Italy, Proceedings of the International Conference on Waste and Biomass Combustion.

PostgreSQL. 2015. Open source database solution. https://www.postgresql.org/ http://energia.fi/sites/default/files/images/solar_cooling_-_reuss_-_mikkeli_25.08.2016.pdf

Reuss, M., Helm, M. & Riepl, M. 2016. Solar thermal cooling. District heating days. August 24–25. Mikkeli. Finnish energy industry. 19 p.

Reda, F., Viot, M., Sipilä, K. & Helm, M. 2016, Energy assessment of solar cooling thermally driven system configurations for an office building in a Nordic country, Applied Energy, Volume 166, 15 March 2016, Pages 27–43, ISSN 0306-2619, http://dx.doi.org/10.1016/j.apenergy.2015.12.119.

RHC. 2014. Solar heating and cooling road map. http://www.rhc-platform.org/fileadmin/user_upload/Structure/Solar_Thermal/Download/Solar_Thermal_Roadmap.pdf

Savo-Solar Oy. 2014. Information on new TPS module. 2014. Available under http://www.Savo-Solar.fi/index.php/en/products-solutions/business-applications/tps-products; Last access: 03.02.2015.

Shi, C., Xu, C. & Hu, H. 2009. Study on falling film generation heat transfer of lithium bromide solution in vertical tubes. DOI: 10.1007/s11630-009-0241-z, Journal of Thermal Science, Vol. 18, No. 3, 241–245.

Sipilä, K. et al. 2015. Distributed Energy Systems (DESY). VTT Technology 224. VTT, Espoo. 186 p. + app. 2 p. http://www.vtt.fi/inf/pdf/technology/2015/T224.pdf

Solar Keymark Database. 2012. Test Results Summary Savo-Solar Collector SF 100-03, 2012. Available under http://www.estif.org/solarkeymark/Links/Internal_links/certif/PSK-036-2013.pdf; Last access: 04.02.2015.

Solar Keymark Database. 2012. Test Results Summary Vaillant VFK 155, 2012.

Available under http://www.dincertco.de/logos/011-7S1937%20F.pdf; Last access: 04.02.2015.

Solar Keymark Database. 2012. Test Results Summary Viessmann Vitosol 300 T, 2012. Available under http://www.dincertco.de/logos/011-7s556_r.pdf; Last access: 04.02.2015.

Solar Keymark Database. 2014. Test Results Summary Viessmann Vitosol 300 F, 2014. Available under http://www.dincertco.de/logos/011-7s2349%20f.pdf; Last access: 04.02.2015.

Vares, S. & Shemeikka, J. 2016. LCA for local energy production and energy storage systems. LCA Nornet workshop, 4.10.2016, 12 p., Nornet LCA Helsinki. http://www.nornetlca.nu/workshops/helsinki/

Viot, M., Hilpinen, J., Kalema, T. & Nyrhinen, J. 2015. Dynamic Building Energy Simulation, Tampere University of Technology, January 2015.

Zuber, N. & Tribus, M., 1958. Further Remarks on the Stability of Boiling Heat Transfer. Report 58-5. Project 34. Los Angeles, USA, University of California, Department of Engineering.

Links

IEA/Solar heating and cooling program:
https://www.iea-shc.org/
http://task48.iea-shc.org/
http://task38.iea-shc.org/

Annex 1a: Weather measurement of SOLCH project. June 3 2016

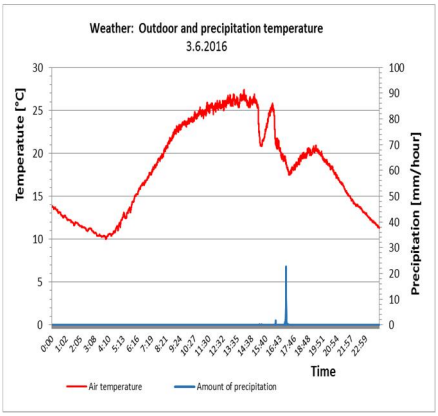

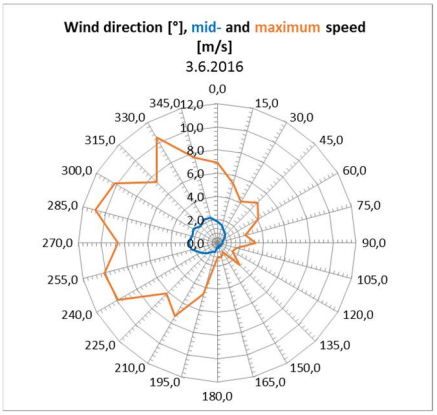

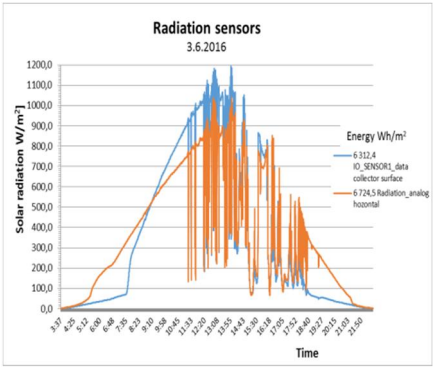

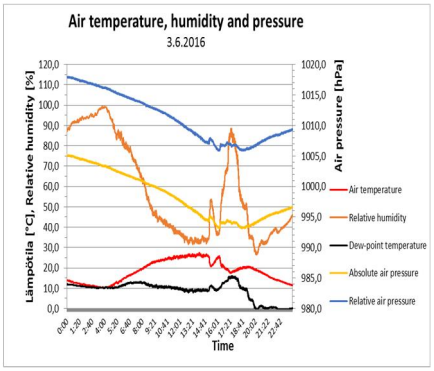

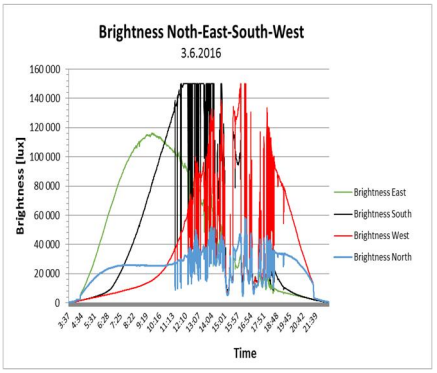

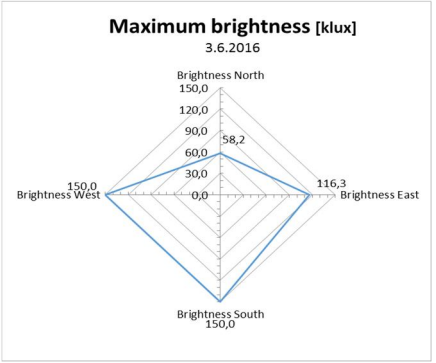

Annex 1b: Solar &Chiller measurement of SOLCH project. June 3 2016

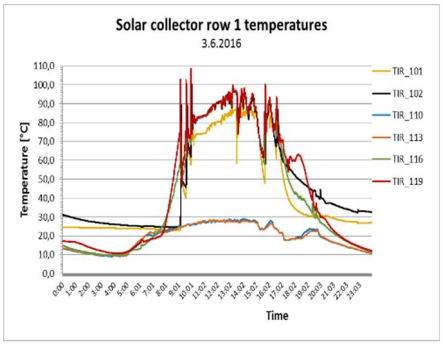

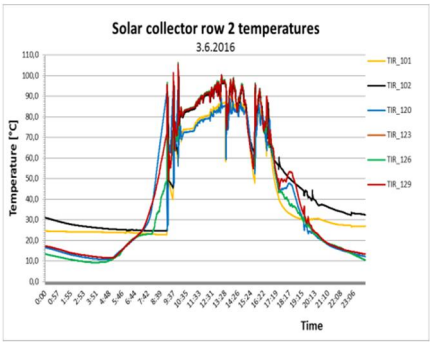

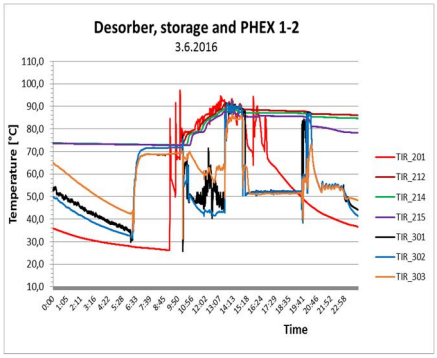

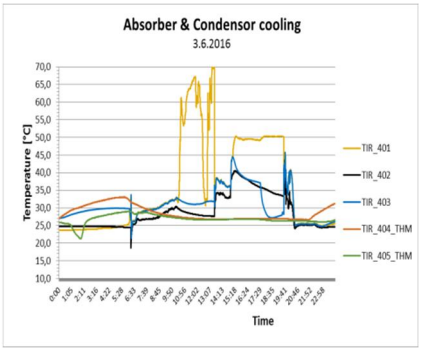

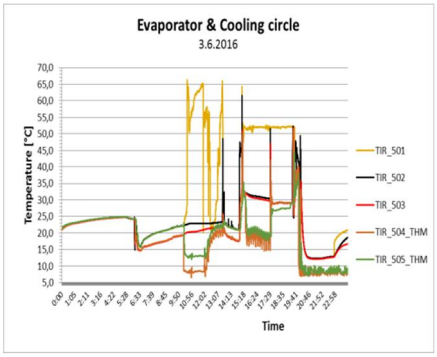

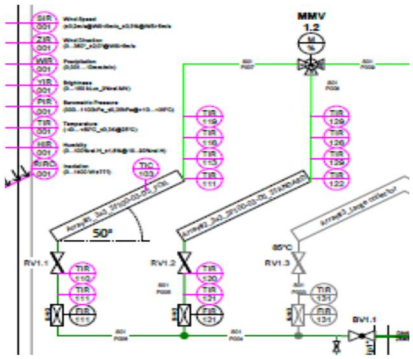

Annex 2: Operation modes of the SHC-System in Mikkeli

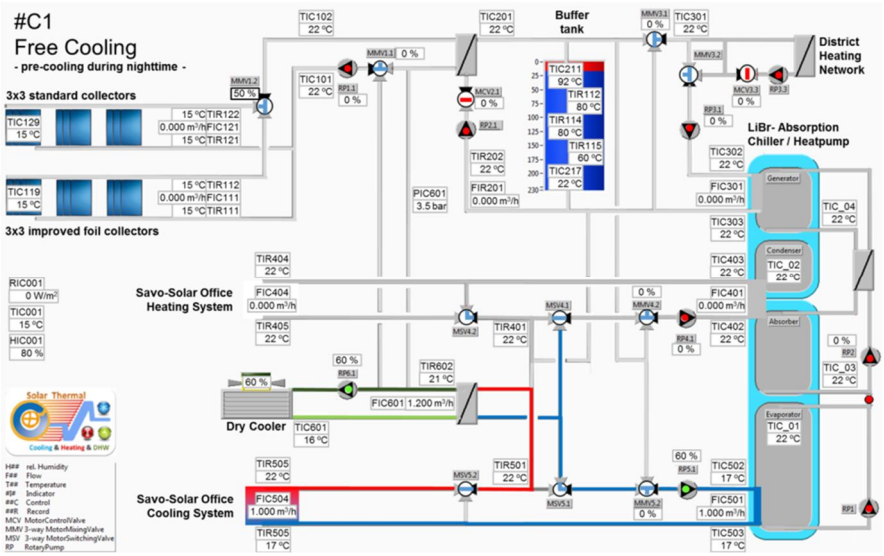

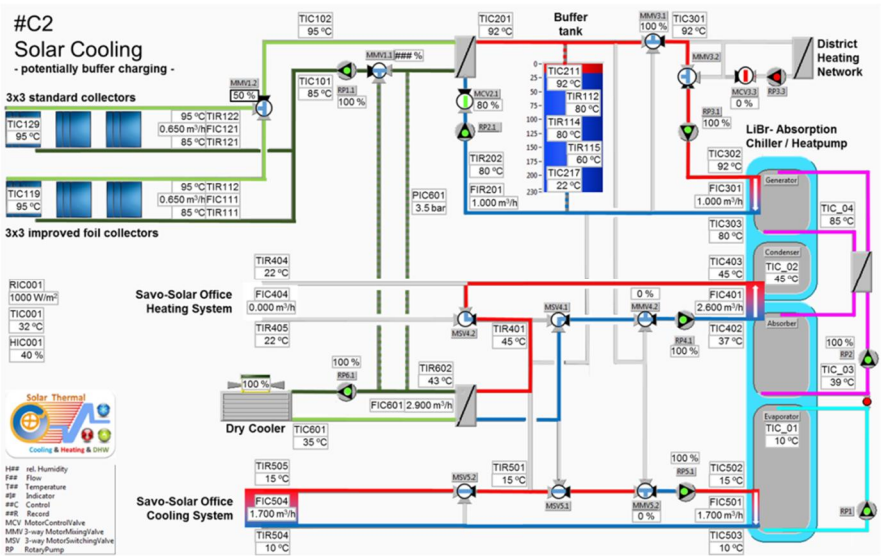

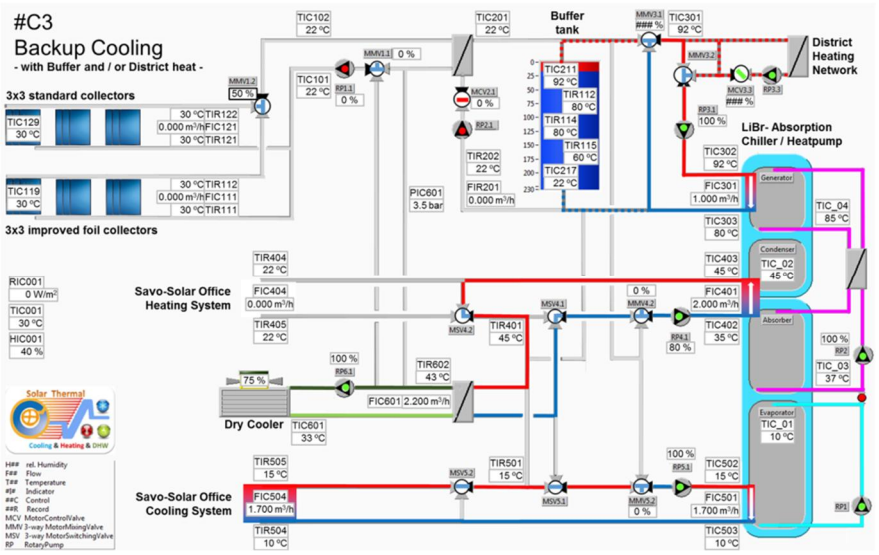
#C3
Backup Cooling
- with Buffer and / or District heat -
3x3 standard collectors
3x3 improved foil collectors
Buffer tank
District Heating Network
LiBr- Absorption Chiller / Heatpump
Savo-Solar Office Heating System
Savo-Solar Office Cooling System
Dry Cooler
Solar Thermal
Cooling & Heating & DHW
Generator
Condenser
Absorber
Evaporator

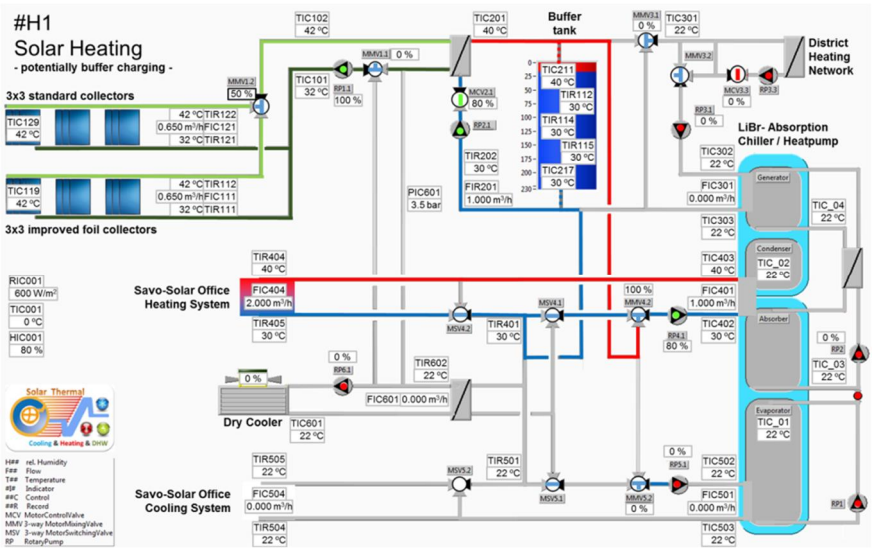
#H1
Solar Heating
- potentially buffer charging -
3x3 standard collectors
3x3 improved foil collectors
Buffer tank
District Heating Network
LiBr- Absorption Chiller / Heatpump
Savo-Solar Office Heating System
Savo-Solar Office Cooling System
Dry Cooler
Solar Thermal
Cooling & Heating & DHW
Generator
Condenser
Absorber
Evaporator

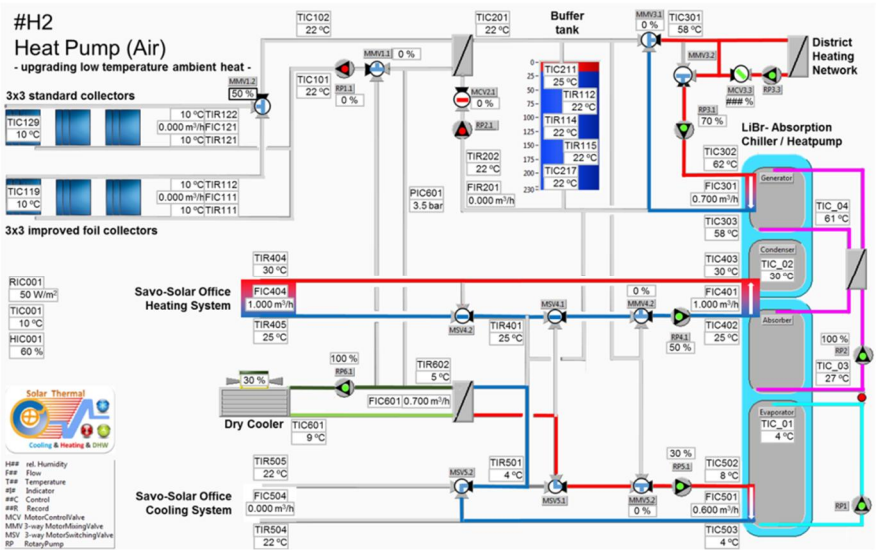
#H2
Heat Pump (Air)
- upgrading low temperature ambient heat -
3x3 standard collectors
3x3 improved foil collectors
Buffer tank
District Heating Network
LiBr- Absorption Chiller / Heatpump
Savo-Solar Office Heating System
Savo-Solar Office Cooling System
Dry Cooler
Generator
Condenser
Absorber
Evaporator
Solar Thermal
Cooling & Heating & DHW

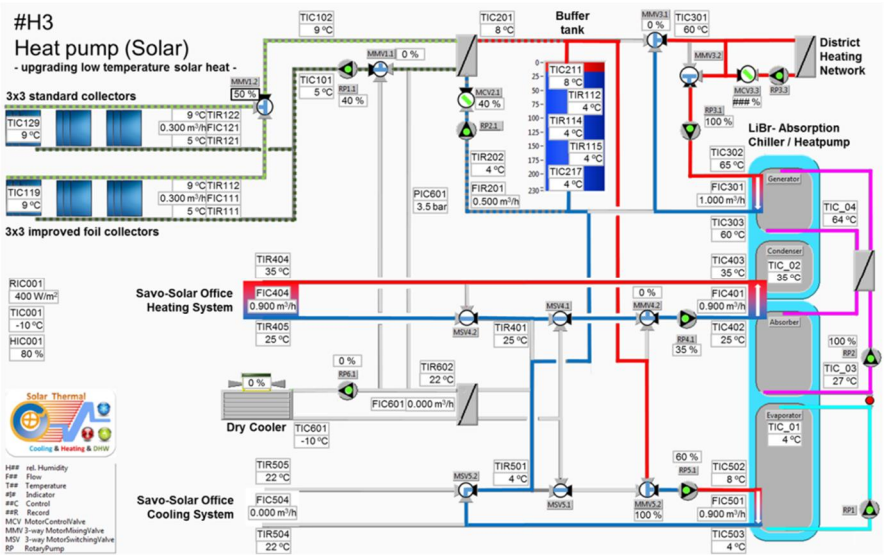
#H3
Heat pump (Solar)
- upgrading low temperature solar heat -
3x3 standard collectors
3x3 improved foil collectors
Buffer tank
District Heating Network
LiBr- Absorption Chiller / Heatpump
Savo-Solar Office Heating System
Savo-Solar Office Cooling System
Dry Cooler
Generator
Condenser
Absorber
Evaporator
Solar Thermal
Cooling & Heating & DHW

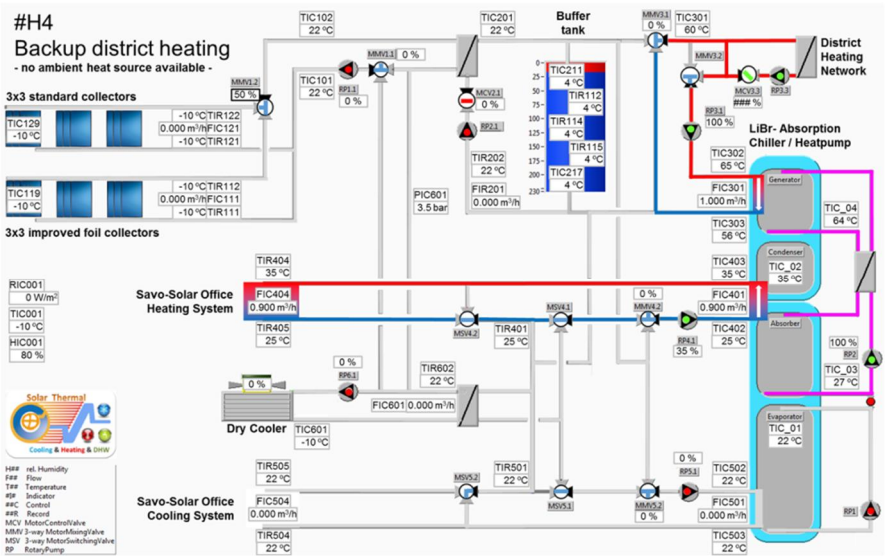
#H4
Backup district heating
- no ambient heat source available -
3x3 standard collectors
3x3 improved foil collectors
Buffer tank
District Heating Network
LiBr- Absorption Chiller / Heatpump
Generator
Condenser
Absorber
Evaporator
Savo-Solar Office Heating System
Savo-Solar Office Cooling System
Dry Cooler
Solar Thermal
Cooling & Heating & DHW
H## rel. Humidity
F## Flow
T## Temperature
#I# Indicator
#C Control
#R Record
MCV MotorControlValve
MMV 3-way MotorMixingValve
MSV 3-way MotorSwitchingValve
RP RotaryPump

Series title and number

VTT Technology 287

Title	**Solar heating and cooling in Northern and Central Europe** Pilot plants in Finland and Germany: Finnish-German joint research project within the European SET-plan strategy
Author(s)	Kari Sipilä, Francesco Reda, Riku Pasonen, Atte Löf, Maxime Viot, Kaj Pischow, Martin Helm, Maximillioan Möckl, Florian Menhard, Peter Osgyan & Manuel Kausche
Abstract	Solar heating and cooling technologies are compatible with almost all sources of backup heat and almost universally applicable due to their ability to deliver hot water, hot air and cold air. In the solar cooling process, the demand and supply of cooling will meet each other. The general objective of this Finnish–German cooperative research project has been to develop an innovative energy system for solar heating, cooling and domestic hot water preparation so as to broaden the application of improved solar thermal systems and absorption heat pumps/chillers for domestic and industrial buildings in Northern and Central European countries. In this project a small scale (10 kW) solar cooling and heating (25 kW) system with a compact absorption chiller/heat pump and improved foil collectors has been developed and successfully demonstrated at the Savo-Solar office building in Mikkeli, Finland. By use of thermally-driven absorption instead of electrically-driven compressor heat pump technology, no additional grid stress or reserve capacity, either in summer or in winter, is caused. The demonstration consists of a solar-heat-driven (36 m2 collectors) absorption chiller, heat storage and district heating or biomass boiler backup (15 kW) for the chiller. The absorption machine can be operated as a chiller or heat pump. Based on simulations, the most suitable V/S (heat storage volume/collector surface) is 55.6 l/m2, so it means 2 m3 in the Savo-Solar case. A practical feasibility study of a biomass (wood chip) -driven double-stage absorption machine was conducted also at the ZAE Bayern laboratory in Munich, Germany. By adding a foil between the glass and aperture area, front-side heat losses have been reduced significantly by up to 11%, especially at higher temperatures, which are required to drive the absorption chiller during summertime. As the future of the solar thermal collector industry is seen to be in large scale applications, it is suggested that the developed techniques are transferred to larger scales as well.
ISBN, ISSN, URN	ISBN 978-951-38-8511-3 (Soft back ed.) ISBN 978-951-38-8510-6 (URL: http://www.vttresearch.com/impact/publications) ISSN-L 2242-1211 ISSN 2242-1211 (Print) ISSN 2242-122X (Online) http://urn.fi/URN:ISBN:978-951-38-8510-6
Date	January 2017
Language	English, Finnish abstract
Pages	161 p. + app. 6 p.
Name of the project	Solar Cooling
Commissioned by	Tekes and Federal Ministry of Economics and Technology, BMWi
Keywords	cooling, heating, absorption chiller, district heating, biomass fuels
Publisher	VTT Technical Research Centre of Finland Ltd P.O. Box 1000, FI-02044 VTT, Finland, Tel. 020 722 111

Julkaisun sarja ja numero

VTT Technology 287

Nimeke	**Aurinkojäähdytys ja -lämmitys Pohjois- ja Keski-Euroopassa** Suomen ja Saksan t&k-yhteistyöprojekti Euroopan SET-strategiasuunnitelmassa
Tekijä(t)	Kari Sipilä, Francesco Reda, Riku Pasonen, Atte Löf, Maxime Viot, Kaj Pischow, Martin Helm, Maximillioan Möckl, Florian Menhard, Peter Osgyan & Manuel Kausche
Tiivistelmä	Aurinkoenergia on hyvin yhteensopiva lähes kaikkien muiden energian tuotantomuotojen kanssa tuottamaan lämmitystä ja jäähdytystä veden ja ilman välityksellä. Aurinkoenergia on myös keino vähentää sähkön käyttöä lämmityksessä ja jäähdytyksessä sekä polttoaineita, joiden hinnat vaihtelevat ja ovat usein myös tuontiriippuvia ja jotka aiheuttavat päästöjä ilmakehään. Aurinkojäähdytyksessä kulutus ja tuotanto kohtaavat sopivalla tavalla ja vältetään energian suurta varastointitarvetta. Tämän Suomen ja Saksan yhteistyöprojektin tavoitteena oli kehittää pieni kompakti aurinkoenergialla, biopolttoaineella tai teollisuusprosessilämmöllä toimiva absorptiojäähdytin kiinteistön tai teollisuusprosessin jäähdytykseen Pohjois- ja Keski-Euroopan olosuhteisiin. Jäähdyttimen tulee toimia myös tarvittaessa lämpöpumppuna. Rinnakkain jäähdytys-lämmitysprojektin kanssa kehitettiin myös Savo-Solarin aurinkokeräintä SF100-03 varustamalla keräin muovikalvolla lasin ja absorptiopinnan väliin. Tavoitteena oli saada merkittävä parannus keräimen hyötysuhteeseen erityisesti suurilla keräimen keskilämpötilan ja ulkolämpötilan eroilla. 10 kW:n absorptiojäähdyttimen sovellutuskohteena oli Savo-Solar Oy:n toimistokiinteistö Mikkelissä. 15 kW:n aurinkolämpöteho tuotetaan Savo-Solarin aurinkokeräimillä (18 x 2 m2). Jos lämmönlähteen tuottama lämpötila tai teho ei riitä jäähdyttimen ajamiseen, lisälämpö otetaan kaukolämmöstä. Absorptiokone toimii myös tarvittaessa 25 KW:n lämpöpumppuna. Järjestelmä on varustettu 2 m3 kuumavesivaraajalla aurinkosäteilytehon vaihtelujen kompensoimiseksi ja ulos sijoitetulla ilmajäähdyttimellä, jonne ajetaan absorptiokoneen välijäähdytyslämpö ja tarvittaessa aurinkokeräinpiirin lämpö ylikuumenemisen välttämiseksi. Lämpöpumppumoodissa lämpö ajetaan teollisuushallin lattialämmitykseen. ZAE Bayernin pilot-kohteessa Münchenissä varalämmön lähteenä on puuhakkeella toimiva biokattila. Suunnitteluvaiheessa koko prosessi simuloitiin TRNSYS-mallilla, jossa todettiin mm. lämpövaraston sopivaksi mitoitusarvoksi 55,6 l/m2 aurinkokeräinpintaa eli Mikkelin tapauksessa 2 m3:n eristetty teräsäiliö varustettuna putkimallisella painovoimaisella lataus-purkausjakajalla. Jäähdytys-lämmityskäytössä lämpövarastoa voidaan hyödyntää 4–110 °C rajoissa. Järjestelmä toimii tavoitteiden mukaisesti, ja 10 kW:n jäähdytysjärjestelmällä on päästy tavoitteisiin eli vähintään 0,7 COP:hen (jäähdytysteho/tarvittava lämpöteho) ja EER 9 -arvoon (jäähdytysteho/käytetty sähköteho). Kehittämällä ohjausstrategiaa ja optimointia paremmin sopivaksi rakennuksen erityistarpeisiin päästään vielä parempiin COP- ja EER-lukuihin.
ISBN, ISSN, URN	ISBN 978-951-38-8511-3 (nid.) ISBN 978-951-38-8510-6 (URL: http://www.vtt.fi/julkaisut) ISSN-L 2242-1211 ISSN 2242-1211 (Painettu) ISSN 2242-122X (Verkkojulkaisu) http://urn.fi/URN:ISBN:978-951-38-8510-6
Julkaisuaika	Tammikuu 2017
Kieli	Englanti, suomenkielinen tiivistelmä
Sivumäärä	161 s. + liitt. 6 s.
Projektin nimi	Aurinkojäähdytys
Rahoittajat	Tekes ja Saksan talous- ja teknlogiaministeriö, BMWi
Avainsanat	jäähdytys, lämmitys, absorptiojäähdytys, kaukolämpö, biopolttoaineet
Julkaisija	Teknologian tutkimuskeskus VTT Oy PL 1000, 02044 VTT, puh. 020 722 111

Solar heating and cooling in Northern and Central Europe

Pilot plants in Finland and Germany

Finnish-German joint research project within the European SET-plan strategy

ISBN 978-951-38-8511-3 (Soft back ed.)
ISBN 978-951-38-8510-6 (URL: http://www.vttresearch.com/impact/publications)
ISSN-L 2242-1211
ISSN 2242-1211 (Print)
ISSN 2242-122X (Online)
http://urn.fi/URN:ISBN:978-951-38-8510-6

VTT TECHNOLOGY 287

Solar heating and cooling in Northern...